UTILIZATION OF NANOSTRUCTURED FLY ASH IN POLYMER MATRIX COMPOSITES

Thesis

Submitted in partial fulfillment of the requirements for the degree of

DOCTOR OF PHILOSOPHY

By

AKSHATA G. PATIL

DEPARTMENT OF METALLURGICAL AND MATERIALS
ENGINEERING

NATIONAL INSTITUTE OF TECHNOLOGY KARNATAKA,

SURATHKAL, MANGALURU – 575 025

December, 2015

DECLARATION

By the Ph.D Research Scholar

I hereby *declare* that the Research Thesis entitled "**Utilization of Nanostructured Fly Ash in Polymer Matrix Composites**", which is being submitted to the **National Institute of Technology Karnataka, Surathkal** in partial fulfillment of the requirements for the award of the Degree of **Doctor of Philosophy** in **Metallurgical and Materials Engineering** is a *bonafide report of the research work carried out by me*. The material contained in this Research Thesis has not been submitted to any University or Institution for the award of any degree.

AKSHATA G. PATIL
Register number: 110674MT11F01
Department of Metallurgical and Materials Engineering
National Institute of Technology Karnataka, Surathkal

Place: NITK-Surathkal
Date:

CERTIFICATE

This is to *certify* that the Research Thesis entitled "**Utilization of Nanostructured Fly Ash in Polymer Matrix Composites**", submitted by **Akshata G. Patil** (Register No: **110674MT11F01**) as the record of the research work carried out by her, is *accepted as the Research Thesis submission* in partial fulfillment of the requirements for the award of degree of **Doctor of Philosophy**.

Dr. S. Anandhan

Research guide

(Signature with date and seal)

Dr. Jagannath Nayak

Chairman-DRPC

(Signature with date and seal)

__Dedicated to my beloved family, friends and well wishers……__

ACKNOWLEDGEMENT

ABSTRACT

Fly ash (FA) is a by-product generated during the combustion of pulverized coal in power generating thermal stations. In this study, a class-F FA was subjected to mechano-chemical activation by high energy ball milling. Mechano-chemical activation was carried out in presence of a surfactant and an inert liquid medium to obtain nanostuctured FA. The morphological, compositional, spectral and structural properties of the mechano-chemically activated FA (MCA-FA) were characterized using scanning electron microscopy, transmission electron microscopy, x-ray diffraction, Fourier transform infrared spectroscopy, dynamic laser scattering and Brunauer-Emmett-Teller surface area analysis. The fresh FA and MCA-FA were incorporated as fillers in ethylene-octene random copolymer and poly(vinyl alcohol) matrices. Morphological studies revealed that interfacial adhesion between the polymer and MCA-FA was good, which accounted for the improvement in mechanical properties of these composites. Thermal properties and flammability of ethylene-octene random copolymer and poly(vinyl alcohol) composites were enhanced on the addition of fresh FA and MCA-FA.

The design of statistical analysis by Taguchi methodology was used to study the influence of milling parameters to obtain nanostructured FA. Ball milling parameters, such as ball-to-powder weight ratio, type and quantity of surfactant and type of medium were varied as guided by the Taguchi design. An orthogonal array and analysis of variance were employed to analyze the effect of milling parameters. According to the results obtained from analysis of variance, the factors ball-to-powder weight ratio and surfactant type emerged as the major contributing factors. Also, a fractal approach was used to characterize the lacunarity of the agglomerates in the MCA-FA. The MCA-FA was characterized by various techniques. Later, chitosan and poly(vinyl chloride) composites were prepared using fresh FA and MCA-FA. The key parameters for the enhancement of the properties of these composites and compatibility between MCA-FA and matrices were interfacial adhesion and morphology of these fillers.

Keywords: Fly ash; High energy ball milling; Mechano-chemical activation; Composite and Nanomaterial.

CONTENTS

PART-I

PART-II

<div align="center">

PART-I

</div>

**CHAPTER 3: MECHANO-CHEMICAL ACTIVATION OF FLY ASH
BY HIGH ENERGY BALL MILLING**

LIST OF FIGURES

iv

LIST OF SCHEMES

LIST OF TABLES

NOMENCLATURE

$\overline{\mathrm{M}}_w$	Average molecular weight
%	Percentage
°	Degree
°C	Degree celsius
μL	Microliter
μm	Micrometer
Å	Angstrom
ANOVA	Analysis of variance
BET	Brunauer-Emmett-Teller surface area analysis
BPR	Ball to powder ratio
BSS	British standard sieves
cm	Centimeter
CMC	Critical micelle concentration
cP	Centipoise
CS	Chitosan
CTAB	N-cetyl-N, N, N-trimethyl ammonium bromide
CuK	Copper k-alpha
DLS	Dynamic light scattering
DSC	Differential scanning calorimetry
DTG	Derivative Thermogravimetric analysis
EDS	Energy dispersive x-ray spectroscopy
EOC	Ethylene-octene random copolymer
Ethanol	E
Ethyl acetate	EA
eV	Electron volt
FA	Fly ash
FESEM	Field emission scanning electron microscopy

FTIR	Fourier transform infrared spectroscopy
g	Gram
GA	Glutaraldehyde
h	Hour
K	Kelvin
kV	Kilovolt
m	Meter
mA	Milliampere
MCA	Mechano-chemically activated
min	Minute
mL	Milliliter
mm	Millimeter
mM	Millimolar
mN	Millinewton
nm	Nanometer
PVA	Poly(vinyl alcohol)
PVC	poly(vinyl chloride)
rev	Revolution
rpm	Revolutions per minute
SAED	Selected area electron diffraction
SD	Standard deviation
sec	Second
SEM	Scanning electron microscopy
SLS	Sodium lauryl sulfate
TEM	Transmission electron microscopy
T_g	Glass transition temperature
TGA	Thermogravimetric analysis
THF	Tetrahydrofuran
Toluene	T
TX-100	Triton X-100
V	Volt

w/v%	Weight by volume percent
w/w%	Weight by weight percent
wt%	Weight percentage
XPS	X-ray photoelectron spectroscopy
XRD	X-ray diffraction
XRF	X-ray fluorescence
Z-avg	Average particle size
	Theta
	Wavelength

CHAPTER 1

CHAPTER 1

INTRODUCTION AND LITERATURE REVIEW

This chapter gives a brief introduction to utilization of fly ash in polymer matrix composites. An over view of the importance of surface modification of fly ash by chemical and mechanical activation process is presented here. The utilization of surface modified fly ash as reinforcement in various polymer matrices is reviewed in brief. The mechanical and thermal properties of fly ash based polymer composites are presented. Finally, the motivation for the present research study along with its scope and objectives are mentioned.

1.1 INTRODUCTION TO FLY ASH

Fly ash (FA) is a by-product generated during the combustion of pulverized coal in power generating thermal stations. During combustion of coal the organic and inorganic minerals (such as clay, feldspar, quartz and shale) fuse in suspension and are carried away from the combustion chamber by the exhaust gases. These suspended particles in the exhaust gases solidify upon cooling into spherical glassy particles, crystalline solids or cluster of agglomerates called as FA. They are collected by the electrostatic precipitators or bag filters [Iyer and Scott 2001].

The physical and chemical properties of FA particles are function of the source, type of minerals in the coal, the combustion conditions, and post-combustion cooling. Fly ashes are light to dark grey in color (**Fig. 1.1a**), abrasive, mostly alkaline, refractory and amorphous in nature. FA is made of fine powdery particles predominantly solid spherical in shape (**Fig. 1.1b**); at times it is a cenosphere that is a hollow spherical shape, which has a wide range of particle size from 0.5 μm to 100 μm. The specific gravity of FA ranges from 2.0 to 2.5. The chemical properties of FA are influenced to a great extent by the four types or ranks of coal, each varying in chemical composition, heating value, ash content, and geological origin. The four types (ranks) of coal are bituminous, sub-bituminous, anthracite and lignite. FAs are heterogeneous consisting of quartz, mullite, kaolinite and ilite as the dominant

mineral phases; and the less predominant minerals include calcite, pyrite and hematite [Ahmaruzzaman 2010, Hamzaoui 2016].
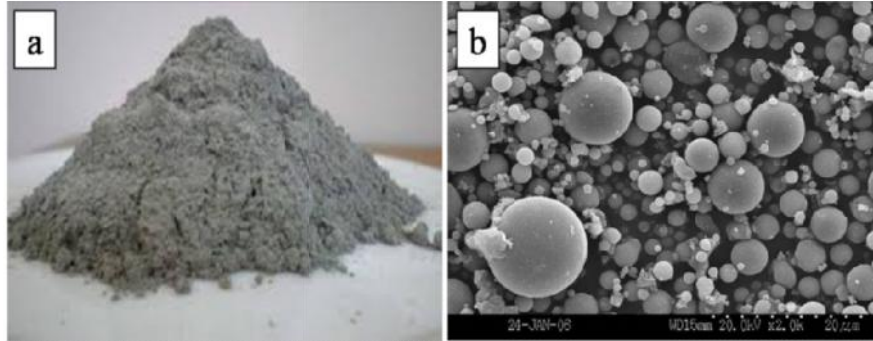
Fig. 1.1 (a) FA and (b) SEM micrograph of FA

As per ASTM C 618-03**,** FA is often divided into two classes: class F and class C on the basis of iron and calcium levels. The FA that contains more than 70 % oxides of silica (SiO_2), alumina (Al_2O_3) and iron oxide (Fe_2O_3) of the total composition with Fe_2O_3 content higher than that of calcium oxide (CaO) belongs to class F [Blissett and Rowson 2012].

FA is considered as an environmental pollutant, because, the extent of dumping the FA is a major problem due to the shortage of space required to accommodate the large volume of its generation. It is necessary to reuse, recycle and ensure safe disposal of FA as it contains toxic elements, such as lead, manganese, arsenic, molybdenum, beryllium, cadmium, mercury, chromium, strontium, cobalt, boron and vanadium, which are hazardous to the people living in the vicinity of disposal sites [Dhadse et al. 2008]. There is an increasing interest in the bulk utilization of FA in various fields as shown in **Fig. 1.2**. Other minor applications include geopolymer, roofing tiles, metal castings, paints, ceramic and glass, and filler in wood and plastic products [Yao et al. 2015]. FA utilization in India stands at a fairly low level of about 15 per cent of the quantity generated; the chief reasons for this being poor understanding of the chemistry and the derivatives of FA for proper end applications, lack of standards and specifications for FA products, poor public awareness about the products and their performance and lack of reliable quality assurance for FA products.

Fig. 1.2 Applications of FA in various fields

1.2 TECHNIQUES OF SURFACE MODIFICATION

Surface modification is a process of enhancing bulk and surface reactivity of fillers/reinforcements through physicochemical changes without altering their overall chemistry to improve the performance of the composites in which these fillers/reinforcements are used. Literature reveals that the surface of FA is modified by either chemical activation, mechanical activation or mechano-chemical activation. In chemical activation, the surface of FA is modified in presence of a surfactant or coupling agent; mechanical activation includes wet or dry ball milling process by fracturing the FA particles to lower size; and mechano-chemical activation is a combined process of chemical as well as mechanical activation.

1.2.1 Chemical activation

Surface modification by chemicals is in general used to obtain a high wetability for a solid surface, a better dispersion of particles, and adhesion of fillers in composite materials. Chemical activation of FA includes surface modification by a surfactant, coupling agent and/or alkali or sulfates. The frequently used surfactant and coupling agents include sodium lauryl sulfate (SLS), furfuryl palmitate, N-2(aminoethyl)-3 aminopropyltrimethoxysilane (KBM-603), silane and triethoxyvinylsilane (TEVS), and alkaline compounds, such as sodium hydroxide, sodium carbonate, potassium hydroxide and calcium hydroxide.

The surface modification of FA by anionic surfactant, sodium lauryl sulphate resulted in an irregular shapes and superior light reflecting quality by the particles [Nath et al 2010]. The surfactant coating on the surface of FA particles facilitated easy dispersion of the filler in poly(vinyl alcohol), which in turn, improved the mechanical properties of the composites. Sengupta et al. [2011] observed that the coating of acid ester of furfuryl alcohol, a low cost renewable chemical, reduced the surface roughness and improved the true porosity (%) of the FA particles. The ether linkages formed by the chemical reaction of the coupling agent (N-2(aminoethyl)-3 aminopropyltrimethoxy-silane) with FA particles is shown in **Fig. 1.3**. This modification improved the interfacial interaction between the filler and epoxy matrix [Chaowasakoo and Sombatsompop 2007].
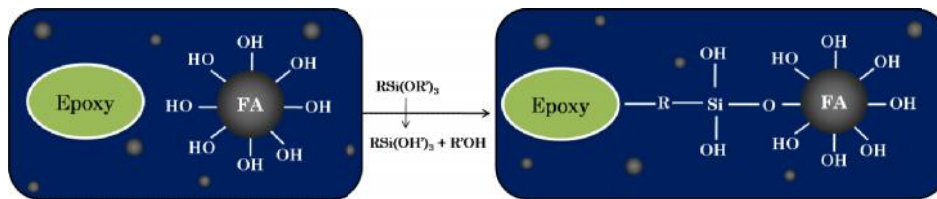
Fig. 1.3 Model for treated FA/epoxy composites using KBM603 at concentration 0.5 wt%

Similarly, Kishore et al. [2002] used three different types of surface modification to improve the adhesion of FA with epoxy matrix. In the first treatment, a simple procedure was followed by cleaning the FA surface with acetone; in the second one, the FA particles were coated with a silane-bearing system; for the third treatment, the FA particles were exposed to paraffin oil. Among the various treatments, the silane treatment was found to be the most effective and yielded better mechanical properties. The particle-particle interaction of the unmodified FA particles disappeared for the modified FA particles and this phenomenon played a significant role in the reduction of agglomeration of particles during fabrication of composite films. This attributes to the presence of triethoxyvinylsilane (TEVS) coupling agent and sodium hydroxide treated FA particles as incorporated in ethylene-octene random copolymer by Anandhan et al. [2012] and poly(vinyl alcohol) matrix by Nath et al. [2010], respectively. The chemical treatment with solutions of NaOH, $NaOH/NH_4HCO_3$, EDTA, and HCl was examined by Sarbak and Kramer [2002].

4

They concluded that chemical modifications of the FA had led to a significant increase in the surface area, mean pore size, and transformation of spherical-shaped structure into stacked layers, rod shape and some agglomerated to undefined shape.

Calcium hydroxide played a dual role of enhancing as well as reducing a few properties of the composites. The improved property was due to the formation of reactive radicals on the FA surface shown in **Fig. 1.4**. This resulted in formation of chemical linkage at the interface and enhanced adhesion between filler and polymer matrix. The deterioration was because of the corroded layer of FA surface that alters the surface chemistry of active FA [Parvaiz et al. 2011]. The FA was treated with calcium hydroxide and then isothermally heated by Yang et al. [2006], which altered the surface morphology and also enhanced the color of FA from dark grey-black to cream-white. The modification of FA surface by a mixture of sulfuric and nitric acids improved dispersion of FA and resulted in better compatibility with nonpolar polymers. These composites have wide application as adsorbent materials in adsorptive separation and purification applications [Khan et al. 2011 and Shawabkeh et al. 2011].
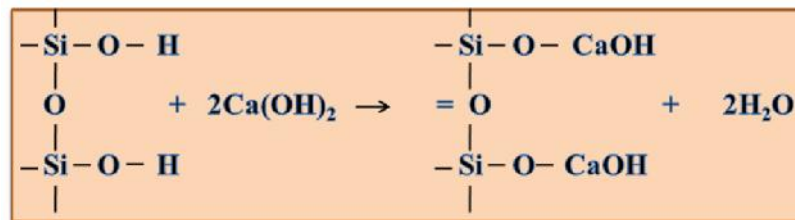
Fig. 1.4 Modification of FA surface with calcium hydroxide

1.2.2 Mechanical activation

Mechanical activation is usually achieved by high energy ball milling,1 which was developed as an industrial process to successfully produce new alloys and phase mixtures in 1970's.

Milling is a traditional way of crushing or blending powders, which is routinely used in mineral processing industries and powder metallurgy. Different types of materials produced by high energy milling are nano-crystalline powders, composite and nanocomposite powders, and intermetallic powders including amorphous alloy. Kong et al. [2001] and, Ghasdi and Alamdari [2010] found high

energy ball milling to be the most efficient route among all the milling processes. They investigated on the quantification and modeling of high-energy milling, which basically depends on the process variables [Zhang et al. 2004].

The variables which influence the milling process are shown in **Fig. 1.5**. All these process variables are not completely independent. For example, the optimum milling time depends on the type of mill, temperature in the vial, ball-to-powder weight ratio and size of the grinding media.
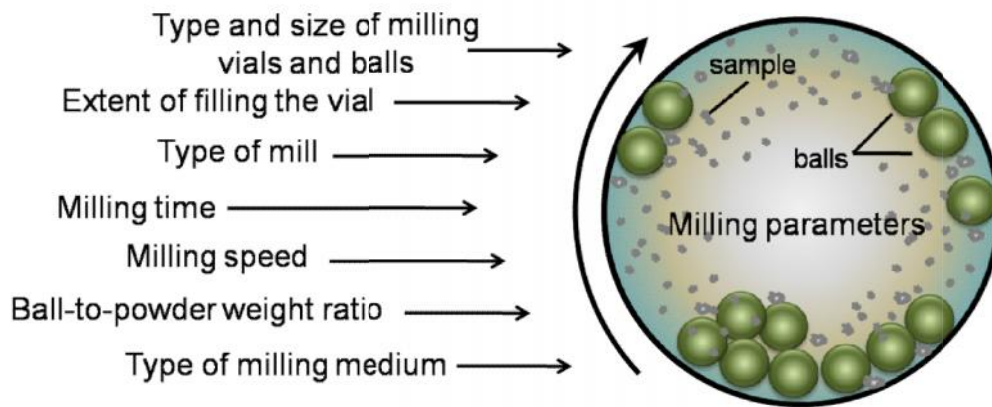
Fig. 1.5 An overview of the process variables to be considered in the milling process

Types of mill: Based on the direction of vial movement the ball mills are classified as conventional mill, attritor mill, planetary ball mill and spex shaker mill as shown in **Fig. 1.6 (a-d)**.

Sakthivel et al. [2008] investigated the grinding behavior in an attritor mill (**Fig. 1.6b**) and found that the efficiency of the mill to produce nanoparticles was low even at a higher milling time. The higher grinding rate of hard materials such as synthetic diamond and alumina in attritor mill was obtained with the larger media size and at a high rotational velocity of the impeller [Shinohara et al. 1999].

From the work of Enayati et al. [2009], it is found that a speed of 350 rpm of the planetary ball mill (**Fig. 1.6c**) provided a higher energy compared to a speed of 750 rpm of the conventional ball mill to produce nanocrystalline tungsten carbide (WC) particles. Ortiz et al. [2012] studied the oxidation of zirconium diboride (ZrB_2) powders in spex shaker mills (**Fig. 1.6d**) and found that high-energy ball-milling in air introduced twice the amount oxygen into the ZrB_2 powders in comparison to attritor mill.
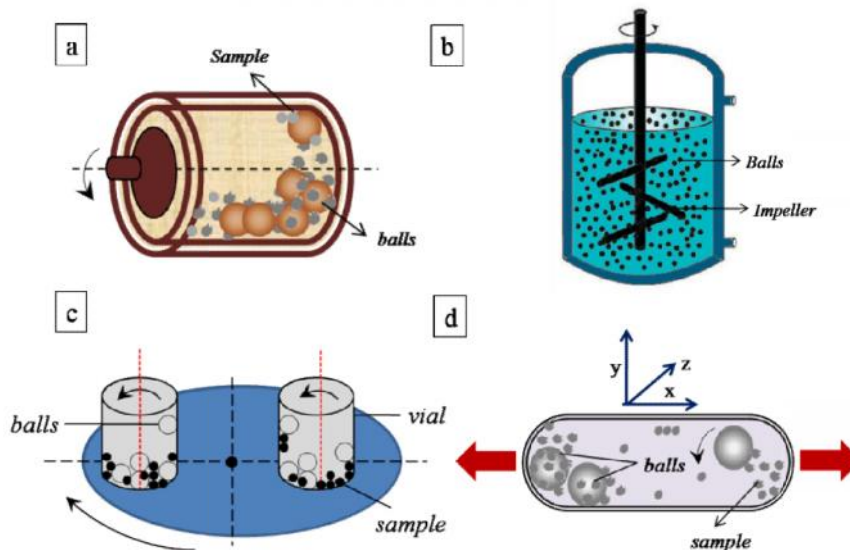
Fig. 1.6 (a) conventional ball mill (b) attritor mill (c) planetary ball mill, and (d) spex shaker mill

Type and size of milling vials and balls: The vials and balls are available in a wide range of sizes and materials, such as hardened steel, tungsten carbide, stainless steel, zirconia, silicon nitride, alumina and agate (**Fig. 1.7**).
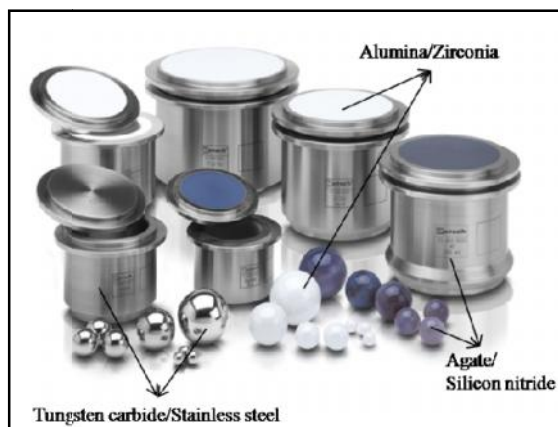
Fig. 1.7 Different varieties of vial and ball materials [www.fishersci.com]

The hard oxide mixture of Bi_2O_3 and TiO_2 were milled in tungsten carbide vial and balls, which resulted in nano-sized bismuth titanate ($Bi_4Ti_3O_{12}$) powder [Kong et al. 2001]. Low density agate vial and balls were used for milling α-Fe_2O_3 particles to reduce the strong magnetic interparticle interaction among the α-Fe_2O_3 particles [Xu et al. 2004].

7

Milling speed: Milling speed is not always directly proportional to the energy input on the sample. Mio et al. [2002] optimized mechanical milling performance by the rotation-to-revolution speed ratio in planetary ball milling. Tan et al. [2004] work suggests that soft metal oxide can be milled at lower rpm to obtain the nano-structured materials. Hard materials, such as hematite were milled with varying mill speeds of 200, 400 and 600 rpm and a higher milling speed of 600 rpm resulted in a minimum average particle size [Arbain et al. 2011].

Milling time: The time of milling is the most important process variable to achieve a steady state between the fracturing and cold welding of the powder particles. There are three different stages observed during the milling process as shown in **Fig. 1.8**.
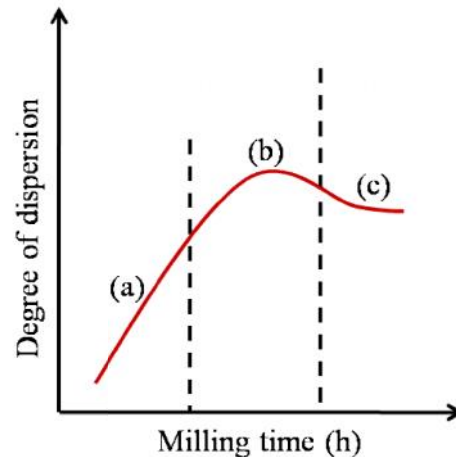
Fig. 1.8 Three stages during high energy milling (a) Rittinger stage (b) aggregation stage and (c) agglomeration stage

The first stage is the *Rittinger stage* **Fig. 1.8a**, where energy input is approximately proportional to the new surface area created by reduction in particle size. Second stage is the *aggregation stage* **Fig. 1.8b** as the new surface area produced is not proportional to the energy input because of particle aggregation. *Agglomeration stage* **Fig. 1.8c** is the last stage; here the dispersion of the particles drops and the surface area decreases because of particle agglomeration. To reduce the average particle size from 500 to 100 nm of lead zirconate titantate (PZT) based ceramics by conventional ball-milling and high energy ball mill took 24 h and 3 h, respectively [Lee et al. 2007]. Hewitt and Kibble [2009] observed that the number of

nanosize WC–Co particles increased with milling time. To avoid the effect of temperature rise during milling, the milling operation was programmed such that the mill was operated for 30 min and kept idle for 30 min [Sharafi and Gomari 2012].

Ball-to-powder weight ratio (BPR): The weight ratio of ball to powder can be varied from a lowest value of 1:1 to the highest value of 200:1, depending on the sample to be milled and type of the mill used. The most commonly used BPR was 10:1 to produce nano-structured materials with SPEX mill [Maweja et al. 2012]. A decrease in crystallite size and particle size with increasing BPR was observed by Zhang et al. [2008] and Ali et al. [2013].

Extent of filling the vial: It is important to consider the utility volume of the vial which varies based on the nominal volume of the container. For example the utility volume of the 250 mL and 500 mL vial is 25-150 mL and 75-300 mL with the maximum sample size of 6 mm and 10 mm, respectively. The maximum recommended ball filling for 250 and 500 mL vials are, 50 and 100 in number of 10 mm diameter and, 12 and 20 number of 20 mm ball diameter. If the numbers of balls are less, then the end results will be impaired due to wear and tear of the balls and the vial. On the other hand, if balls are large then there is no sufficient space for the balls to move around and the impact is less on samples. A 250-mL tungsten carbide vial and 10 tungsten carbide balls with diameter of 20 mm were used to prepare nano-sized lead lanthanum zirconate titanate powders at room temperature [Kong et al. 2001].

Type of milling medium: The milling process can be done either in presence or absence of a liquid medium, which are called as wet milling and dry milling, respectively. The effect of wet milling and dry milling on the physicochemical properties of milled boron particles was investigated by Jung et al. [2014]. They observed that wet milling process resulted in a narrower size distribution, smooth surface morphology, and reduced agglomerated particles than the dry milling process. From literature it was found that the wet milling process is advantageous over dry milling, as sample does not stick to the surface of balls and inner walls of the vial. It also acts as a cooling agent due to the heat generated by the rotation of the ball mill and reduces the agglomeration of the particles [Akcçay et al. 2004]. Fadda et al.

[2009] proposed a model to study the transition from the breakage to the agglomerative regime of fragile materials in dry milling process.

1.2.3 Mechano-chemical activation

Mechano-chemical activation is a process in which mechanical energy, such as impact and shear forces act on solid particles in presence of a chemical agent, such as a surfactant. It is an efficient technique for the low cost, large scale production of nanopowders than the conventional methods. However, conventional techniques have some drawbacks, such as low stirring and degree of mixing, uneven dispersion of the surfactant and in particular, high rate of aggregation of particles. The use of surfactants offers a potential path of controlling the structural and morphological characteristics of milled products. The surfactants provide a steric and/or electrostatic repulsive force to reduce the aggregation and agglomeration of the particles. Steric stabilization is achieved by wrapping the particles with polymers, which provide steric barrier to prevent close contact of the fine particles. Electrostatic stabilization occurs by the repulsive force between the like electrical charges and involves the creation of an electrical double layer by adsorption of ions on particle surface. Eisermann et al. [2012] investigated the phase transformation from alumina to aluminum hydroxide with electrostatic and steric stabilization methods.

Alumina-titanium diboride (TiB_2–Al_2O_3) nano-composite was prepared by mechano-chemical reduction processes and the homogeneity of the composite powder was highlighted by Rabiezadeh et al. [2012]. Lomayeva et al. [2000] and Zheng et al. [2012] milled pure iron and Sm_2Co_{17} in presence of a liquid medium (heptane) and surfactants (oleic acid). The presence of a surfactant increased the dispersion of powder particles and their magnetic characteristics. Sodium oleate (SDO) was incorporated as a surface modifier while grinding calcite by Yo urtcuo lu et al. [2011], which turned the hydrophilic surface of calcite to hydrophobic. The study by Pelovski et al. [2001] and Baláž et al. [2011] proved the possibility of mechano-chemically activating dolomite and arsenic sulphide particles by high energy ball milling. This led to lower average particle size and higher specific surface area. Nanocrystalline soft magnetic powders of Ni_3Fe were obtained in presence of benzene as a process control agent to reduce cold welding [Neamtu et al. 2011]. The objective

of Hennart et al. [2012] was to characterize a sub-micron grinding process and agglomeration of fines inside the grinding chamber. The milling process was carried out in presence of a surfactant CTAB (cetyltrimetyl-ammonium bromide) to prevent aggregation of small particles and stabilize the particle suspension. The nano-structured FA was obtained by milling for 30 h and 60 h in presence of anionic surfactant and toluene medium by Paul et al. [2007] and swami et al. [2010]. This resulted in 405 times reduction in particle size, the surface area increased more than 100% and the morphological studies revealed the FA particles were deformed into irregular shape with rough surface.

1.3 DESIGN OF EXPERIMENTS (DOE)

DOE is a statistical technique, which deals with planning, conducting, analyzing and interpreting controlled tests to evaluate multiple variables simultaneously. It is necessary to integrate a simple and powerful statistical method into the experimental design methodology to draw conclusions effectively and efficiently. The most important stage in the design of an experiment lies in the selection of control factors.

1.3.1 Taguchi Method

Taguchi created a standard orthogonal array to accommodate various factors and levels in design with defined logical procedure or algorithm implementation. The Taguchi technique provides a simple, efficient and systematic approach to determine the influence of parameters in a manufacturing process. It is used to study the entire parameters' space with only a small number of experiments [Taguchi 1986]. Moreover, an analysis of variance (ANOVA) and main effect plot is employed to estimate the error variance and determine the percentage contribution of the individual factors [Roy 2001 and Ross 1996]. The response surface method (RSM) is used to build the relationship between the input factors and output responses, and used as the fitness function to measure the fitness value of the genetic algorithm (GA).

Mechanical alloying is a complex process and hence involves optimization of a number of variables to achieve the desired product phase and/or microstructure. Ghani et al. [2004] worked on the Taguchi optimization methodology for cutting parameters in end milling and, analyzed the results by signal-to-noise (S/N) ratio and ANOVA. The preparation of ZnO nano-particles using statistical experimental design

11

by Kim et al. [2008] observed the particle and crystallite size were dependent on the milling time and mass ratio of ball to powder. Zhang et al. [2008] optimized the parameters in the planetary ball milling of nano-structured tungsten carbide/cobalt powder by the Taguchi method. The factors were weight ratio of ball to powder, type of medium, size of milling balls, rotation speed and volume of milling medium. It was found that all the factors other than weight ratio of ball to powder were very significant on specific surface area results. The most influential factor for preparing the lead-free piezoelectric ceramic of $Bi_{0.5}Na_{0.5}TiO_3$ was the sintering temperature determined using Taguchi method, which had a percentage contribution up to 94.94% as indicated by ANOVA [Chou et al. 2010]. Hennart et al. [2010, 2012] used factorial design for ball milling of water soluble organic products and developed a model to study the agglomeration phenomena. Shrivastava et al. [2011] demonstrated that statistical modeling improved the understanding of experimental data by the main effects plots and regression analysis to predict the optimal conditions of attritor mill. Taguchi's design of experiments with four factors and three levels (3^4) of L_9 orthogonal array was performed to study the formation of silicon nitride and silicon carbide whiskers using the carbothermal nitridation process [Mustapha et al. 2013]. Canakci et al. [2013] carried out a Taguchi design of L_{16} (4^4) to assess the effect of mechanical milling parameters to obtain nanocrystalline Al 2024 powder. Similarly, many researchers [Ho et al. 2009, Heng et al. 2012, Kuram et al. 2013, Jamshidi et al. 2014 and Fruhstorfer et al. 2014] worked on Taguchi statistical experiments to optimize the combinatorial effects of milling process.

1.4 POLYMER MATRIX COMPOSITES

Polymers are a large class of materials consisting of many small molecules (called monomers) that can be linked together to form long chains, thus they are known as macromolecules. They are classified as natural and synthetic polymers, where natural polymers occur in nature and are usually biopolymer. The examples for natural polymers are silk, wool, cotton, DNA, cellulose and proteins. Synthetic polymers are derived from petroleum products, and made by scientists and engineers to meet the demands of industries to manufacture stiffer, stronger and lightweight materials.

Pristine polymer materials do not meet completely the technological requirements of the present industries. So, to make the polymer materials more commercially useful, they are admixed with certain supplement additives, modifiers, compatibilizers and reinforcing materials such as particulate fillers and fibers. Polymer composite materials can be well-defined as an amalgamation of two or more constituent materials of distinct phases with significantly different physical or chemical properties, resulting in a heterogeneous material having bulk properties different from that of the individual constituents.

There are three main constituents in any composite: the matrix, the reinforcement, and the interfacial region. The primary constituent that forms the continuous phase is termed as the matrix and the secondary constituent is referred to as the reinforcing phase, or reinforcement, as it is embedded in the matrix [Chawla 2012]. The interfacial region is responsible for communication between the matrix and filler. This is conventionally ascribed properties different from the bulk matrix because of its proximity to the surface of the filler.

Many researchers have reinforced organic and inorganic materials as reinforcement in polymer matrix. The properties of the composites is a function of the characteristics of the reinforcement, such as its size, shape and distribution, color, volume fraction, aspect ratio, and the interfacial adhesion between the surface of reinforcement and polymer. Polymer composites exhibit a combination of properties of the reinforcement and polymer matrix.

1.4.1 Reinforcements

The reinforcements are usually fibers or particulates. Particulate based composites have dimensions that are almost the same in all directions with the varying sizes from few microns to nano meters. Micro/nano-composites of polymer are extensively studied their use lowers the material cost by reducing the volume of matrix resin and enhances the overall performance of the composites. The fillers are tougher, stronger, harder and stiffer than the matrix, and thereby provide durability, strength and stiffness to the composites. Many micro/nano fillers exhibit multi-functionality in polymer matrices, as they exhibit improved mechanical properties, electrical properties, thermal properties and flammability properties. A wide variety of fillers,

such as silica [Reynaud et al. 2001], graphene [Stankovich et al. 2006], $CaCO_3$ [Kaully et al. 2008], montmorillonite [Anandhan et al. 2011], CNT [Ghorabi et al. 2012] and TiO_2 [Wang et al. 2014] were used in a range of polymer matrices. The incorporation of ceramic fillers into a more flexible and low thermal resistance polymer matrix substantially improves its stiffness and thermal stability. Compared to most of the expensive and toxic fillers, FA when used as reinforcement in polymer matrix composites could reduce the consumption of the other commonly used mineral fillers, such as silica thereby reducing the green house emissions.

FA in un-modified or the surface modified state has been widely used as filler in various polymer matrices, such as epoxy [Kulkarni and Kishore 2002, Gu et al. 2007 and, Chaowasakoo and Sombatsompop 2007], polyester [Devi et al.1998, Guhanathan et al. 2001, Rohatgi et al. 2009], ethylene–octene copolymer [Anandhan et al. 2011], poly(vinyl alcohol) (PVA) [Yunsheng et al. 2006, Nath et al. 2010], polypropylene [Sengupta et al. 2011, Satapathy et al. 2011], poly(etheretherketone) [Parvaiz et al. 2011], polyurea [Qiao et al. 2011], acrylonitrile butadiene styrene (ABS) terpolymer [Kulkarni et al. 2014].

The use of polymer composites is increasing in many important applications, such as civil infrastructure, electronic appliances, medical equipments, packaging and sports materials, automotives and aerospace industries. Presently, the world's annual consumption of polymer composites has exceeded that of the other materials such as wood and metals. This is because of the outstanding properties of the polymer composites, for instance high strength, corrosion resistance, high chemical stability, elastic stiffness and low density.

1.4.2 Role of Polymer matrix

Polymers are the perfect matrix as they can be processed easily, have low density and possess desirable mechanical properties. The physical properties of the matrix, which influence the behavior of composites are shrinkage during cure, ultimate elongation, modulus of elasticity, fracture toughness and strength (tensile, compressive and shear). Polymer matrix consists of either a thermoset or thermoplastic resin, which binds the reinforcement or filler together; and transfer applied stresses from the matrix to the reinforcement. The processability and defects in a composite material depend

strongly on the thermal characteristics, such as viscosity, melting point, and curing temperature of the matrix.

1.4.2.1 Thermoplastic resin

Thermoplastic resins, also called engineering plastics, include polymers such as nylon, polyethylene, teflon, polyvinylchloride, polypropylene and polyether-etherketone (PEEK). Thermoplastic polymers are either amorphous or semicrystalline in nature, synthesized by addition or condensation polymerization. They are widely used in household appliances, cable insulators, textiles and packaging materials [Muzzy 2000 and Rudin et al. 2012].

Poly(vinyl alcohol) (PVA): PVA is a biodegradable water-soluble semicrystalline polymer synthesized by alcoholysis of poly(vinyl acetate). A number of biodegradable polymers of natural and synthetic origin indicated significant developments in engineering applications. Unfortunately, biodegradable polymers have inferior mechanical and thermal properties. As a result, attempts have been made by many researchers to improve their strength by incorporating inorganic fillers, such as FA.

FA particles modified by sodium hydroxide [Nath et al. 2010] and sodium lauryl sulfate [Nath et al. 2010] improved the mechanical properties of the PVA composites. The tensile strength improved by 289% and 33% for the modified FA composites in comparison with unmodified FA and neat PVA. This was attributed to elimination of particle–particle interactions and uniform distribution of particles in PVA matrix.

PVA fiber-reinforced fly ash-geopolymer boards (SFRFGBs) were manufactured by extrusion technique. The FA content and fiber volume fraction changed the impact failure mode of those boards from brittle to ductile, resulting in a great increase in impact toughness for SFRFGBs [Yunsheng et al. 2006].

Polyethylene (PE): Polyethylene belongs to a family of polyolefin resins obtained from the polymerization of ethylene. It is the most common thermoplastic, having long hydrocarbon chains and has widely been used as a packing material. The different grades of polyethylene are low density PE (LDPE), medium density PE (MDPE), and high density PE (HDPE). Others very low density PE (VLDPE), linear

low density PE (LLDPE), ultra high molecular weight PE (UHMWPE) and ultra high molecular weight high density PE (UHMWHDPE).

In 1998 Li et al. prepared composite material from FA and post-consumer poly(ethylene terephthalate) (PET). They observed that addition of FA reduced the thermal decomposition of PET and improved the compressive strength. The study by Sharma and Mahanwar [2010] showed the effect of particle size of FA on recycled poly(ethylene terephthalate)/FA composites. The composites with smaller particles of FA showed better mechanical properties than those with a larger particle size, due to better interlink between the filler and polymer matrix. Larger particles of FA led to an improvement in dielectric strength and flammability of those composites.

The mechanical properties and thermal stability of high density polyethylene composites was improved by reinforcing the FA cenospheres modified by silane coupling agent and HDPE-g-dibutyl maleate as compatibilizer [Deepthi et al. 2010]. Similar improvement in the properties of LDPE composites was observed by modifying oil fly ash (OFA) with COOH group and polyethylene-grafted-maleic anhydride as a compatibilizer [Khan et al. 2011].

The article by satapathy et al. [2012] highlighted the results of reinforcing FA and nano structured FA in waste polyethylene (WPE) matrix. The decrease in particle size of FA from micron to nano level by ball milling was an efficient technique for enhancement in the properties of the composites. Similar trend of physico-mechanical, thermal and dynamic mechanical properties were observed for high density polyethylene composites incorporated with FA and nano FA [satapathy et al. 2013].

Polypropylene (PP): The semicrystalline polypropylene polymer and its composites have been widely used in many engineering applications. The semicrystalline PP forms three different crystallographic phases, viz., -monoclinic phase, -pseudohexagonal phase and γ-orthorhombic phase. The mechanical properties of PP were improved by the addition of natural clay, as it generally influences the crystallization of , and γ forms [Nath et al. 2010], which is evident from the crystallization kinetics of the PP composites. A study on non-isothermal crystallization kinetics of FA filled isotactic-polypropylene (PP) composites revealed

some interesting phenomena [Nath et al. 2010]. Addition of FA to PP acted as a heterogeneous -nucleating agent and induced a secondary -crystalline phase in the PP–FA composites. From dynamic mechanical properties they observed that there was a significant enhancement in storage (E') and loss moduli (E'') of these composites compared with those of neat PP [Nath et al. 2011].

FA particles coated with furfuryl palmitate (FP) were incorporated as filler in recycled polypropylene (RPP) matrix composites by Sengupta et al. [2011]. The flexural strength, breaking energy and modulus were increased by 6.4%, 64% and 1.4%, respectively. Satapathy et al. [2011] observed a ductile-to-brittle transition in the cenosphere-filled PP composites. Many researchers [Yang et al. 2006, Bandyopadhyay et al. 2010 and Zaeni et al. 2010] worked on the color control of FA as a combined function of particle size, chemical composition and isothermal heating and incorporated in PP matrix. This improved the esthetic appearance with brighter and reflecting surfaces of the composites.

Ethylene-octene random copolymer (EOC): EOC is a new random copolymer of ethylene and 1-octene, which is commercially available as a polyolefin plastomer. It possesses high flexibility and the melt processability of thermoplastics. Anandhan et al. [2012] reinforced FA particles modified by triethoxyvinylsilane (TEVS) into EOC. The improvement of EOC with modified FA composites was nearly 150% in tensile strength at a filler loading of 20%. This indicates that modified FA can be an effective reinforcement in EOC matrix.

Polyurea: Polyurea (PU) is produced by the chemical reaction between an isocyanate component and polymer resin. The PU composites filled with larger FA particles displayed inferior mechanical properties in comparison with those filled with small- and medium-sized FA [Qiao and Wu 2011].

Similarly, thermoplastics such as acrylonitrile butadiene styrene (ABS) terpolymer [Kulkarni et al. 2014], metakaolin-based geopolymeric composites [Wang et al. 2011] and poly(ether ether ketone) (PEEK) [Parvaiz et al. 2011] reinforced with FA cenosphere and FA surface modified with calcium hydroxide improved the mechanical properties (tensile and flexural strength), thermal insulation and interfacial adhesion between filler and polymer matrix.

1.4.2.2 Thermoset resin

Thermoset resins are usually low molecular weight oligomers or monomers having functional groups for cross-linking reaction. The three-dimensional network of thermosets tends to have high dimensional stability, high-temperature resistance, and good mechanical properties and resistance to solvents. Although thermosets are difficult to reform, they have many distinct applications in defense, aerospace, and electronic industries for materials that can retain useful properties at elevated temperatures. Polyesters, vinylesters, epoxies, and polyamides are the most commonly used thermoset resins [Varma and Gupta 2000; and Carraher 2003].

Epoxy resin: Epoxy resins are widely used family of thermosets. The advantages of epoxy resin are reasonably stable to chemical attacks and low shrinkage during curing. The epoxy resin filled with FA is involved to obtain a promising advanced low density composite.

The poor interfacial bonding between hydrophobic thermosetting epoxy polymer and hydrophilic FA particles resulted in reduced mechanical properties. Many researchers modified the FA surface by various silane coupling agents promoting the adhesion between the thermosetting matrices and the FA. The FA was treated with three different chemicals (acetone, combination of both acetone and silane, and paraffin oil) by Kishore et al. [2002] as discussed in the chemical activation section 1.2.1. Among the various treatments, the silane treated and acetone-cleaned FA particles improved the overall properties of the system, especially strength and load bearing capacities. The epoxy composites with lower average particle size exhibited improved strength and better adherence for the silane treated particles by kulkarni and kishore [2002]. Similarly, Ramos et al. [2005] prepared hybrid composites using epoxy resin (ER), carboxyl-terminated butadiene acrylonitrile copolymer (CTBN) and FA microspheres in different proportions. The results showed that the impact resistance of CTBN modified ER were superior to that of the pure epoxy resin.

Chaowasakoo and Sombatsompop [2007] suggested that the tensile and flexural moduli of the composites increased with increasing FA content in epoxy matrix. The comparative studies of fly ash/epoxy composites using conventional

thermal and microwave curing methods showed higher tensile and flexural moduli for the conventional thermal cure. A series of epoxy composites filled with FA of different volume fraction was prepared by Gu et al. [2007], who observed better interfacial adhesion with γ-aminopropyltriethoxy silane treated FA particles.

Polyester resins: Polyester resins are long-chain polymers, which are chemically composed of an ester and a dihydric alcohol and a terephthalic acid. Polyesters are hydrophobic in nature, widely used for insulation because of their durability and chemical resistance, low stretching and shrinking, wrinkle resistance and abrasion resistance.

The mechanical properties of fly ash-filled unsaturated polyester resin (FPR) were compared with that of calcium carbonate-filled polyester resin (CPR) and polyester resin (PR) [Devi et al. 1998]. It was observed that FPR was inferior to CPR and PR composites with respect to tensile and flexural strengths. Further, the work was upgraded by modifying the surface of FA by two different silane coupling agents (CAs) such as 3-aminopropyl-trimethoxysilane (AMP) and vinyltriethoxysilane (VES). AMP coupling agents was found to be better than VES coupling agents, with increased tensile, flexural, compressive, and impact strengths of the composites [Guhanathan et al. 2001, 2004].

Rohatgi et al. [2009] fabricated polyester/FA composites with cenospheres. As the volume fraction of FA increased in the composite the compressive modulus increased and compressive strength decreased. This was attributed to the numerous defects present in FA particles, which contributed to their early fracture and reduced strength of the composite.

1.5 SCOPE AND OBJECTIVES OF THE PRESENT STUDY

1.5.1   Scope

About 75 % of India's energy supply is coal based and shall be so for the next few decades. There are about 82 utility thermal power stations to produce approximately 110 million tonnes of FA per annum in the country. Nearly 38% of the FA waste is utilized in the country at present in various fields. Attempts have been made earlier to utilize this FA waste in the polymer industry in making polymeric composites, where FA is being used as inorganic particulate filler. Mechanically modifying the FA by

high energy ball milling could be used to convert it into a nanostructured particle and incorporate as filler in polymer matrix composites to produce new materials for various applications. Even though mechano-chemically activated FA prepared by the proposed method involves some additional cost, it will be cheaper as compared with the currently used synthetic ceramic nanoparticles or nanotubes. This will also be an effective way of utilizing the plentiful resource of this inexpensive, abundant industrial by-product and will also help reduce the environmental pollution.

1.5.2 Objectives

The objectives of the work are divided into part-I and part-II based on the FA collected from two different thermal power stations.

Part-I

In this part of the study, the FA was obtained from Tuticorin Thermal Power Station, Thoothukudi, Tamil Nadu, India. The objectives are:

- Preparation of nanostructured FA by mechano-chemical activation using high energy planetary ball mill.
- Characterization of fresh and mechano-chemically activated FA by x-ray diffraction (XRD), scanning electron microscopy (SEM), transmission electron microscopy (TEM), Fourier transform infrared (FTIR) spectroscopy, BET surface area and particle size analyzer.
- Synthesis of composites from the mechano-chemically activated FA with ethylene-octene random copolymer and poly(vinyl alcohol) matrices.
- To study the mechanical, morphological and thermal properties of the composites.

Part-II

In this part of the study, the FA was obtained from Raichur (NTPC) Thermal Power Station, Karnataka, India. The objectives are:

- To study the influence of parameters of planetary ball milling on the mechano-chemical activation of FA by Taguchi method-design of experiments.
- Characterization of fresh and mechano-chemically activated FA by x-ray diffraction (XRD), x-ray fluorescence spectroscopy (XRF), scanning electron

microscopy (SEM), field emission scanning electron microscopy (FESEM), transmission electron microscopy (TEM), Fourier transform infrared (FTIR) spectroscopy, x-ray photoelectron spectroscopy (XPS), BET surface area and particle size analyzer.

- Synthesis of chitosan and poly(vinyl chloride) composites based on the fresh FA and nanostructured mechano-chemically actived FA obtained using the Taguchi method.
- To study the mechanical, morphological and thermal properties of the polymer composites.

1.6 LAYOUT OF THE THESIS

The dissertation has nine chapters, which are divided into part-I and part-II based on the FA that is collected from two different thermal power stations. The contents of each chapter are organized as follows:

Chapter 1 gives a brief introduction and a review of literature on to FA, surface modification of FA and its utilization as filler in various polymer matrices.

Chapter 2 details the materials used and methodology followed for the pre-treatment of FA, mechano-chemical activation of FA and preparation of the polymer nanocomposites. It also discusses the characterization techniques used to study the properties of fresh FA, mechano-chemically activated FA and their composites.

Part-I: In this part of the study, the FA was obtained from Tuticorin Thermal Power Station, Thoothukudi, Tamil Nadu, India.

Chapter 3 focuses on the preparation and characterization of mechano-chemically activated FA obtained by high energy planetary ball milling in presence of a surfactant and an inert liquid medium.

Chapter 4 discusses the preparation and characterization of ethylene-octene random copolymer based composites reinforced with fresh FA and mechano-chemically activated FA.

Chapter 5 details the preparation and characterization of biodegradable poly(vinyl alcohol) based composites incorporated with fresh FA and mechano-chemically activated FA.

Part-II: In this part of the study, the FA was collected from Raichur (NTPC) Thermal Power Station, Karnataka, India.

Chapter 6 focuses on the influence of planetary ball milling parameters on the mechano-chemical activation of FA to obtain nanostructured FA using design of statistical analysis by Taguchi methodology. It also covers the characterization of mechano-chemically activated FA.

Chapter 7 is on the preparation and characterization of biodegradable chitosan composites reinforced with fresh FA and mechano-chemically activated FA.

Chapter 8 details the preparation and characterization of poly(vinyl chloride) composites incorporated with fresh FA and mechano-chemically activated FA.

Chapter 9 conclusions obtained from the present investigation.

CHAPTER 2

CHAPTER 2

MATERIALS AND METHODS

———————————————————————————————

This chapter discusses the details of the materials used for the surface modification of FA by mechano-chemical activation process. The statistical Taguchi design was applied to study the influence of experimental parameters on the preparation of mechano-chemically activated FA (MCA-FA). This MCA-FA was reinforced in various polymers matrix to obtain nanocomposites. The process of pre-treatment of FA, mechano-chemical activation of FA and preparation of the polymer nanocomposites are discussed followed by a concise description on the several characterization techniques used in this study.

PART – I

This section discusses the details of characterization of the Class-F FA obtained from a Tuticorin thermal power station and subjected to high energy ball milling induced mechano-chemical activation in presence of an inert liquid medium and surfactant. Subsequently, the resultant FA was used as a nano-structured reinforcement in ethylene-octene random copolymer (EOC) and Poly(vinyl alcohol) (PVA) matrices. This is followed by a description of the various techniques used to characterize the nanocomposites.

2.1. MATERIALS

FA was kindly supplied by Tuticorin thermal power station, Thoothukudi, Tamil Nadu, India. The anionic surfactant, sodium lauryl sulfate (SLS) was obtained from Sisco research laboratories, Mumbai, India. The cross-linking agent, glutaraldehyde (GA: 25% content in water) and solvents (toluene and xylene) were procured from Nice chemicals Pvt. Ltd, Kochi, Kerala, India with purity < 99% and were used without further purification.

Ethylene-octene random copolymer (EOC) (ENGAGE-8200^{TM} with octene content of 38%) was kindly provided by Dow elastomers, USA, through Bhimrajka

Impex, India. It had a melt index of 5 dg min^{-1} at 190 °C/2.16 kg (ASTM D 1238); density 0.870 g cm^{-3} (ASTM D 792); Mooney viscosity 8, ML_{1+4}@121 °C (ASTM D 1646); hardness 66 (shore A, 10 s ASTM D 2240-81). Poly(vinyl alcohol) (PVA) ($\overline{M}_w$: 125,000 g mol^{-1} and the degree of hydrolysis was approximately 89%) and solvent (cyclohexane) were obtained from Central drug house Pvt. Ltd., New Delhi, India.

2.2 METHODOLOGY

Pre-processing and mechano-chemical activation of the FA were carried out and the mecahno-chemically activated FA (MCA-FA) was further characterized by various techniques. The preparation of polymer composites with fresh FA and MCA-FA in EOC and PVA matrices are discussed.

2.2.1 Pre-treatment of FA

Demineralized water was used to wash the as-received FA to eliminate the carbon present in it; this was followed by drying for 5 h at 100 °C. The dried FA is called as fresh FA. The fresh FA was sieved using British standard sieves of mesh no. 150 to 350. The maximum amount (25% by weight) of the FA retained on mesh no. 200 and passed through mesh no. 170 was collected. This FA is mentioned as sieved FA. Later, magnetic impurities were removed through manual magnetic separation and the FA obtained was subjected to mechano-chemical activation. The pre-treatment of FA is shown in **Fig. 2.1**.

Fig. 2.1 Pre-treatment of FA

2.2.2 Mechano-chemical activation of FA

Mechano-chemical activation of pre-treated FA was achieved using a high-energy planetary ball mill (model: PM 100; Retsch, Germany) as shown in **Fig. 2.2**. The milling conditions were as follows: the milling vial and the grinding media were of

tungsten carbide, weight ratio of ball-to-FA was 10:1, and the ball diameter was 10 mm. The milling was carried out for 30 h and 60 h in toluene medium along with 1 wt% of SLS surfactant to reduce the agglomeration between FA particles. The rotation speed of the planetary carrier was 300 rev min^{-1}. The resultant FA is called as as MCA-FA. Fresh FA, 30 h and 60 h MCA-FA had specific gravities of 2.01, 1.32 and 1.15, respectively, as determined by the pycnometer method as per ASTM D854-10.
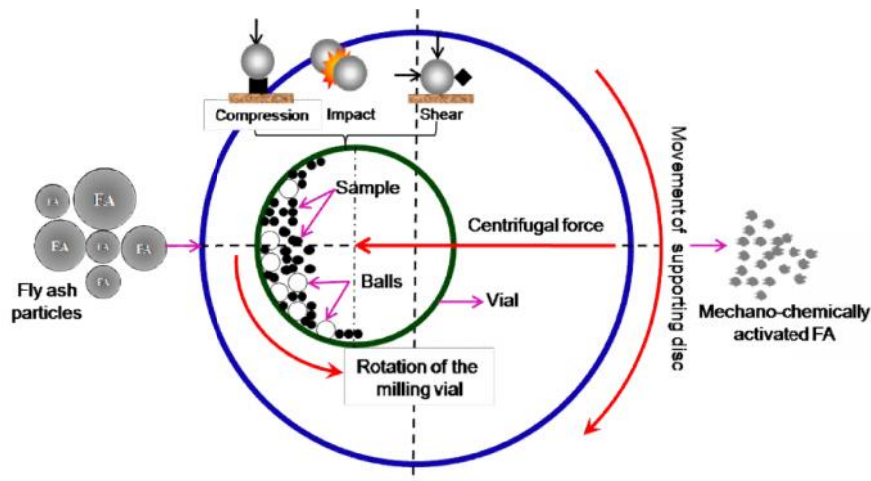
Fig. 2.2 Mechano-chemical activation of FA

2.2.3 Preparation of EOC/fresh FA and EOC/MCA-FA composites

Three sets of composites with 1, 3 and 5 wt% of fresh FA and FA mechano-chemically activated for 30 and 60 h, were prepared by solution casting method. About 6 g of EOC polymer were added to 100 mL of a 3:2 mixture of cyclohexane and xylene. The setup was kept under magnetic stirring until the entire polymer dissolved in the solvent. The predetermined amount of filler was added to the solution and ultrasonicated for 30 min. The solution was then transferred to clean glass petri-dishes and the mixtures were allowed to dry at room temperature. The residual solvent in the film was removed by drying the latter in a vacuum oven at 40 °C to a constant weight. After the complete evaporation of the solvent, the films were peeled off the glass petri-dishes and used for testing and characterization. The thickness of the films was 0.4 mm. The designations of the samples are given in **Table 2.1**.

Table 2.1 Designations of the EOC/fresh FA and EOC/MCA-FA composites

Samples	Designation
Neat EOC	EFA0
EOC/1 wt% of fresh FA	EFA1
EOC/3 wt% of fresh FA	EFA3
EOC/5 wt% of fresh FA	EFA5
EOC/1 wt% of 30 h MCA-FA	$EMFA_{30}1$
EOC/3 wt% of 30 h MCA-FA	$EMFA_{30}3$
EOC/5 wt% of 30 h MCA-FA	$EMFA_{30}5$
EOC/1 wt% of 60 h MCA-FA	$EMFA_{60}1$
EOC/3 wt% of 60 h MCA-FA	$EMFA_{60}3$
EOC/5 wt% of 60 h MCA-FA	$EMFA_{60}5$

2.2.4 Preparation of PVA/fresh FA and PVA/MCA-FA composites

Three sets of PVA matrix composites, containing 1, 3, and 5 wt% of fresh FA and FA that was mechano-chemically activated (MCA-FA) for 30 and 60 h, were prepared by solution casting method. Neat PVA was dissolved in demineralized water at 80 °C under vigorous agitation in a covered beaker to prepare a 6% (w/v) solution. For the preparation of cross-linked composite films, 1 N hydrochloric acid (50 µL) and 1 wt% GA solutions (0.50 mL) were added. A predetermined amount of filler was added to the PVA solution, and the mixture was ultrasonicated for 30 min. The solution was then transferred to a clean petri-dish and dried at ambient temperature. Subsequently, they were kept in a vacuum oven for 4 h at 60 °C to remove the residual solvent until a constant weight was obtained. After the complete evaporation of the solvent, the films were peeled off the glass petri-dishes and used for testing and characterization. The thickness of the films was approximately nearly 0.3 mm. The designations of the samples are given in **Table 2.2**.

Table 2.2 Designations of the PVA/fresh FA and PVA/MCA-FA composites

Samples	Designation
Neat PVA	PFA0
PVA/1 wt% of fresh FA	PFA1
PVA/3 wt% of fresh FA	PFA3
PVA/5 wt% of fresh FA	PFA5
PVA/1 wt% of 30 h MCA-FA	$PMFA_{30}1$
PVA/3 wt% of 30 h MCA-FA	$PMFA_{30}3$
PVA/5 wt% of 30 h MCA-FA	$PMFA_{30}5$
PVA/1 wt% of 60 h MCA-FA	$PMFA_{60}1$
PVA/3 wt% of 60 h MCA-FA	$PMFA_{60}3$
PVA/5 wt% of 60 h MCA-FA	$PMFA_{60}5$

PART II

In this part of study the FA was obtained from Raichur thermal power station, karantaka. India. This section illustrates the design of statistical analysis by Taguchi methodology to obtain nanostructured FA. An orthogonal array was formed by considering the various factors and levels that influences experimental parameters during mechano-chemical activation of FA by planetary ball milling. Subsequently, chitosan and poly(vinyl chloride) composite reinforced with fresh FA and MCA-FA were prepared by solution casting. This is followed by a description of the various techniques used to characterize the nanocomposites.

2.3 MATERIALS

FA was collected from Raichur (NTPC) Thermal Power Station, Karnataka, India. Analytical grade surfactants, sodium lauryl sulfate ($\overline{M}_w$:288.38 g mol^{-1}) (SLS), N-cetyl-N, N, N-trimethyl ammonium bromide ($\overline{M}_w$: 364.46 g mol^{-1}) (CTAB), Triton X-100 ($\overline{M}_w$: 646.87 g mol^{-1}) (TX-100) and crosslinking agent, glutaraldehyde (GA) (25% content in water) were procured from Sisco research laboratories, Mumbai, India. Toluene (T), ethanol (E) and ethyl acetate (EA) were obtained from Nice

chemicals private limited, Kochi, Kerala, India. The solvent tetrahydrofuran was obtained from Central drug house Pvt. Ltd, New Delhi, India. All the reagents were of analytical grade (purity > 99%) and used without further purification.

Chitosan (CS) ($\overline{M}_w$: 190,000-310,000 g mol^{-1}) was procured from Sigma Aldrich, St. Louis, USA. Poly(vinyl chloride) (PVC) ($\overline{M}_w$: 48,000 g mol^{-1}) was procured from Rolex chemical industries, Mumbai, India.

2.4 METHODOLOGY

2.4.1 Pre-treatment of FA

The pre-treatment for FA was performed in the same way as discussed in **part-I section 2.2.1.**

2.4.2 Experimental design: selection of factors and their levels

The most important stage in the design of an experiment lies in the selection of control factors. Taguchi created a standard orthogonal array to accommodate the various factors and levels in the design. The experimental design chosen for mechano-chemical activation of FA with four factors and three levels (3^4) is shown in **Table 2.3**.

Table 2.3 Assignment of factors and levels of L$_9$ (3^4) orthogonal array

Levels	Factors			
	A	**B**	**C**	**D**
	Surfactant type	**Surfactant quantity (wt%)**	**Medium**	**Ball to powder ratio**
1	Anionic (SLS)	2	Toluene (T)	10:1
2	Cationic (CTAB)	4	Ethanol (E)	12:1
3	Non-Ionic (TX-100)	6	Ethyl acetate (EA)	8:1

2.4.3 Mechano-chemical activation of FA

Mechano-chemical activation of pre-treated FA was achieved by using a high energy planetary ball mill (PM 100; Retsch, Germany). FA was charged into a 250 mL

tungsten carbide lined vial of the planetary carrier and tungsten carbide balls of 10 mm diameter were used for milling the FA powder. The milling was carried out for 48 h at 250 rpm. The optimum rotational speed of the mill was determined using **equation (2.1)** proposed by Rose and Sullivan [1953]; Watanabe, H. [1999].

$$N_c = \frac{1}{2f}\sqrt{\frac{g}{R\sqrt{1-r}}} \qquad\qquad (2.1)$$

Where, N_c is the critical rotation speed of the ball mill, g is the acceleration due to gravity, R is the inner radius of a vial and   is the volumetric filling ratio of the particles.

For every 2 h of continuous milling, a break time of 60 s was given at an interval of 30 min to avoid heat build-up. This FA is called as MCA-FA.

Fresh FA and MCA-FA had specific gravities of 2.00 and 2.6, respectively determined by the pycnometer method as per ASTM D854-10.

2.4.4 Preparation of CS/fresh FA and CS/MCA-FA composites

CS matrix composites containing 1, 3 and 5 wt% of fresh FA and MCA-FA were prepared by solution casting method. CS solution was prepared with 2% (w/v) CS in 5% glacial acetic acid at room temperature by magnetic stirring. A pre-determined amount of filler was added to the CS solution and the mixture was stirred overnight and ultrasonicated. The solution was then transferred to Teflon coated petri-dishes and dried at ambient temperature. To convert CS acetate into CS, all the dried membranes were immersed in 1M NaOH solution for 24 h. The excess of NaOH and solvents was removed by washing the CS composites with distilled water. For the preparation of cross-linked composite films, GA solution was diluted into 0.1% solution using distilled water and CS composites were dipped in it for 30 min. The cross-linked CS composites thus obtained were washed several times with distilled water and dried at 40 °C for 4 h. The thickness of the films was   0.3 mm. The designations of the samples are given in **Table 2.4.**

Table 2.4 Designations of the CS/fresh FA and CS/MCA-FA composites

Samples	Designation
Neat chitosan	CFA0
chitosan/1 wt% of fresh FA	CFA1
chitosan/3 wt% of fresh FA	CFA3
chitosan/5 wt% of fresh FA	CFA5
chitosan/1 wt% of MCA-FA	CMFA1
chitosan/3 wt% of MCA-FA	CMFA3
chitosan/5 wt% of MCA-FA	CMFA5

2.4.5 Preparation of PVC/fresh FA and PVC/MCA-FA composites

Two sets of PVC composites were prepared by solution casting method with 1, 3 and 5 wt% of fresh FA and MCA-FA. PVC solution was prepared by dissolving 14 g of PVC in 100 mL of tetrahydrofuran at room temperature by magnetic stirring in a closed beaker. A predetermined quantity of filler was added to the PVC solution with vigorous agitation overnight. The solution was ultrasonicated for 30 min and then poured into glass petri-dishes. These solutions were dried at ambient temperature and covered with an aluminum foil to protect it from dirt and other foreign materials. They were further dried in a hot air oven for 4 h at 50 °C to eliminate the residual solvent. The films were peeled out from the petri-dishes, which had a thickness of ~0.3 mm. **Table 2.5** shows the designations of the samples.

Table 2.5 Designations of the PVC/fresh FA and PVC/MCA-FA composites

Samples	Designation
Neat PVC	VFA0
PVC/1 wt% of fresh FA	VFA1
PVC/3 wt% of fresh FA	VFA3
PVC/5 wt% of fresh FA	VFA5
PVC/1 wt% of MCA-FA	VMFA1
PVC/3 wt% of MCA-FA	VMFA3
PVC/5 wt% of MCA-FA	VMFA5

2.5 CHARACTERIZATION OF FRESH FA, MCA-FA AND THEIR COMPOSITE WITH EOC, PVA, CS AND PVC MATRICES

Morphology Studies: The texture and morphology of fresh FA, MCA-FA, and their composites with EOC, PVA, CS and PVC matrices were determined by a scanning electron microscope (SEM; JEOL-JSM-6380LA SEM, Peabody, Massachusetts, USA). Prior to the studies of cryo-fractured EOC composites and fractography of tensile fractured PVA, CS and PVC composites were sputtered with gold using a sputtering unit (JEOL JFC 1600, auto fine coater, USA) to make their surfaces conductive. The images were recorded at suitable accelerating voltages for the best possible resolution using secondary electron imaging.

The elemental composition of fresh FA and MCA-FA, and the particle distribution and dispersion of filler in the composites were determined by silicon elemental mapping with an energy dispersive x-ray spectroscopy (EDS) (Link ISIS-300 Micro-analytical System, Oxford Instruments, UK). Each EDS map of a specified area was divided into nine equal regions in the sample. The number of particles in each area was analyzed using Image-J software, and the degree of inhomogeneity of the dispersion was quantified as the standard deviation (σ). The standard deviation among the number of particles per unit area was estimated by the following equation [Friel 2000]:

$$= \sqrt{\frac{1}{n}\sum_i \left(N_{Ai} - \overline{N_A}\right)^2} \tag{2.2}$$

Where,

N_{Ai}: Observed number of inclusion per unit area in the ith location

$\overline{N_A}$: Number of particles in unit area

 : Standard deviation, a degree of inhomogeneity of the dispersion.

The maximum homogeneity is characterized by the minimum standard deviation and the degree of homogeneity increased with a decrease in the standard deviation.

A transmission electron microscopy (TEM; JEOL-JEM 2100 TEM, Japan) was used to study the particle morphology as well as surface texture of the MCA-FA. The MCA-FA particles were dispersed in ethanol under sonication and a drop of this

dispersion was transferred onto a 200-mesh carbon-coated copper (Cu) grid. The TEM images were obtained at an accelerating voltage of 120 kV, and the selected area electron diffraction (SAED) patterns were also obtained to study the crystalline nature of MCA-FA.

FESEM (LEO SUPRA55, Carl Zeiss, Germany) was used to study the texture and morphology of fresh and MCA-FA. The samples for FESEM were prepared by dip coating the dispersions of the samples in ethyl acetate on a silicon wafer. The images were taken at suitable accelerating voltages for the best possible resolution using back scattered electron detector.

Wettability Measurements: Even though MCA-FA consists of irregular and rough surfaced nano-particles, the surface energy mismatch between MCA-FA and polymer (EOC/PVA/CS/PVC) matrices should not be high, so that a strong interface can form between them. To demonstrate the change in the nature of the surface of FA upon its mechano-chemical activation, the fresh FA and MCA-FA for 30 and 60 h were mixed with demineralized water in different vials. The beakers were ultrasonicated and then digital photographs were snapped. In addition, a dynamic contact angle analyzer (FTÅ 200, First Ten Angstroms, Portsmouth, Virginia, USA) was used to study the surface wetability of fresh FA and MCA-FA pellets obtained by using a hydraulic press. Ten micro-liters of the test liquid (double-distilled water and polymer solutions) were dispensed using a micropipette onto the surfaces of the fresh FA and MCA-FA pellets. The images of the liquid spreading were recorded at specific intervals of time. The captured images were analyzed by FTA software to determine the static contact angles of the droplets on the pellets.

Particle Size Analysis (PSA): Dynamic laser scattering (DLS) (Scatteroscope I, Qudix Inc, South Korea) was used to analyze the hydrodynamic sizes and size distributions of fresh FA and MCA-FA particles in aqueous or glycerol media.

Specific Surface Area (SSA): The specific surface area of the MCA-FA was measured by a computerized surface area analyzer (Smart Sorb 92/93, Smart Instruments, Dombivli, Maharashtra, India) as per ASTM D3037 standard. It was calculated at an accuracy of ±5% for 1 g of sample by the Brunauer-Emmett-Teller (BET) method. Sample surface was first regenerated to remove the adsorbed gases

and moisture by degassing in vacuum at 350 °C. Specific surface area was calculated by measuring the volume of N_2 adsorbed using a modified single point BET equation.

X-ray Fluorescence (XRF) spectroscopy: The elemental compositions of fresh FA, sieved FA and magnetic separated FA were determined by an x-ray fluorescence (XRF) spectrometer (Axios^{mAX} PANalytical, Netherlands) using glass discs prepared by fusing the FA sample with lithium tetraborate.

X-ray photoelectron (XPS) spectroscopy: XPS data of fresh FA and MCA-FA were obtained using a Thermo Fisher K-alpha x-ray photoelectron spectrometer (Thermo Fisher Scientific, USA) using Al K radiation (12 kV, 6 mA). The powder samples were pelletized and mounted with a double-sided adhesive tape onto the probe tip. The working pressure in the spectrometer was 10^{-8} to 10^{-9} Pa and the electron take-off angle was 90°. The area under Si 2p, O 1s, C 1s and Al 2p peaks were divided by the photo-ionization cross-sectional area to calculate the concentration of each element present in the sample.

Fourier Transform Infrared (FTIR) Spectroscopy: A Fourier transform infrared spectrometer (FTIR-4200, Jasco, Japan) was employed for examining the chemical functional groups of surfactant, fresh FA and MCA-FA in transmission mode by a KBr pellet method and the spectrum was recorded with the resolution of 0.5 cm^{-1} in the wave number range of 4000-400 cm^{-1} at an average of 32 scans.

The vibrational spectra of EOC, PVA, CS and PVC composite films incorporated with fresh FA and MCA-FA were analyzed to examine the polymer-filler interaction in the ATR mode between the wave number range of 4000-650 cm^{-1} at a spectral resolution of 0.5 cm^{-1} with an average of 32 scans.

X-ray Diffraction (XRD): X-ray diffraction measurements were carried out to find the crystallite size and lattice strain of the quartz phase of fresh FA and MCA-FA, with the help of a goniometer (DX-GE-2P, JEOL, Japan) using CuK radiation (= 1.5418 Å) at an accelerating voltage of 30 kV and a beam current of 20 mA. The samples were scanned at a speed of 2° min^{-1} in the 2 range of 10-90°.

The PVA and PVC composites reinforced with fresh FA and MCA-FA were scanned at a speed of 2° min^{-1} in the 2 range of 10-40° at 25 °C.

The average crystallite size was calculated from the full width at half maximum (FWHM) of the XRD peak using the Scherrer's formula:

$$t = \frac{k}{cos}$$

(2.3)

Where, t is the particle diameter, is the wavelength of the x-rays, is the FWHM of the diffraction peak, is the diffraction angle and k is the Scherrer's constant of the order of unity for usual crystals [Cullity 2001].

The relationship between the half width of the broadened diffraction peaks, B_d and the distortion of lattice, (d/d) was described by Yang et al. [2000]. The lattice distortion (d/d) can be obtained from the following equation:

$$\frac{\Delta d}{d} = \frac{B_d}{(4 \tan_{,,})}$$

(2.4)

Where, B_d is half width of the broadened diffraction peak; is half of the diffraction angle.

Mechanical Properties of EOC, PVA, CS and PVC Composites with fresh FA and MCA-FA: A universal testing machine (H25KS, Hounsfield, UK) was used to determine tensile strength, elongation at break and stresses at 100% and 300% strains (denoted at M100 and M300). The testing was performed at 25± 2 °C as per ASTM D638-10 at a cross head speed of 50 mm.min^{-1}. Dumb-bell specimens of the composites were punched out by using an ASTM D412-06a die. The reported values of mechanical properties results are the averages of five values. Maximum deviations in the results of tensile strength, M100, M300 and elongation at break were ±5%.

The relationship between strain at break and filler volume fraction of EOC, PVA, CS and PVC composites was described by Nielsen's equation [Nielsen 1966].

$$\vee_c = \vee_m (1 - V_f^{1/3})\qquad(2.5)$$

Where, ϵ_c is strain at break of composite, ϵ_m is strain at break of polymer matrix, and V_f is volume fraction of filler.

To understand the mechanical results further, the "interfacial interaction" between the filler and the matrices (CS and PVC) was evaluated by the following equation.

$$B_{\tau y} = \frac{1}{w_f}\log\frac{\tau_y}{\tau_{ym}}\left[\frac{1 + 2.5w_f}{1 - w_f}\right]\qquad(2.6)$$

Where

$B_{\tau y}$ - interfacial interaction parameter

ϕ_f - volume fraction of the filler particles

τ_y and τ_{ym} - yield stresses of the composite and the polymer matrix, respectively

Film solubility and swelling behavior of CS/fresh FA and CS/MCA-FA composites: The film solubility and swelling behavior were used to determine the water resistance of films. Film pieces (2×2 cm) were dried at 80 °C for 24 h in a hot air oven to get the initial dry weight (W_1). Then the films were dipped in beakers containing 30 mL distilled water and covered with aluminum foil at room temperature for 24 h. The left over water from the beakers was discarded and the residual film pieces (W_2) were dried superficially with filter paper. Later the residual film pieces were dried at 80 °C for 24 h in a hot air oven to determine the final dry weight (W_3). Three readings were taken for each composite sample. Film solubility and degree of swelling were calculated using the following equations, respectively [Tanabe et al. 2002, Amin and Panhuis 2012]:

$$\text{Film solubility} = \frac{(W_1 - W_3)}{W_1}\times 100\qquad(2.7)$$

$$\text{Degree of swelling} = \frac{(W_2 - W_1)}{W_1}\qquad(2.8)$$

Flammability of EOC and PVC composites with fresh FA and MCA-FA: The limiting oxygen index (LOI) method, which describes the tendency of a material to sustain a flame, is widely used as a tool to investigate the flammability of polymers. The LOI of the control and composite samples was determined by using a LOI analyzer (Dynisco, Franklin, MA, USA) according to ASTM D2863. A numerical index, the LOI, is defined as the minimum concentration of oxygen in an oxygen-nitrogen mixture, required to just support downward burning of a vertically mounted test specimen. Hence, higher LOI values represent better flame retardance. The LOI was calculated by using the following formula:

$$\text{LOI}(\%) = \frac{[O_2]}{[O_2] + [N_2]} \times 100 \qquad (2.9)$$

Where, $[O_2]$ is the volumetric flow rate of oxygen ($cm^3 sec^{-1}$) and $[N_2]$ is that of nitrogen.

Differential Scanning Calorimetry of EOC, PVA, CS and PVC Composites with fresh FA and MCA-FA: For DSC measurements, about 5 mg of the samples were heated in hermetically sealed aluminum pans kept in the furnace of a DSC analyzer (822e -Mettler Toledo, USA) from 0-100 °C for EOC composites, (Netzsch DSC 200 F3 Maia®, Germany) in the range of 0-250 °C for PVA composites and (Q series-TQ10, TA Instruments, USA) for CS and PVC composites. The heating rate was 10 °C min^{-1} under a dynamic N_2 atmosphere flowing at a rate of 50 mL min^{-1}.

The % crystallinity (X_c) of the EOC and PVA composites was calculated according to equation given below:

$$X_c = \frac{\Delta H_f}{W_i \times \Delta H_{f\,100\,\%}} \times 100 \qquad (2.10)$$

Where, H_f is the enthalpy of fusion of the composite, W_i is the weight fraction of the polymer in the composite and $H_{f100\,\%}$ is the enthalpy of fusion of the perfect crystal of polyethylene and PVA having a value of 277.1 Jg^{-1} [Shi et al. 2008] and

36

138.60 Jg^{-1} [Guirguis and Moselhey 2011; Saroj and Singh 2012; and Guo et al. 2010], respectively.

Thermogravimetric Analysis (TGA) of CS and PVC with fresh FA and MCA-FA composites: Thermogravimetric (TGA) measurements were performed with ~6 mg samples under a nitrogen atmosphere flowing at a rate of 25 mL min^{-1} (TGA 4000, Perkin Elmer, USA). A constant heating rate of 10 °C min^{-1} was maintained and the weight loss vs. temperature curves was recorded over a temperature range of 30-800 °C.

PART - I

CHAPTER 3

CHAPTER 3

MECHANO-CHEMICAL ACTIVATION OF FLY ASH BY HIGH ENERGY BALL MILLING
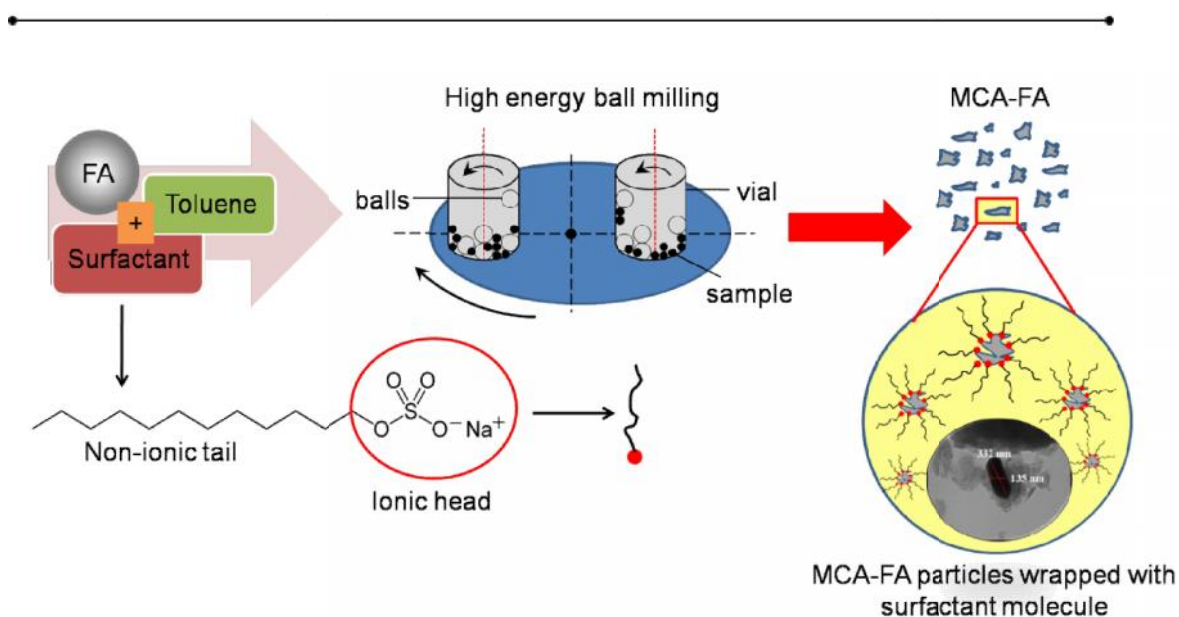
Scheme 3.1 Preparation of the mechano-chemically activated FA

This chapter discusses the mechano-chemical activation of FA by high energy ball milling in presence of a surfactant and an inert liquid medium. The morphological, compositional and spectral properties of the MCA-FA were studied by scanning electron microscopy (SEM), transmission electron microscopy (TEM), energy dispersive x-ray spectroscopy (EDS) and Fourier transform infrared (FTIR) spectroscopy. The reduction in crystallite size and average particle size with increased specific surface area during mechano-chemical activation of FA was determined by x-ray diffraction (XRD), dynamic laser scattering (DLS) and BET surface area analyzer. The effect of surface modification of the MCA-FA was analyzed by wettability studies and dynamic contact angle measurements.

3.1 RESULTS AND DISCUSSION

3.1.1 Characterization of fresh FA and mechano-chemically activated FA

3.1.1.1 Morphological studies
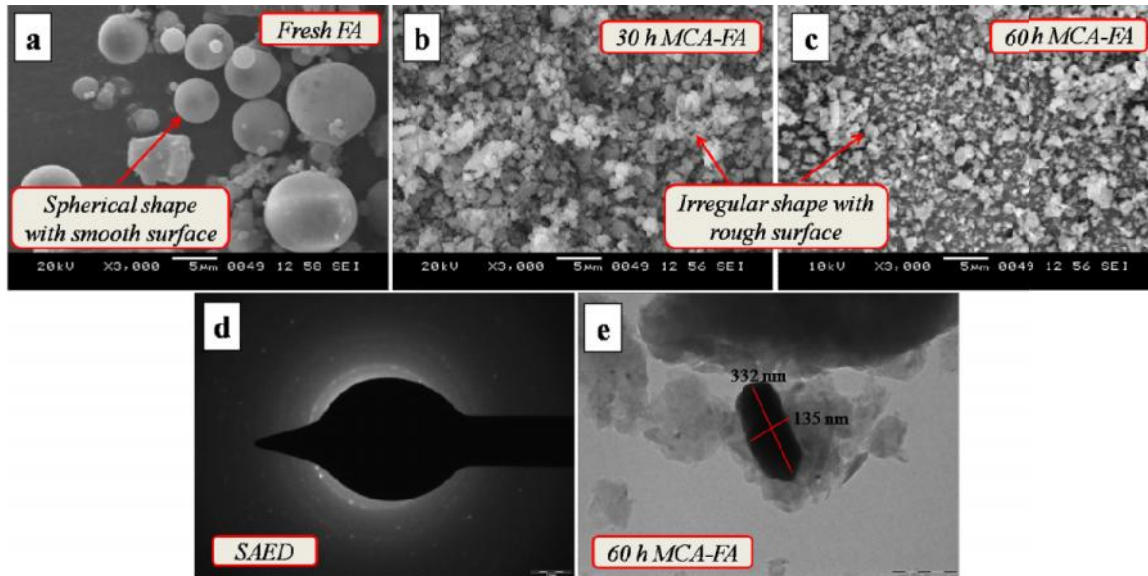
Fig. 3.1 SEM images of (a) fresh FA (b) 30 h MCA-FA (c) 60 h MCA-FA, (d) SAED pattern and (e) TEM micrograph of 60 h MCA-FA

The surface morphology and texture of the fresh FA as well as MCA-FA was determined by SEM and TEM images from **Fig. 3.1**. **Fig. 3.1a** shows the SEM image of fresh FA, which has a smooth surface and majority of the particles are spherical in shape. Along with the solid spheres, smaller particles are adhering on the surfaces of the larger ones. The morphology of FA particles depends on operating temperature of the furnace and cooling rate of the flue gases. If sufficient time is given for cooling of FA particles, the majority of the particles will assume a spherical shape to reduce their surface tensions. Due to rapid cooling, inter-particle fusing occurs and FA particles agglomerate, resulting in an irregular shape [Dhadse et al. 2008 and Swami et al. 2009]. **Fig. 3.1b and c** are the SEM images of the FA after 30 h and 60 h of mechano-chemical activation. The MCA-FA particles are of irregular shapes with rough surfaces and their sizes are few

hundred nanometers. The 60 h MCA-FA sample has more structural breaks as shown in **Fig. 3.1c**.

Fig. 3.1d shows the SAED pattern of 60 h MCA-FA. Which indicates the polycrystalline nature of the MCA-FA obtained after 60 h of milling; as the crystal size is small, a large number of crystals are included in the diffraction rings. The individual crystals are randomly distributed and oriented differently, but, then fall on rings of constant radius [Ashby et al. 2009]. **Fig. 3.1e** shows the TEM image of MCA-FA particle to illustrate the morphological changes by mechano-chemical activation. It is observed that the particles attained irregular shape with rough surface. The size of a single particle is typically in nanometer range with narrow crystalline needle-like shape. The surfactant layer on the surfaces of nano-FA particles is expected to play a significant role in reducing the agglomeration of particles, which, in turn, is supposed to improve the mechanical strength of the composites based on nano-FA.

3.1.1.2 Wettability study
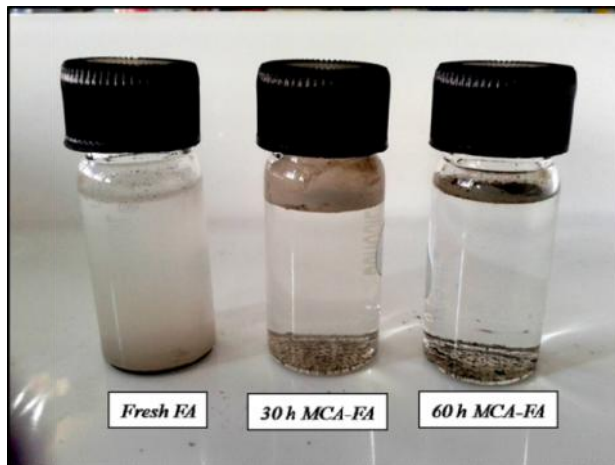
Fig. 3.2 Dispersion behaviors of fresh FA, 30 h and 60 h MCA-FA in demineralized water

The silanol groups on the surface of fresh FA particles make them hydrophilic. To demonstrate the change in the nature of FA surface upon its mechano-chemical activation, the fresh FA and MCA-FA were mixed with demineralized water in three

different vials of 10-mL capacity. The vials were ultrasonicated for 15 min and then digital photographs were snapped (**Fig. 3.2**).

It can be seen from **Fig. 3.2** that the MCA-FA particles float on water, while that of the fresh FA are found dispersed in water. The surface chemistry of fresh FA allows its particles to be wet by water through formation of hydrogen bonds with water. The wettability of MCA-FA by water is less as the surfactant molecules are adsorbed on to the surfaces of FA particles, in such a way that the polar heads of the surfactant molecules orient towards the surfaces of the FA particles and the non-polar tails orient themselves away from the FA surface. The structure of the MCA-FA can hence look like an inverse micelle in which the FA particle surrounded by the ionic heads form the core and the non-polar tails for the outer core. The proposed model is shown in **Scheme 3.1**. This results in a partially hydrophobic surface of MCA-FA. From **Fig. 3.2**, it can be seen that some fraction of MCA-FA sinks in water due to the agglomeration taking place during the ball milling process, which may be due to non uniform adsorption of surfactant molecules over individual FA particles. Behavior of a surfactant at the interface is determined by a number of forces, including electrostatic attraction, covalent bonding, hydrogen bonding, and hydrophobic bonding [Paria and Khilar 2004].
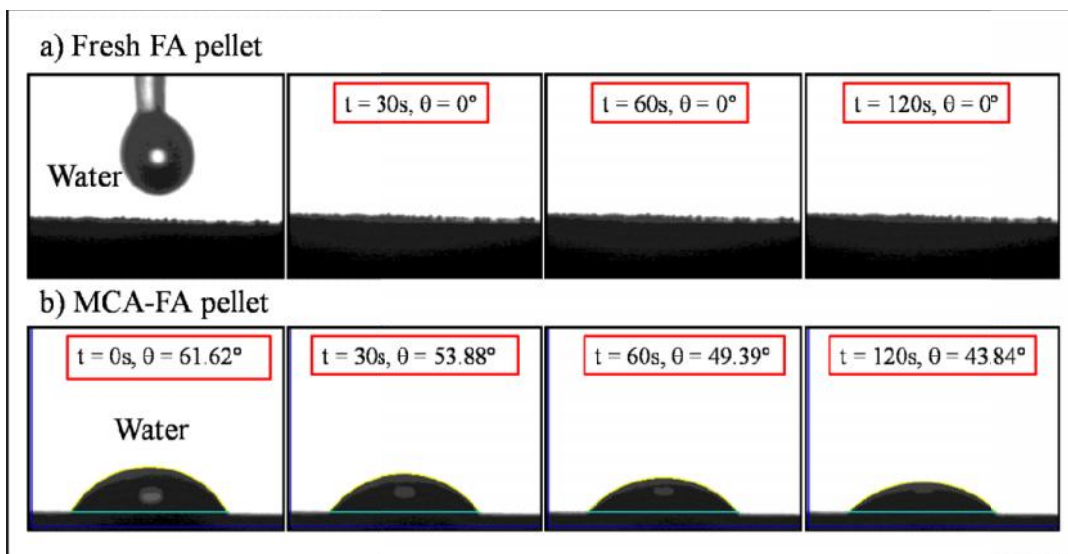
Fig. 3.3 Static contact angle measurements on (a) fresh FA and (b) MCA-FA pellets with water

42

This interpretation is substantiated by the contact angle measurements (**Fig. 3.3a**), where the surface tension of the fresh FA surface is greater than that of water due to which the water droplet spread rapidly and got absorbed by the pellet. In contrast, as the critical surface tension of the 60 h MCA-FA is less than that of water, the water droplet is repelled (**Fig. 3.3b**). The contact area between the water droplet and surface is minimized in MCA-FA, which is attributed to the presence of the surfactant layer on the MCA-FA particles [He et al. 2009]. Thus the surfactant coated MCA-FA particles reduces water pickup and aids in better dispersion in the polymer matrices.

3.1.1.3 Particle size analysis

The effects of mechano-chemical activation on the particle size of the FA samples are represented graphically in **Fig. 3.4**. The figure represents the variation in particle diameter (in meter) with respect to intensity distribution. The broad bimodal distribution of sieved FA particles changed to monomodal (**Fig. 3.4**) for milled FA because of the continuous collision between grinding media and FA particles. This is more vigorous for higher milling hours, which lead to tremendous stress energy being imparted on the particles, resulting in massive strain in the particles. This trend provides evidence supporting that more plastic deformation and disordering of the FA particles occur under intensive grinding, resulting in nanoscale dimensions [Arbain et al. 2011 and Zheng et al. 2012]. Further, the use of surfactant and toluene as process-enhancing agents in the milling clearly offers the potential for reduction in particles size.

From the distribution curves obtained, values of D_{10}, D_{50}, and D_{90}, representing the sizes, from which 10%, 50%, and 90% (by volume% and by number%) of the particles in the sample were smaller or greater than, could be determined. D_{50} represents the median of the respective distribution. The particle sizes at D_{10}, D_{50}, and D_{90} of FAs are shown in **Table 3.1.**
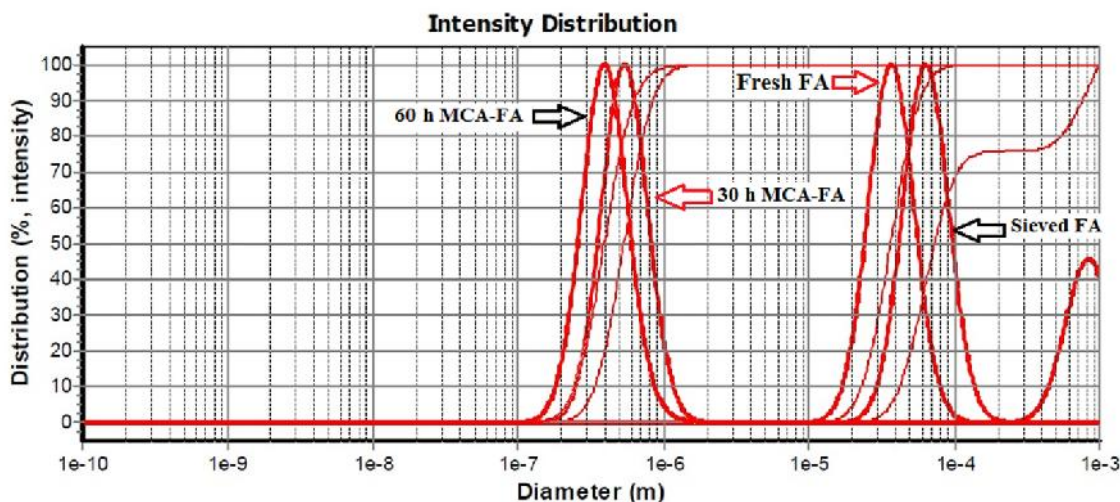
Fig. 3.4 Particle size distribution of fresh FA, sieved FA, 30 h and 60 h MCA-FA

The average particle size of fresh FA was 36.5 μm at D_{50} (median size), which implies that 50 % volume of the particles are less than 36.5 μm and remaining 50 % are greater than 36.5 μm. The particle size of sieved FA, which passed through mesh number 170 and retained on mesh number 200 was 79.4 μm. Mechano-chemical activation for 30 and 60 h intensified the reduction in particles size of sieved FA from 79.4 μm (D_{50}) to 538 nm and 392 nm, respectively (**Table 3.1**). It is anticipated that the actual values of the particle size of the MCA-FA could be slightly less than that revealed by the DLS technique. This is due to the simple fact that during the mechano-chemical activation the surfactant molecules form an outer layer on the surfaces of the FA particles (**Scheme 3.1**). This in turn, will lead to a slightly higher hydrodynamic volume than it should have been. Also, dispersing MCA-FA was difficult as it tends to repel water as evidenced by the contact angle measurement. Hence, there is a possibility of some error in the measured particle size values. Toluene along with SLS might be sorbed onto the surface of FA and its micro-cracks, and also could reduce the hardness of FA because of its low surface tension (surface tension of toluene in air at 20 °C is 28.40 mN.m^{-1} [www.surface-tension.de]. The surface tension of toluene may further get reduced by the surfactant. Hence, a different milling medium and/or surfactant could yield a different particle size and size distribution for MCA-FA.

44

Table 3.1 Particle sizes at (D_{10}), (D_{50}) and (D_{90}) of FA and MCA-FA

Samples	D_{10}*	D_{50}*	D_{90}*
Fresh FA	23.2 μm	36.5 μm	58.4 μm
Sieved FA (-170# +200#)	43.2 μm	79.4 μm	999 μm
MCA-FA for 30 h	336 nm	538 nm	846 nm
MCA-FA for 60 h	245 nm	392 nm	637 nm

3.1.1.4 Specific surface area

The specific surface area had increased from 12.35 $m^2\,g^{-1}$ for 30 h MCA-FA to 18.87 $m^2\,g^{-1}$ for 60 h MCA-FA (specific surface area of fresh and sieved FA could not be determined due to experimental difficulties). The presence of an organic coating on the surface of MCA-FA facilitated its dispersion in the polymer matrix; the change of the particle size and surface area enhanced the mechanical property of the MCA-FA composites as discussed in the later chapters of mechanical properties section.

3.1.1.5 EDS analysis

Chemical compositions of fresh FA and 60 h MCA-FA were determined by EDS and their spectra are shown in **Fig. 3.5a** and **b**, respectively. Class-F and class-C are the two major classes of FA. Class-F FA contains 70 % of oxides of silicon, aluminium and iron of the total composition and a higher Fe_2O_3 content than CaO. On the other hand, class-C FA has higher lime content than Fe_2O_3 [ASTM C618-03]. **Table 3.2** shows the elemental compositions obtained from an average of measurements done at 10 different locations on the surface of the fresh FA and 60 h MCA-FA samples. It is obvious that the % of calcium oxide, which is 0.51 %, is less than that of iron whose value is 4.7 % implying that the FA belongs to class-F [Paul et al. 2007]. The elemental compositions of fresh FA and 60 h MCA-FA have a negligible difference.
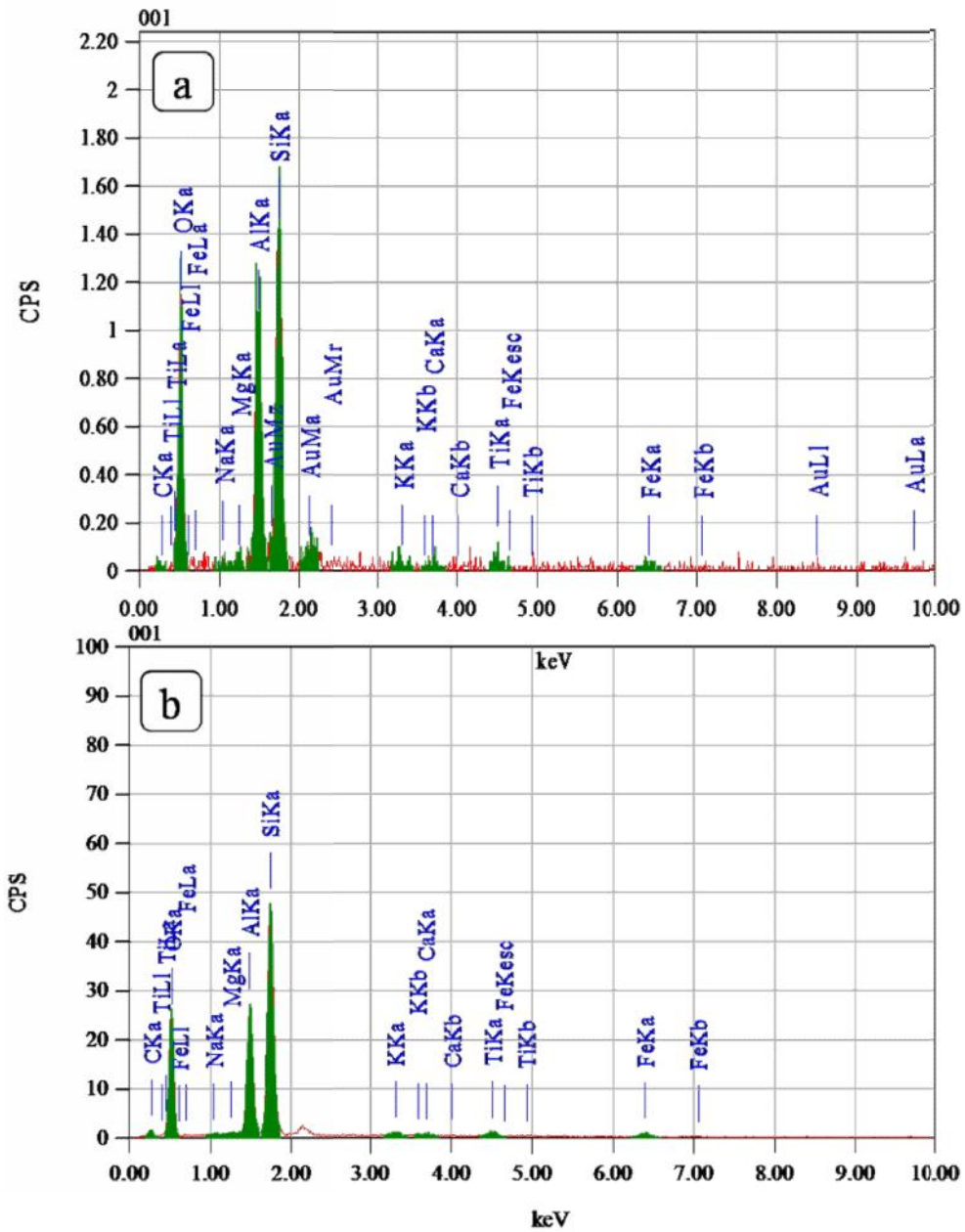
Fig. 3.5 EDS of (a) fresh FA and (b) 60 h MCA-FA

Table 3.2 Elemental composition of fresh FA and MCA-FA

Elemental composition of fresh FA		Elemental composition of 60 h MCA-FA	
Component	Content (wt%)	Component	Content (wt%)
Silicon	31.01 ± 0.2	Silicon	31.14 ± 0.2
Aluminum	16.53 ± 0.2	Aluminum	15.24 ± 0.2
Iron	2.2 ± 0.1	Iron	2.15 ± 0.1
Titanium	1.04 ± 0.01	Titanium	1.24 ± 0.01
Potassium	0.94 ± 0.1	Potassium	0.68 ± 0.1
Sodium	0.38 ± 0.02	Sodium	0.20 ± 0.02
Calcium	0.23 ± 0.02	Calcium	0.44 ± 0.02
Magnesium	0.32 ± 0.01	Magnesium	0.21 ± 0.01
Oxygen	47.34 ± 0.2	Oxygen	47.41 ± 0.2

3.1.1.6 XRD results

Fig. 3.6 shows the x-ray diffraction patterns of fresh FA, 30 h and 60 h MCA-FA. The analysis was done using X'pert high score software, which revealed a lower degree of crystallinity for fresh FA and showed a few numbers of crystalline peaks in the diffraction pattern. In all the diffraction patterns, an amorphous hump was observed between 2 values of approximately 14° to 35°, which is due to the presence of amorphous glassy materials. According to the x-ray diffraction patterns the FA consists of a major proportions of quartz (SiO_2), mullite ($3Al_2O_3. 2SiO_2$), calcium oxide (CaO) and iron oxide (Fe_2O_3).

The average crystallite sizes of the quartz phase present in the fresh FA and MCA-FA were determined by the full width at half maximum (FWHM) of the x-ray diffraction peak using the Scherrer's formula given in **chapter 2, equation 2.3**.

There was reduction in intensity of the peak with an increase in the milling time. The crystallite size of quartz phase present in fresh FA was 56 nm, which got reduced to 33.6 nm and 28 nm after 30 h and 60 h of milling, respectively (**Fig. 3.7**). There was

broadening of this peak and a shift in the peak angles, due to the existence of residual stress in the MCA-FA, which resulted in lattice distortions of the quartz crystallites.

The lattice distortion was calculated from the **equation 2.4** given in **chapter 2**. The relative lattice strain of quartz phase increased from 0.26 % in fresh FA to 0.44 % and 0.53 % in 30 h and 60 h milled FA, respectively. This increase in strain must be due to the intense mechanical deformation combined with the sorption of the milling medium on the surface pores on the FA particles during the high energy milling [Baláž 2008].
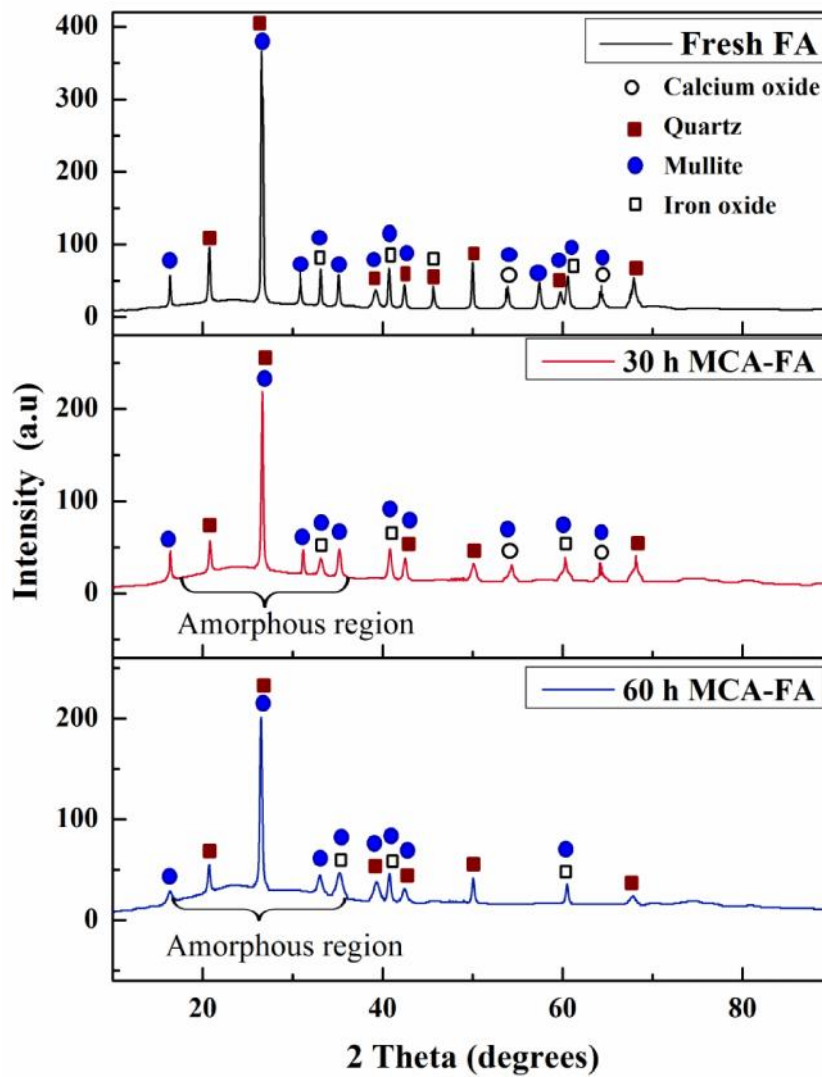
Fig. 3.6 XRD patterns of fresh and MCA-FA prepared by ball milling for 30 h and 60 h
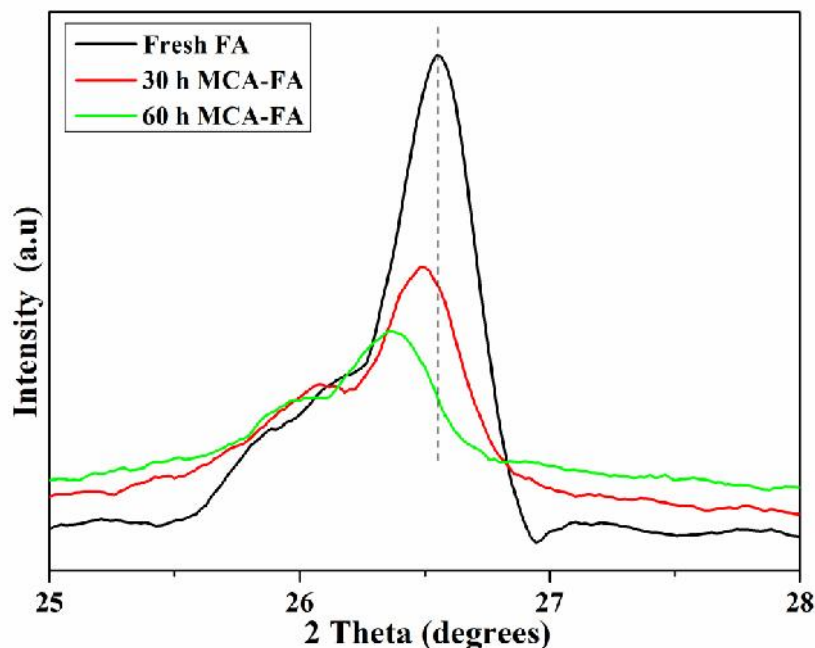
Fig. 3.7 XRD patterns showing variation in the quartz peaks (2 = 26.52°) of fresh FA and MCA-FA for 30 h and 60 h

3.1.1.7 FTIR Spectroscopy

The FTIR spectra of the SLS, fresh FA, 30 h and 60 h MCA-FA are shown in **Fig. 3.8**. The FTIR spectrum of SLS shows the O-H stretching band at 3475 cm^{-1}. The 2920 and 2855 cm^{-1} bands correspond to C-H stretching. The major sulfate asymmetric and symmetric characteristic stretching vibration bands are observed at 1220 and 1080, 1140-900 cm^{-1}, respectively [Viana et al. 2012].

The FTIR spectrum of FA showed characteristic stretching vibration bands at 1092, 797 and 570 cm^{-1}. The strong broad band at 1092 cm^{-1} can be related to Si-O-Si asymmetric stretching vibration, while 797 cm^{-1} band can be related to Si-O-Si symmetric stretching vibration [Smith 1998] as well as AlO$_4$ vibrations. The Si-O-Si bending is observed at 465 cm^{-1}.

The peak at 1092 cm^{-1} has broadened and its intensity has increased in 30 h and 60 h MCA-FA as compared to fresh FA, which is due to the interaction of sulfate vibration band of SLS and Si-O-Si stretching of FA. This attributes to the presence of

sulfate and silanol (Si-OH) functional groups in the FA. The peak at 3440 cm^{-1}, which was insignificant in the fresh FA, has become conspicuous in case of 30 h and 60 h MCA-FA; this is because of the interaction of O-H stretching band of FA with that of SLS.
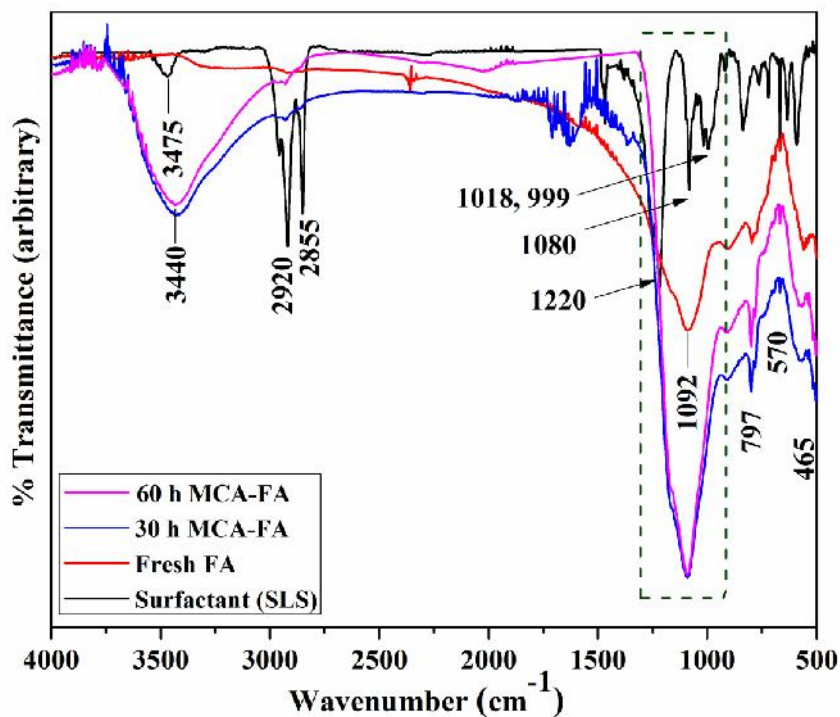
Fig. 3.8 FTIR spectra of SLS, Fresh FA 30 h and 60 h MCA-FA

3.2 CONCLUSIONS

In summary, EDX analysis revealed that the FA used for this study belongs to class F. The mechano-chemical activation of FA considerably reduced the size of a single particle to a few hundred nanometers with a rough surface and an irregular shape. The average particle size of fresh FA was 36.5 μm, which got reduced to 538 nm and 392 nm after 30 h and 60 h of mechano-chemical activation, respectively. The specific surface area value increased from 12.35 m^2 g^{-1} for 30 h MCA-FA to 18.87 m^2 g^{-1} for 60 h MCA-FA. The crystallite size of quartz phase present in the fresh FA was 56 nm, which got reduced to 33.6 nm and 28 nm after 30 h and 60 h of milling, respectively. The relative lattice strain of the quartz phase was also increased from 0.23 % to 0.33 % after 60 h of milling.

50

CHAPTER 4

CHAPTER 4

PREPARATION AND CHARACTERIZATION OF ETHYLENE-OCTENE RANDOM COPOLYMER BASED COMPOSITES REINFORCED WITH NANOSTRUCTURED FLY ASH

This chapter discusses the preparation of ethylene-octene random copolymer (EOC) composites with fresh FA and MCA-FA as filler by solution casting. The distribution and dispersion of the filler particles were determined by measuring number density distribution or spare sampling or grid counting in the composites. The surfactant molecules wrapped on the surface of the MCA-FA accounted for a good interaction with polymer matrix. The composites were cryo-fractured to evaluate the texture and morphology. Morphological studies revealed that interfacial adhesion between the polymer and MCA-FA was good and this accounted for the improvement in mechanical properties of the composites. Flammability of the composites was determined by limiting oxygen index (LOI) method, which resulted in improved flame retardance.

4.1 RESULTS AND DISCUSSION

4.1.1 Characterization of EOC/fresh FA and EOC/MCA-FA Composites

4.1.1.1 Wettability study

Fig. 4.1a and **b** show the contact angle measurements of EOC solution on fresh FA and MCA-FA, respectively. Initially a contact angle of 86.62° was observed for the EOC droplet on the surface of fresh FA pellet, which gradually decreased to 9.25° after 20 min. But, EOC droplet made a contact angle of 65.29° on the MCA-FA pellet surface initially, which then decreased to 11.69° after 10 min. This implies that MCA-FA can be easily wet by the EOC solution, which can lead to a good interaction between the MCA-FA particles and the polymer matrix.
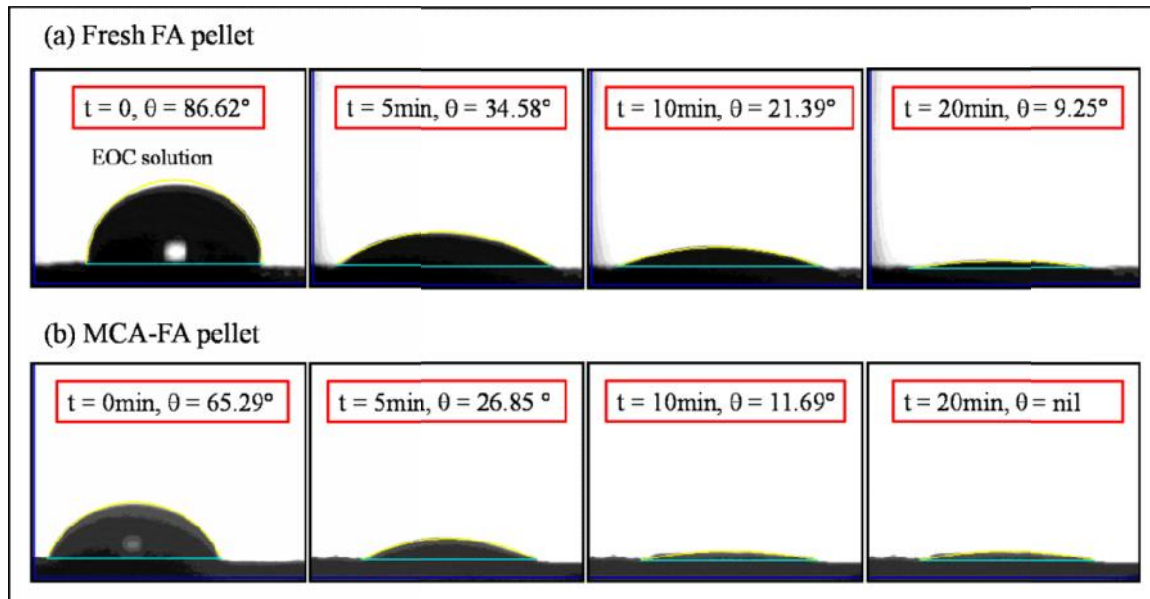
Fig. 4.1 Static contact angle measurements on (a) fresh FA and (b) MCA-FA pellets with EOC solution

4.1.1.2 Morphological studies
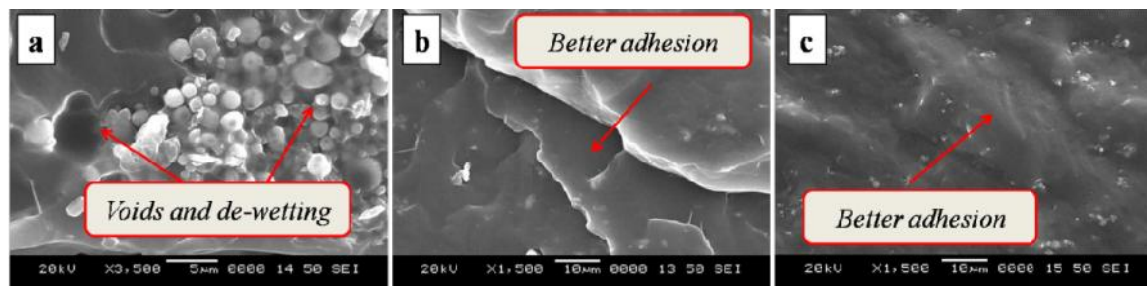
Fig. 4.2 Scanning electron micrographs of EOC composite with 5 wt% (a) fresh FA, (b) 30 h MCA-FA and (c) 60 h MCA-FA

Fig. 4.2a reveals the morphology of the cryo-fractured surface of EOC reinforced with 5 wt% of fresh FA. It can be observed that due to smooth surface and spherical shape of fresh FA, the particles are poorly wet by the matrix resulting in segregation. The formation of voids in the bulk of this sample leads to stress concentration and reduced mechanical strength [Nath et al. 2009]. On the other hand, the morphologies of the EOC composites reinforced with 5 wt% of 30 h and 60 h MCA-FA (**Fig. 4.2b** and **c**)

52

demonstrate an efficient wetting of the particles of MCA-FA by the matrix along with minimal amounts of interstitial voids or porosities. The uniform distribution of MCA-FA particles in the matrix is due to the surfactant wrapping on their surfaces during mechano-chemical activation, which alters their surface energies and reduces the particle agglomerations resulting in an efficient polymer-filler interaction [Nath et al. 2010a].

4.1.1.3 Elemental mapping of filler distribution and dispersion
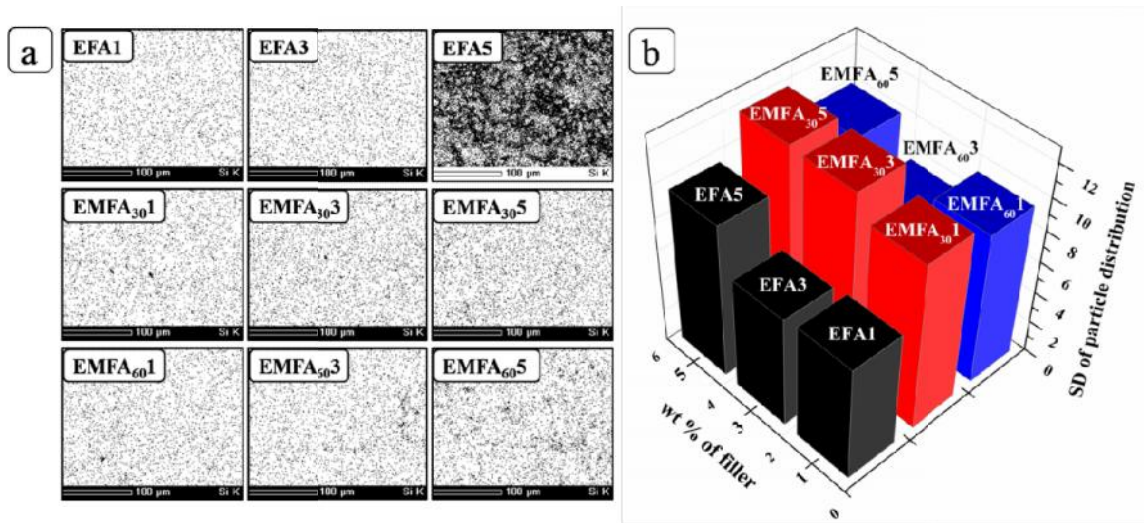
Fig. 4.3 (a) Silicon elemental mapping showing filler distribution in composites; and (b) standard deviations of filler distribution calculated from elemental maps by image-J toola

This technique is based on measurements of number density distribution or sparse sampling or grid quadrant counting to analyze the degree of dispersion of particles in composite [Friel 2000]. **Fig. 4.3a** shows the silicon elemental maps of filler distribution in the EOC/fresh FA and EOC/MCA-FA composites. Each EDX map was divided into a sample area of 400 μm $\times$ 400 μm and the degree of inhomogeneity of the dispersion was quantified as the standard deviation,   given in **chapter 2, equation 2.2**.

Fig. 4.3b shows the bar chart of standard deviation ( ) of filler distribution in these composites. From **Fig. 4.3a** and **b**, it can be observed that as the filler content increases in EOC/fresh FA composite the -value also increases indicating a non-uniform distribution of the filler particles in the matrix due to extensive particle-particle interaction. The micrographs of the EOC/MCA-FA composites reveal a uniform

distribution of filler particles, even at a higher loading (**Fig. 4.3a**). The maximum homogeneity in EOC composites is observed for 30 h and 60 h MCA-FA at 1 and 3 wt% of filler content, respectively, which is evident from their minimum -values (**Fig. 4.3b**).

4.1.1.4 FTIR spectroscopy
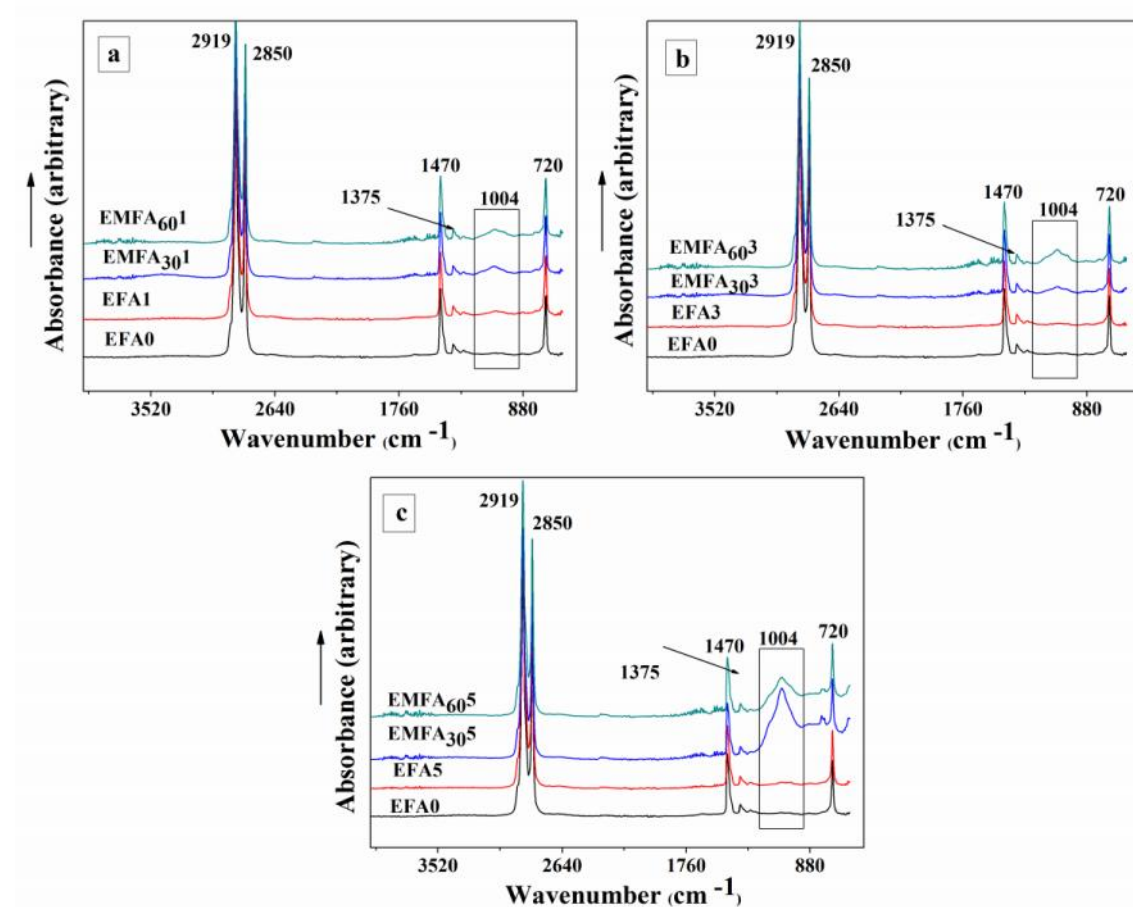
Fig. 4.4 FTIR spectra of neat EOC and EOC composites with (a) 1 wt%, (b) 3 wt% and (c) 5 wt% of fresh FA, 30 h and 60 h MCA-FA

Fig. 4.4 shows the vibrational spectra of neat EOC and the composites with 1, 3 and 5 wt% of fresh FA, 30 h and 60 h MCA-FA. The major peaks at 2919 and 2850 cm^{-1} are that of C-H asymmetric stretching of -CH_2 or -CH_3 and CH symmetric stretching of -CH_2 or CH_3, respectively, which are observed in the spectra of all the composites. The C-H bending and CH_2 rocking peaks are observed respectively at 1470 and 720 cm^{-1}. The

peaks at 1375 and 1300 cm^{-1} are less prominent, which correspond to C-H rocking and CH wagging, respectively. An additional peak at 1004 cm^{-1} is observed only in the EOC composites reinforced with MCA- FA, where the intensity of this peak increases with an increase in filler loading. This peak corresponds to the vibrations of sulfate and Si-O-Si, which was insignificant in the neat EOC and EOC/fresh FA composites, has become conspicuous in case of EOC/MCA-FA composites [Smith 1998]. These results show that MCA-FA is successfully incorporated into the EOC matrix.

4.1.1.5 Mechanical properties

Load bearing properties of composites depend on the effectiveness of load transferred from the matrix on to reinforcement [Nath et al. 2010 and Guhanathan et al. 2001]. **Fig. 4.5(a-d)** shows the variation in tensile strength (TS), elongation at break (EB), modulus at 100 % and 300 % elongation of the composites EOC/fresh FA, EOC/30 h MCA-FA and EOC/60 h MCA-FA.

Neat EOC exhibited a tensile strength value of 9.7 MPa. In EOC/fresh FA composites (**Fig. 4.5a**), there was no much improvement in tensile strength at 1 and 3 wt% of filler loading, but, at a loading of 5 wt%, the tensile strength exhibited a value of 11.3 MPa (% enhancement = 16.5). The incompatibility between the hydrophilic filler and hydrophobic matrix leads to a poor dispersion of the filler particles in the matrix (the formation of agglomerates) and a low degree of homogeneity of the composite as a whole. The presence of spherical particles with glassy surfaces leads to a weak interface formation between the matrix and filler [Anandhan et al. 2012]. M100 and M300, which are considered as indicators of good polymer-filler interaction in rubbers, remain unchanged at 1 and 3 wt% of filler loading and suddenly increase at a loading of 5 wt%.

In EOC/30 h MCA-FA composites, the tensile strength attained the maximum value (% enhancement = 29) at a filler loading of 1 wt% and then decreased at higher filler loading. A similar trend was observed for the M100 and M300. The optimum filler content for EOC/30 h MCA-FA composite was 1 wt%, which enables a relatively high interfacial bonding between the filler and EOC. The good distribution of the filler particles throughout the matrix inhibits crack propagation and thereby improves the

mechanical properties. This is attributed to an increase in tensile strength of composites even at the minimum filler content. The decrease in the tensile properties at high filler loading is related to a larger particle size of 30 h MCA-FA combined with non-uniform distribution of the filler particles in the matrix. This probably reduces the interaction between the matrix and filler and thus resulting in a decreased tensile strength. This explanation for the changes in tensile properties of the composites is supported by the SEM micrographs in **Fig. 4.2**, showing the cryo-fracture surfaces of the EOC/30 h MCA-FA composites.
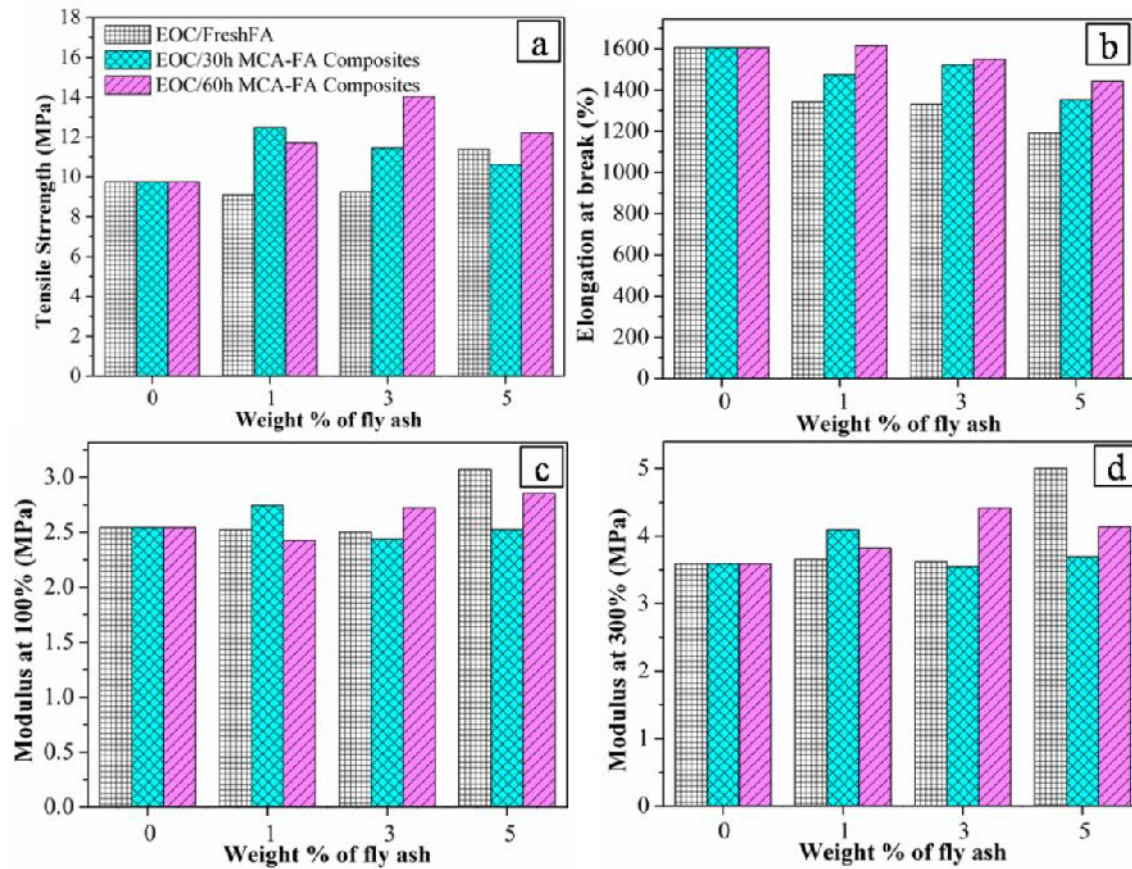
Fig. 4.5 Variations in mechanical properties of composites EOC/fresh FA, EOC/30 h MCA-FA and EOC/60 h MCA-FA as a function of wt% of filler: (a) tensile strength, (b) elongation at break, (c) modulus at 100 % elongation and modulus at 300 % elongation

The tensile strength was maximum (% enhancement = 45 %) at a filler loading of 3 wt% in EOC/60 h MCA-FA composites, which attributes to the uniform distribution of

filler having minimum -value (**Fig. 4.3**). The irregular shape and rough surface along with the surfactant wrapping on MCA-FA particles enable them better interaction and bonding with the matrix. At a higher filler loading, tensile strength decreases due to insufficient wetting of the filler particles by the matrix. EOC/30 h MCA-FA and EOC/60 h MCA-FA have similar tensile strength values at a filler loading of 1 wt%. But, the tensile strength decreases at higher filler loading for the former whereas it increases with filler loading for the latter. Earlier, Anandhan et al. [2012] reported that there was an enhancement in tensile strength by a factor of 50 % in extruded EOC/silane-modified FA composites at a filler loading of 20 wt%. In the present EOC/60 h MCA-FA composites, 45 % improvement is observed in tensile strength at filler loading of 3 wt%. Hence, it is obvious that the MCA-FA is very effective in reinforcing the mechanical properties of EOC.

The theoretical values of the elongation at break of the composites, obtained by using Neilsen equation given in **chapter 2 equation no. 2.5**, were compared with the experimental ones. It was observed that the elongation at break decreases abruptly with an increase in volume fraction of filler (V_f) for the theoretical values as shown in **Fig. 4.6.**

In case of EOC/fresh FA composites, there is a very close match between theoretical and experimental values at all filler loading (**Fig. 4.6a**). In case of EOC composites containing 30 h and 60 h MCA-FA (**Fig. 4.6b** and **c**), there is a large difference between the experimental and theoretical values, i.e., the experimental values are higher than the theoretical ones. Usually in composite systems, when tensile strength increases, the elongation at break tends to decrease. But, for the EOC/MCA-FA composites the tensile strength and elongation at break values increase simultaneously! This means that these composites become stronger and more ductile when loaded with MCA-FA. A spherical particle regardless of its size has the lowest aspect ratio, as the filler shape changes from a spherical to an irregular one, the aspect ratio increases. The irregularly shaped, rough textured, surfactant-wrapped particles of MCA-FA form a strong interface with the polymer matrix due to mechanical interlocking combined with

dispersion and van der Waals forces. It is obvious from the D_{50} values that mechano-chemical activation resulted in a reduction in particle size of FA and this reduction was more for the 60 h MCA-FA. It is an established fact that the reduction of particle dimensions would lead to an increase in the specific surface area [Ashby et al. 2009]. Also, during the application of mechanical stress on the MCA-FA based composites, the stress is transferred to the surfactant wrapped on the MCA-FA particles. Due to these reasons, it is anticipated that the EOC matrix becomes more ductile in the presence of MCA-FA, resulting in its higher ultimate elongation values.
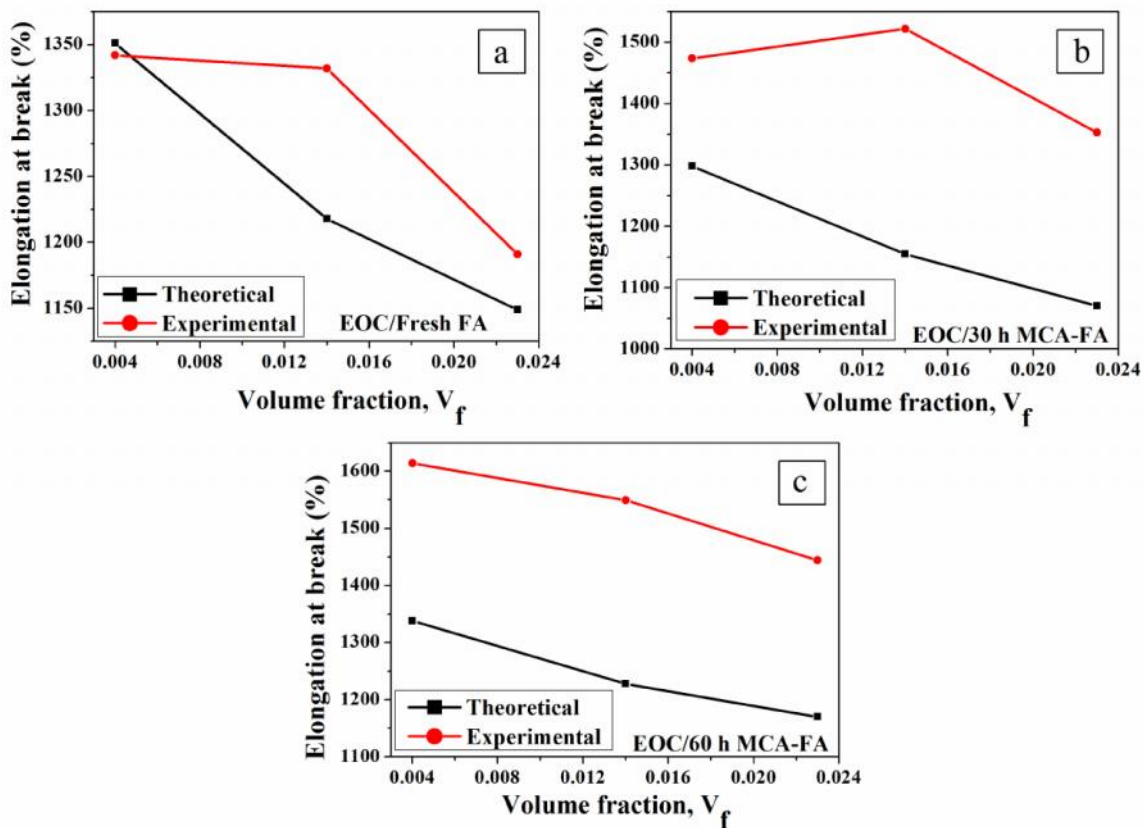
Fig. 4.6 Elongation at break versus volume fraction of filler of composites: (a) EOC/fresh FA, (b) EOC/30 h MCA-FA and (c) EOC/60 h MCA-FA

4.1.1.6 Flammability study

The LOI was calculated using **equation no. 2.9** from **chapter 2**. **Table 4.1** shows the LOI results of neat EOC, EOC/fresh FA and EOC/MCA-FA composites.

Table 4.1 LOI, H_f and X_c values of the composites

Designation	LOI (%)	$H_f (Jg^{-1})$	X_c (%)
EFA0	16	-31.43	11.35
EFA1	18	-35.70	12.89
EFA3	19	-22.90	8.27
EFA5	20	-20.96	7.57
EMFA$_{30}$1	18	-30.03	10.84
EMFA$_{30}$3	22	-27.54	9.94
EMFA$_{30}$5	25	-28.18	10.17
EMFA$_{60}$1	18	-36.57	13.20
EMFA$_{60}$3	20	-33.78	12.19
EMFA$_{60}$5	24	-35.26	12.73

The composites with filler loadings of 3 and 5 wt% are more fire retardant than the neat EOC as the LOI values of these composites are higher than that of EOC [Nelson 2001]. As fresh FA and MCA-FA are ceramic materials they tend to improve the fire retardance of EOC. The marginally higher values of LOI for the composites containing a higher loading MCA-FA stands a proof for their good dispersion and better interaction with EOC. Materials of LOI greater than 28 are generally considered self-extinguishing [Búcsi and Rychlý 1992]. The present composite systems did not become self-extinguishing even at the highest filler loading used in this study. From flammability point of view, it seems that a still higher filler loading is necessary to improve the flame retardance of EOC.

4.1.1.7 DSC results

DSC results help characterize the crystallization and melting behavior of neat EOC, EOC/fresh FA and EOC/MCA-FA composites. It is expected that both neat EOC and EOC/FA composite seem to have long ethylene blocks, which are easy to crystallize in the usual manner. However, depending on its inherent molecular architecture, crystalline melting temperature (T_c) of neat EOC was 45 °C. **Fig. 4.7** shows the DSC traces of neat EOC and EOC/FA composites with 1, 3 and 5 wt% of fresh FA, 30 h and 60 h MCA-FA. EOC exhibited multiple melting endotherms in its DSC curve. That is because ethylene-octene random copolymers possess only some residual crystallinity and that is due to the ethylene sequences.
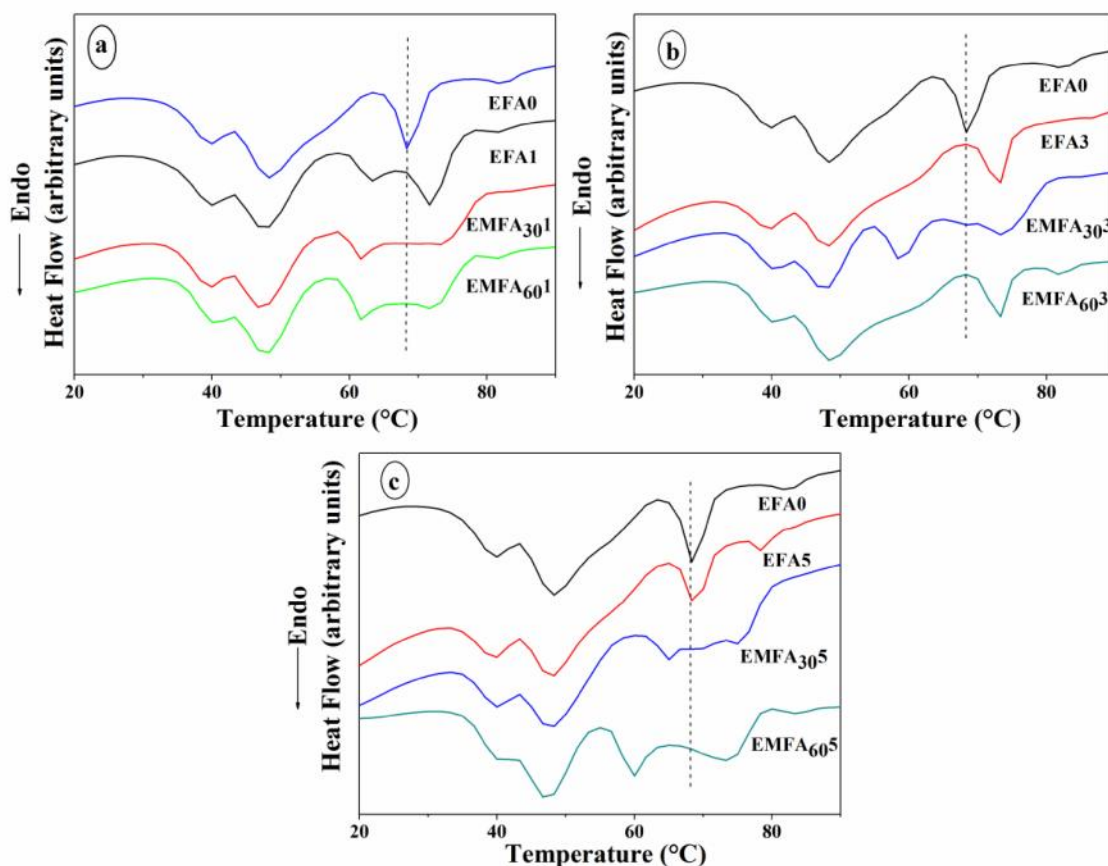
Fig. 4.7 DSC traces of composites with filler loadings of (a) 1 wt% (b) 3 wt% and (c) 5 wt%

60

The % crystallinity (X_c) of the composites was calculated according to **equation no. 2.10 in chapter 2**. The H_f and X_c of the composites are shown in **Table 4.1**. It was difficult to assess the significance of this slight reduction in crystallinity of the composites. There was a slight broadening of the melting endotherm for the composites with increased filler concentrations, reflecting a distribution of crystallite size and perfection as a consequence of the disruption of the EOC crystal morphology by the filler. The minor change in H_f and X_c can be explained on the basis of grafting of EOC on filler that limits the crystallization tendency.

Crystallization of the sequences occurs predominantly for longer sequences of monomers; shorter sequences of monomers cannot participate in crystal formation at ambient temperatures. Due to the multi-layer build-up, these EOC composites exhibit several melting peaks. It revealed that the crystallization peaks of EOC shifted to higher temperature with fresh FA content and to lower temperature with MCA-FA. The observed effects can be attributed to the nucleating effect of filler in EOC crystallization process, the crystallization peak shifts to lower temperature as the filler content increases. This suggests that the MCA-FA reduces the stereoregularity of ethylene macromolecular chain and the crystallization is restricted to a certain degree. The majority of the peaks in neat EOC and EOC/fresh FA composites remained same. Overloading of filler (5 wt%) in composite, however, showed no further change in crystallization peak. EOC composites with 30 h MCA-FA and 60 h MCA-FA showed lower crystallization temperature. The over loaded filler particles may aggregate in EOC matrix and the aggregated MCA-FA have lower nucleating ability due to the reduced specific surface area. Further, a weak endothermic peak at about 45 °C was observed for all the samples, which can be attributed to a secondary, less organized, crystal phase [Liu et al. 2009 and Shangguan et al. 2005].

4.2 CONCLUSIONS

One of the principal problems that occurred whenever FA has been used as filler in polyolefin polymers the interface formation between the polymer and FA has been a challenge. In this work, an attempt was made to improve the compatibility between the

non-polar EOC matrix and the polar filler by modifying the surface of the FA by mechano-chemical treatment. Surface modification and better interaction of filler and polymer matrix were determined by contact angle measurement. Morphological studies revealed that interfacial adhesion between EOC and the MCA-FA was good which resulted in improved mechanical properties. Flame retardance of EOC was enhanced by the addition of FA and MCA-FA. The improvement in physico-mechanical and flammability of these composites is encouraging as this strategy could help eliminate environmental pollution due to FA in a very profitable manner.

CHAPTER 5

CHAPTER 5

PREPARATION AND CHARACTERIZATION OF BIODEGRADABLE POLY(VINYL ALCOHOL) BASED COMPOSITES REINFORCED WITH NANOSTRUCTURED FLY ASH
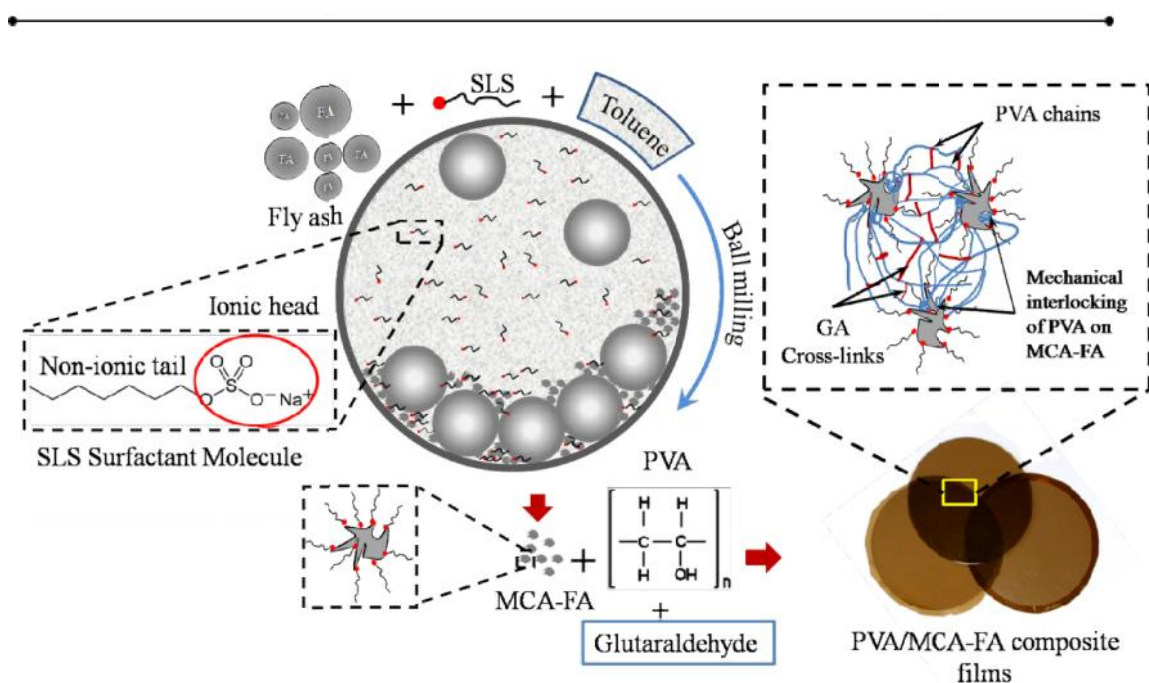
Scheme 5.1 Preparation of PVA composites reinforced with MCA-FA

This chapter discusses the incorporation of fresh FA and MCA-FA into biodegradable poly(vinyl alcohol) (PVA) matrix by solution mixing and ultrasonication. Fourier transform infrared spectroscopy revealed a thermodynamically favorable interaction between the MCA-FA and PVA matrix. The distribution and dispersion of the filler particles was determined from silicon elemental mapping by energy dispersive x-ray spectroscopy (EDS). Thermal properties of the composites were determined by differential scanning calorimetry (DSC), which revealed an improved crystallinity and glass transition temperature of the composites.

5.1 RESULTS AND DISCUSSION

5.1.1 Characterization of PVA/fresh FA and PVA/MCA-FA composites

5.1.1.1 Wettability study

Fig. 5.1a and **b** shows the contact angle measurements of PVA solution on fresh FA and MCA-FA pellets, respectively. Initially a contact angle of 20.12° was observed for the PVA droplet on the surface of fresh FA pellet, which gradually decreased to 9.75° after 10 min. But, the PVA droplet initially made a contact angle of 70.65° on the MCA-FA pellet surface, which then decreased to 20.57° after 20 min. This implies that PVA behaves similar to water, as it is a polar polymer. In addition, after modification, the filler surface became rough, which, in turn, leads to an increment in contact angle.

(a) Fresh FA pellet

t = 0, θ = 20.12°   PVA solution

t = 5min, θ = 9.66°

t = 10min, θ = 9.75°

t = 20, θ = nil

(b) MCA-FA pellet

t = 0, θ = 70.65°   PVA solution

t = 5min, θ = 52.37°

t = 10min, θ = 38.85°

t = 20min, θ = 20.57°
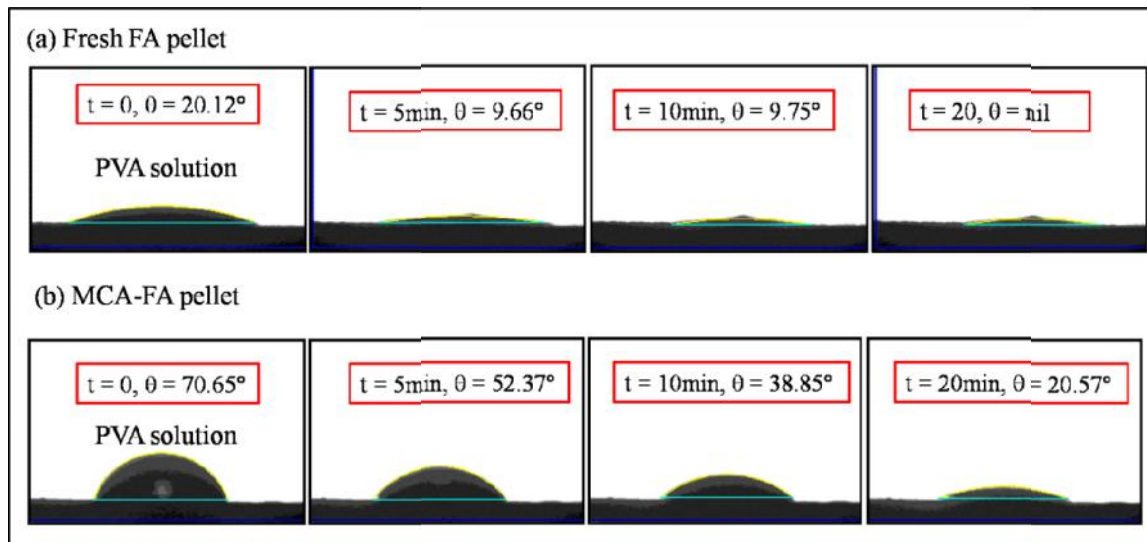
Fig. 5.1 Static contact angle measurements on (a) fresh FA and (b) MCA-FA pellets with PVA solution

5.1.1.2 Elemental mapping of filler distribution and dispersion

Fig. 5.2 shows the silicon elemental maps and standard deviation measurement of filler distribution in the PVA/fresh FA and PVA/MCA-FA composites. The technique of grid quadrant counting was used to analyze the degree of dispersion of particles in the PVA-based composites [Friel 2000]. Each EDS map was divided into nine equal regions of a

sample area of $150 \times 150 \ \mu m^2$. The number of particles in each area was analyzed using Image-J software, and the degree of inhomogeneity of the dispersion was quantified as the standard deviation (σ) by the **equation 2.2 chapter 2**.
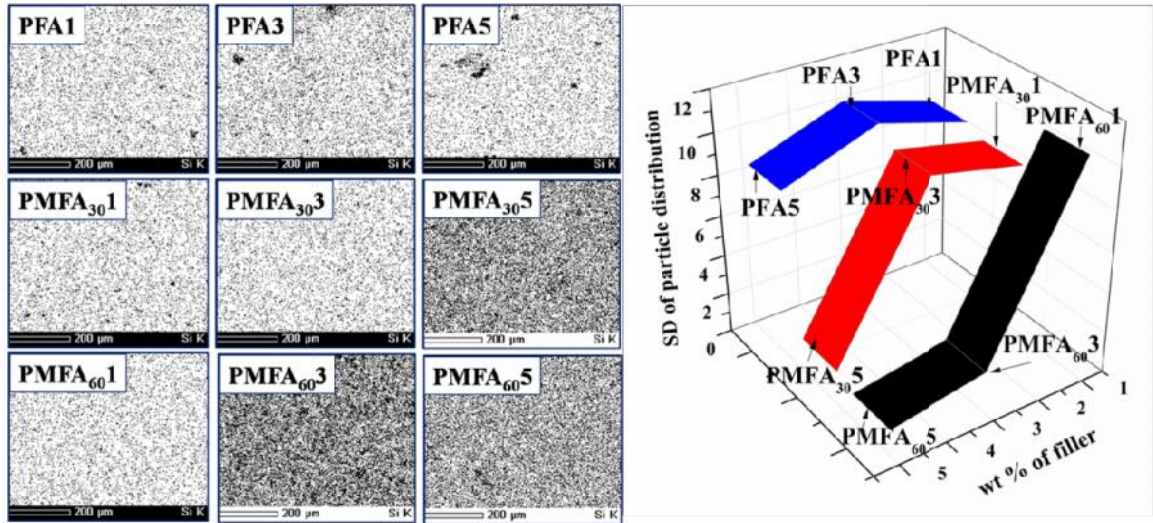
Fig. 5.2 Silicon elemental mapping and standard deviation of particle size distribution of PVA composites

Each spot in the elemental maps represents a filler particle, and as the filler loading is increased, the number of particles is more and so is the number of agglomeration. The σ values decreased with higher filler loading, which signifies that the agglomerated particles are considered as individual particles. This super saturation of FA concentration has resulted in a decline of mechanical properties as discussed in mechanical properties section. The clustering of fillers due to particle–particle interaction, and nonuniform distribution of surfactant led to lower load transfer between matrix and filler that resulted in stress generation in the composites before failure.

5.1.1.3 FTIR spectroscopy

Fig. 5.3 shows the FTIR spectra of neat PVA and its composites containing 5 wt% fresh FA, 30 h and 60 h MCA-FA. All major peaks related to hydroxyl and acetate groups were observed. The intense peaks observed between 3550 cm^{-1} and 3200 cm^{-1} are due to O-H stretching arising from the intermolecular and intramolecular hydrogen bonds. The

vibrational band observed at 2920 and 1727 cm^{-1} refer to the C-H stretching from alkyl groups and C=O stretching from acetate group of neat PVA, respectively. O-H bending and C-O-C stretching peaks appeared at 1423 and 1256 cm^{-1}, respectively [Sudhamani et al. 2003 and Pal et al. 2007].
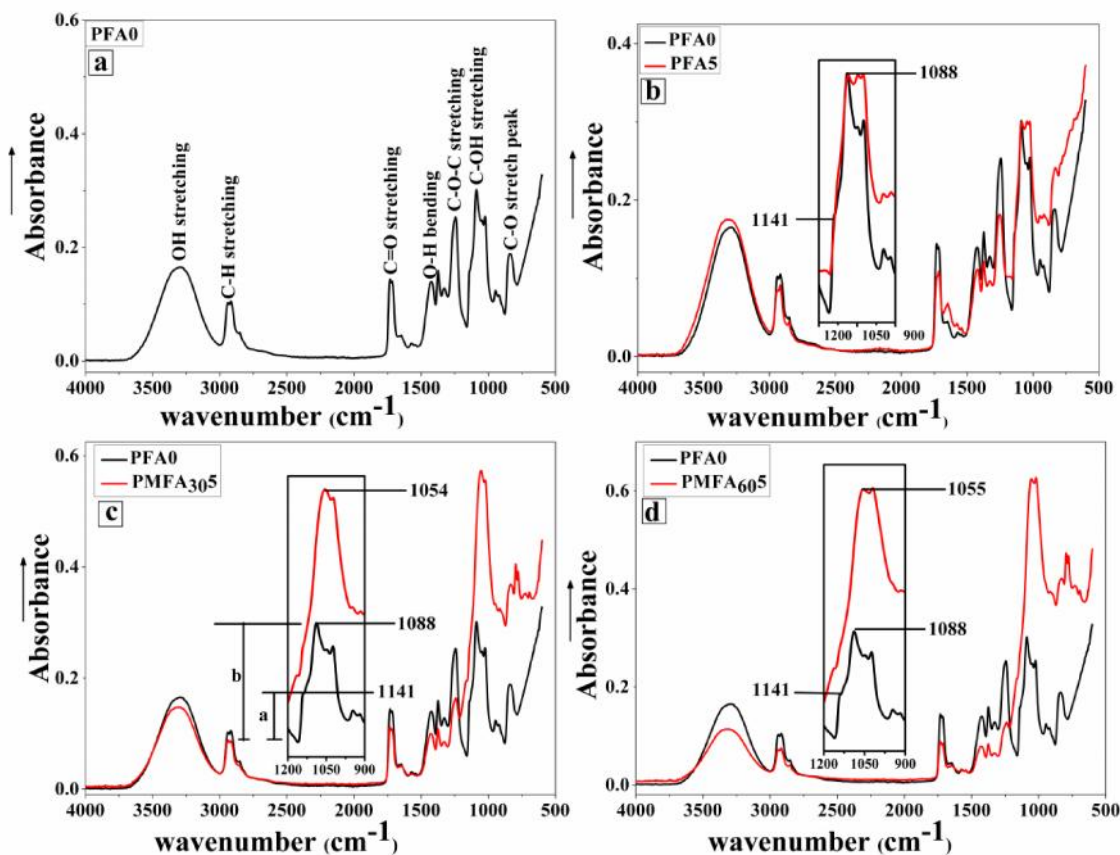
Fig. 5.3 FTIR spectra of neat PVA and PVA composites with 5 wt% of fresh FA, 30 h and 60 h MCA-FA

The composites containing MCA-FA, in comparison with the neat PVA, exhibited significant peak shifts to lower wave numbers with increased intensities. The peak shift is observed at 1088 cm^{-1} of C-O stretch of secondary alcoholic groups C-OH stretching to 1054 cm^{-1} and 1055 cm^{-1}, respectively. This attributes to the intermolecular H-bonding between the C-OH group of PVA and Si-O-Si group of MCA-FA (**Fig. 5.3c** and **d**) [Mansur et al. 2008]. This is explained by a plausible mechanism shown in **Fig. 5.4**.

Meanwhile, the PVA/fresh FA composite did not show any such peak shift (**Fig. 5.3b**). This indicates that the mechano-chemical activation process leads to enhanced polymer-filler interaction in the PVA-based composites. The effective polymer-filler interaction combined with good dispersion and distribution of the filler is expected to help in enhancing the mechanical properties of these composites.
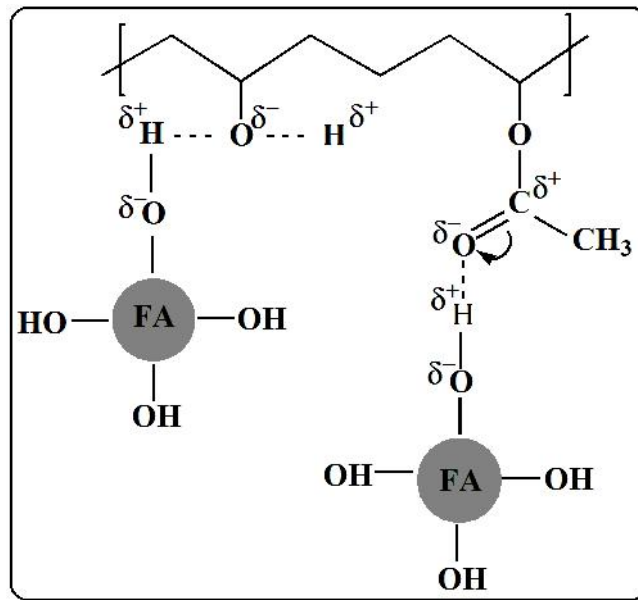
Fig. 5.4 Plausible mechanism of hydrogen bonding between PVA and FA based on the FTIR results of the composite films

To quantify the interaction and compatibility between the polymer matrix and the nanofiller, Fowkes' equation (**equation 5.1**) was employed, which relates the change in IR peak position with enthalpy of interaction between the phases in a multiphase polymer system such as a blend or composite.

$$\Delta H = 0.236 \times \Delta \bar{v} \qquad (5.1)$$

where H is the enthalpy of interaction between the phases in the binary polymer system, and $\Delta \bar{v}$ is the shift in peak position (corresponding to a functional group of the polymer that is involved in interactions such as H-bonding).

The 	∆*H* values of interaction between PVA and MCA-FA in the composites containing 30 h and 60 h MCA-FA were calculated to be -8 and -7.8 kcal mol^{-1}, respectively. The change in Gibbs free energy is related to the enthalpy change as follows:

$$\Delta G = \Delta H - T\Delta S \qquad\qquad (5.2)$$

∆G value will be is negative, when ∆H is negative and ∆S are positive. When ∆G value is negative, the interaction between the filler and polymer is thermodynamically favored [Anandhan et al. 2011]. Thus, in this study, the interaction between PVA and MCA-FA is thermodynamically favored.

5.1.1.4 Mechanical properties

The variation in tensile strength, elongation at break, and modulus at 100% elongation of PVA composites with 1, 3, and 5 wt% of fresh FA, 30 h and 60 h MCA-FA are presented in **Fig. 5.5(a-c)**. The key factor for improvement in tensile properties is the good interfacial interaction between the filler and the polymer matrix, which facilitates stress transfer from matrix to reinforcement. In PVA/fresh FA composites (**Fig. 5.5a**), the tensile strength increases initially at a filler loading of 1 wt% and then decreases at a higher filler loading. The decrease in strength at a higher filler loading is possibly due to extensive filler–filler interaction rather than the filler–polymer interaction, which attributes to the slippage of the polymer chains over the smooth surfaces of the spherical particles of fresh FA. There is a possibility of super saturation of FA concentration, which results in the reduction of intimate contact area between fresh FA and PVA [George and Bhowmick 2007]. A similar trend was observed for elongation at break (**Fig. 5.5b**), leading to transformation from ductile-to-brittle fracture of composite.

Fig. 5.5a shows a decrease in tensile strength with 30 h MCA-FA due to an uneven distribution and agglomeration of filler particles, which were inferred from the SEM elemental mapping. This effectively weakens the number of available reinforcing particles. On the other hand, tensile strength values of the composites containing 60 h MCA-FA are higher than those of the other systems. This attributes to the fact that there

is good dispersion of the 60 h MCA-FA particles in the PVA matrix and the existence of efficient filler–polymer interaction as confirmed by the FTIR results. MCA-FA nanoparticles arranged on the nanometer scale with a high aspect ratio and/or an extremely large surface area into polymers matrix significantly improves their mechanical performance [Tjong 2006]. The stiffness of the filler contributes to the immobilization of polymer phase by molecular interaction as discussed by Kader et al. 2006. This mechanism may proceed through two different pathways. In the first one, the aggregated cluster of particles breakdown in the aqueous PVA solution and the polymer chains can penetrate into the asperities on the surface of MCA-FA. In the second one, the polymer chains get entrapped into the MCA-FA wrapped with surfactant during the vigorous stirring and sonication processes.
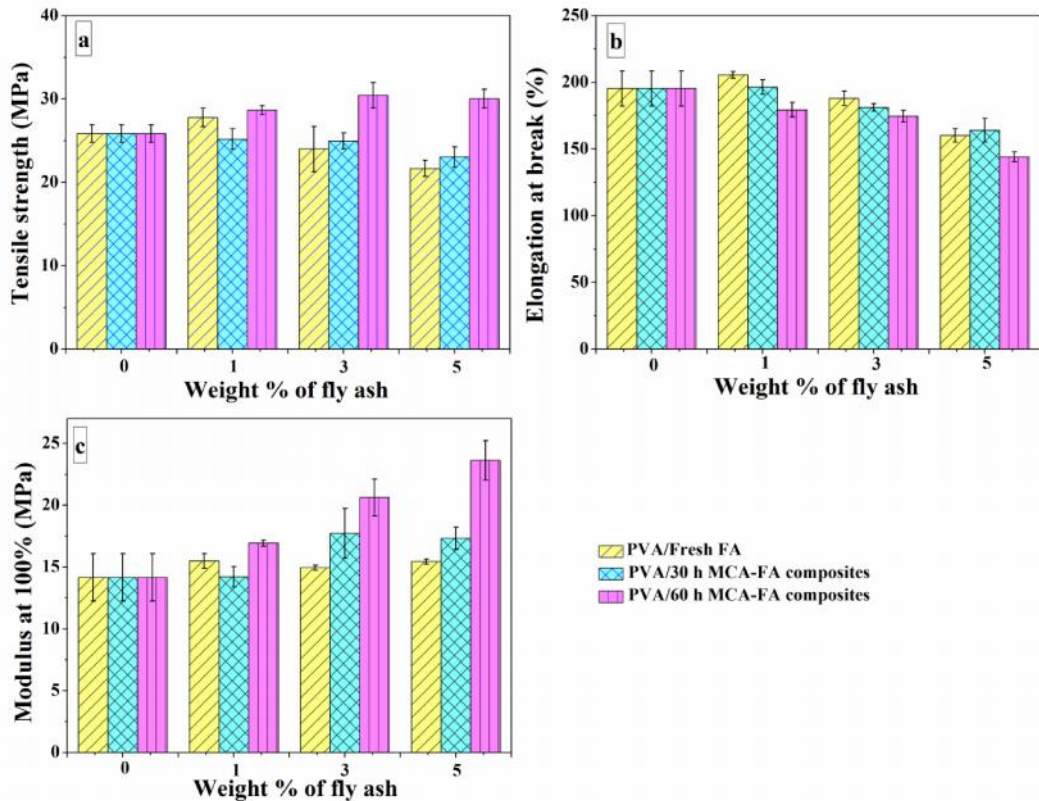
Fig. 5.5 Variations in mechanical properties of PVA/fresh FA, PVA/30 h MCA-FA, and PVA/60 h MCA-FA composites as a function of wt% of filler (a) tensile strength, (b) elongation at break, and (c) modulus at 100%

The ongoing discussion is corroborated by the results of TEM, DLS, and elemental mapping, which reveal the presence of rough, irregular nanosized filler particles in MCA-FA that got uniformly distributed and dispersed in the PVA matrix. These factors, in turn, help in strengthening of the PVA matrix by the MCA-FA particles. An attempt has been made to explore the relationship between strain at break and filler volume fraction in these composites using Nielsen's [1966] equation given in **chapter 2 equation no. 2.5**.
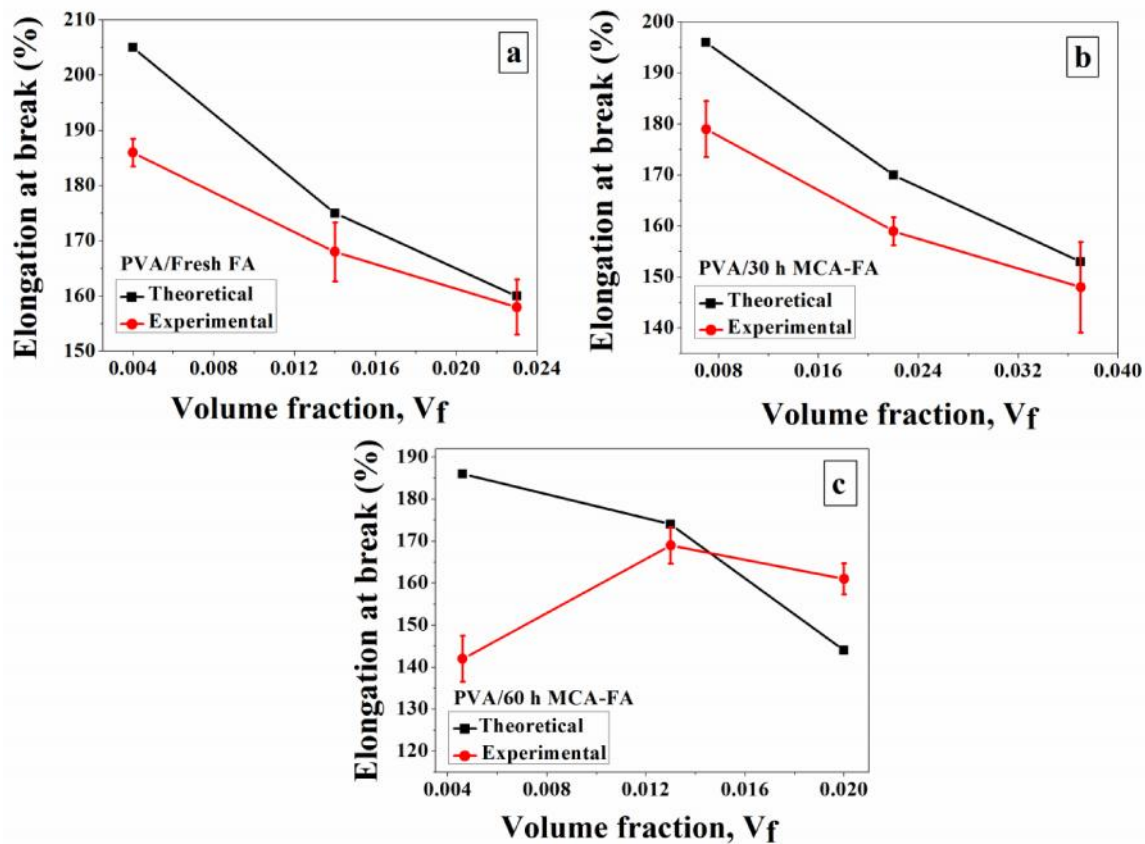
Fig. 5.6 Elongation at break versus volume fraction of filler of (a) PVA/fresh FA, (b) PVA/30 h MCA-FA and (c) PVA/60 h MCA-FA composites

The theoretical and experimental values of elongation at break with respect to volume fraction of the filler were compared as shown in **Fig. 5.6(a-c)**. It was observed that on reinforcing PVA with fresh FA and 30 h MCA-FA, elongation at break decreases

70

with an increase in volume fraction of the filler (**Fig. 5.6a and b**). But, there is a close match between the theoretical and experimental values of elongations at break of these composites. Interestingly, the abrupt decrease in elongation at break in the composite with 1 wt% of 6 h MCA-FA (**Fig. 5.6c**) signifies interruption of crack propagation through the polymer matrix by the filler particles. This is due to strong polymer-filler interaction as discussed before. Nicolais and coworkers [D'Amore et al. 1988] indicated that some fillers might promote craze formation in polymer matrices and that, in turn, might give rise to an increase in ultimate elongation at higher filler loading, which is observed at a filler loading of 5 wt% of 60 h MCA-FA [Anandhan et al. 2012].

5.1.1.5 Fractography of the composites

SEM images were analyzed to determine the nature of adhesion, failure, and the relationship between morphology and mechanical properties of the tensile-fractured surfaces of these composites. **Fig. 5.7(a-d)** displays the SEM micrographs of the tensile-fractured surfaces of the PVA composites with 3 wt% of filler loading.

Tensile fracture surfaces of neat PVA showed the presence of two distinct regions, initial region with a very smooth and flat surface and other region with surface roughness and presence of conical marks due to less crystal flows of semi-crystalline PVA (**Fig. 5.7a**).

Fig. 5.7b illustrates the fractured surface of the PVA/fresh FA composites showing brittle failure and poor filler–matrix adhesion. The presence of the interfacial voids and debonding at the interface occurred probably due to the selective chemical reaction of -CHO groups of glutaraldehyde and -OH groups of PVA in the formation of acetal ring and ether linkage. The bulky acetal rings might occupy considerable space that retards the intimate contact of PVA chains and FA particles [Nath et al. 2010]. In addition, it was observed that many of the randomly oriented FA particles subjected to tensile stress are acting perpendicular to the plane; therefore, the crack propagation occurs parallel to the plane [Deepthi et al. 2010 and Ramos et al. 2005].

Conversely, the morphologies of the PVA composites reinforced with 3 wt% of 30 h and 60 h MCA-FA (**Fig. 5.7c and d**) displayed better polymer-filler adhesion. The

71

superior performance of PVA/MCA-FA composites in mechanical testing attributes to the uniform distribution and efficient packing of MCA-FA. This attributes to the wrapping of surfactant on MCA-FA particles and filler size in nanoscales, which makes the surface highly accessible to the PVA chains (**Scheme 5.1**).
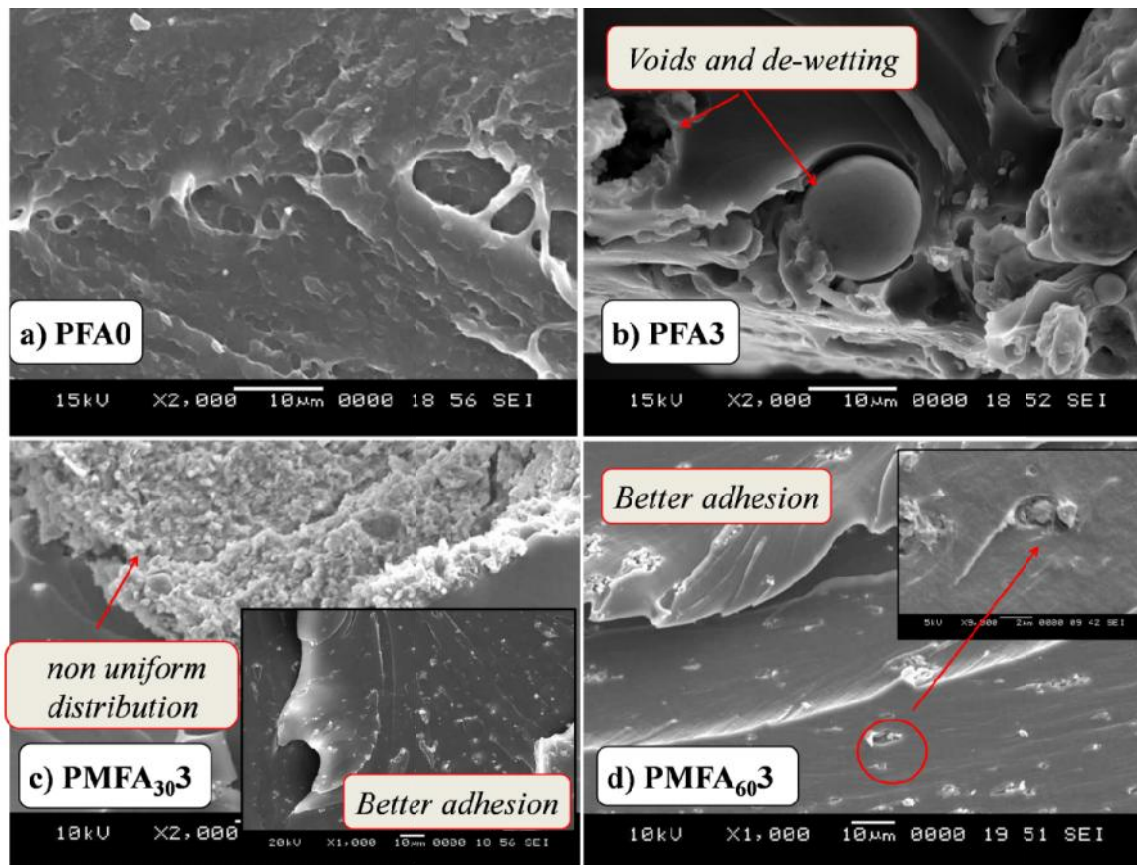
Fig. 5.7 Scanning electron micrographs of the tensile fracture surfaces of (a) neat PVA and PVA composites with 3 wt% of (b) fresh FA, (c) 30 h MCA FA, and (d) 60 h MCA-FA

5.1.1.6 XRD results

The XRD patterns of neat PVA, PVA/fresh FA, and PVA/MCA-FA composites with the loading of 1, 3, and 5 wt% of filler are shown in **Fig. 5.8(a-c)**. The crystallite size of the composites was calculated using **equation no. 2.3** given in **chapter 2**. The appearance of a sharp reflection at 2θ angle of $19.5°$ and a diffuse scattering between $15°$ and $25°$ was

observed for a neat PVA film, which, respectively, is the characteristic of crystalline and amorphous phases of conventional semicrystalline polymers. The crystallinity index depends on the synthetic process and the physical aging of polymers [Bhadra and Sarkar 2011 and Su et al. 2013].
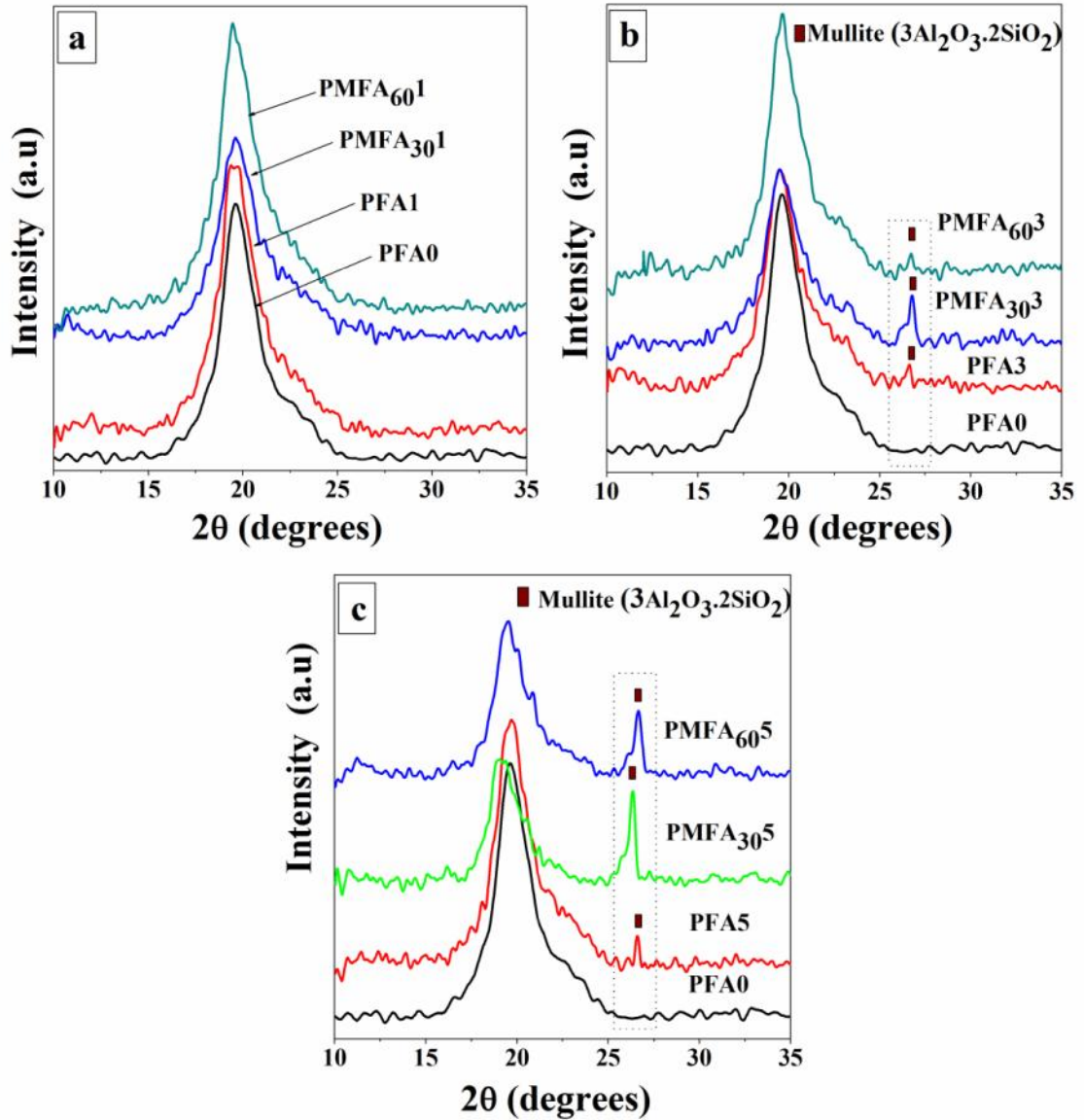
Fig. 5.8 XRD patterns of neat PVA and PVA composites with (a) 1 wt% (b) 3 wt% and (c) 5 wt% of fresh FA, 30 h and 60 h MCA-FA

The XRD patterns of the composites with filler loading of 3 and 5 wt% of fresh FA, 30 h and 60 h MCA-FA exhibit prominent crystalline peaks at 2θ angle of 26.5° with the d spacing of 3.4 Å (**Fig. 5.8b and c**). This peak corresponds to the mullite phase of FA ($3Al_2O_3.2SiO_2$) as reported by the software X'Pert High Score Plus (ref code: 00-002-0428) having an orthorhombic crystal system with $a = 7.52$ Å, $b = 7.65$ Å, and $c = 2.89$ Å. At 1 wt% of filler loading, there was no significant crystalline peak showing the presence of FA (**Fig. 5.8a**), which may be due to the lower concentration of filler. More specifically, the absence of peak might be misinterpreted. There are many factors, such as concentration and order of the filler, which can influence the XRD patterns. For example, samples where the filler is not uniformly distributed will fail to produce a Bragg diffraction peak.

The incorporation of the fresh FA, 30 h and 60 h MCA-FA influenced the crystallite size of PVA as shown in **Table 5.1**. There is only a marginal change in crystallite size; this is probably due to the nucleating effect of MCA-FA.

Table 5.1 Crystallite size of PVA composites from XRD analysis

Designation	2θ (degree)	β (degree)	Crystallite size (Å)
PFA0	19.60	2.149	37.61
PFA1	19.56	2.419	33.35
PFA3	19.49	2.294	35.22
PFA5	19.70	2.337	34.48
PMFA$_{30}$1	19.61	2.313	34.92
PMFA$_{30}$3	19.49	2.494	32.39
PMFA$_{30}$5	19.2	2.342	34.44
PMFA$_{60}$1	19.45	2.382	33.89
PMFA$_{60}$3	19.64	2.281	35.38
PMFA$_{60}$5	19.52	2.34	34.47

5.1.1.7 DSC results

Fig. 5.9(a-c) shows the DSC traces of neat PVA and its composites reinforced with 1, 3, and 5 wt% of fresh FA, 30 h and 60 h MCA-FA. The DSC results (**Fig. 5.9a-c**) refer to the second heating cycles of the samples, as the first heating was done to eliminate the thermal history of the samples. PVA is a semicrystalline polymer exhibiting both a glass transition temperature (T_g; characteristic of amorphous phase) and a melting endotherm (T_m; characteristic of crystalline phase) due to high physical interchain and intrachain interactions of hydroxyl groups by hydrogen bonds [Liu et al. 2007; and Agrawal and Awadhia 2004]. The discontinuity at 5-10 °C is due to the glass transition of PVA, and the sharp endothermic peak in the range of 170-200 °C is attributed to the melting of the crystallites of PVA [Guo et al. 2010; and Xiao and Yang 2006]. The values of melting temperature, heat of fusion, and degree of crystallinity (X_c%) of the composite samples was calculated by **equation no. 2.10** given in **chapter 2**. The results are summarized in **Table 5.2**.

Table 5.2 H_f and X_c values and degree of crystallinity of the composites from DSC analysis

Designation	T_m (°C)	H_f (Jg^{-1}])	Crystallinity (X_c%)
PFA0	181.1	-93.77	67.65
PFA1	189.9	-46.96	35.66
PFA3	180.5	-60.31	43.72
PFA5	175.7	-99.36	73.90
PFA5	189.9	-46.96	35.66
PMFA$_{30}$1	174.9	-98.9	72.07
PMFA$_{30}$3	187.9	-63.86	46.86
PMFA$_{30}$5	187.2	-56.73	43.08
PMFA$_{60}$1	174.9	-100.3	73.09
PMFA$_{60}$3	190.2	-41.08	30.55
PMFA$_{60}$5	193.0	-34.82	26.44

The nominal value of crystallinity, obtained from the DSC curve of pure PVA, was 67%. The crystallization peak of PVA shifted to a higher temperature and X_c% decreased at a filler content of 1 and 3 wt% of fresh FA. The crystallinity slightly increased at a fresh FA loading of 5 wt%. At a lower filler content (1 wt%) of 30 h MCA-FA and 60 h MCA-FA, the melting point was less than that of pure PVA. But, X_c% value was more. This could be due to the nucleating effect of the MCA-FA, which induces the formation of a large number of crystallites that have a broad size distribution [Ikejima et al. 1999 and Othman et al. 2011].
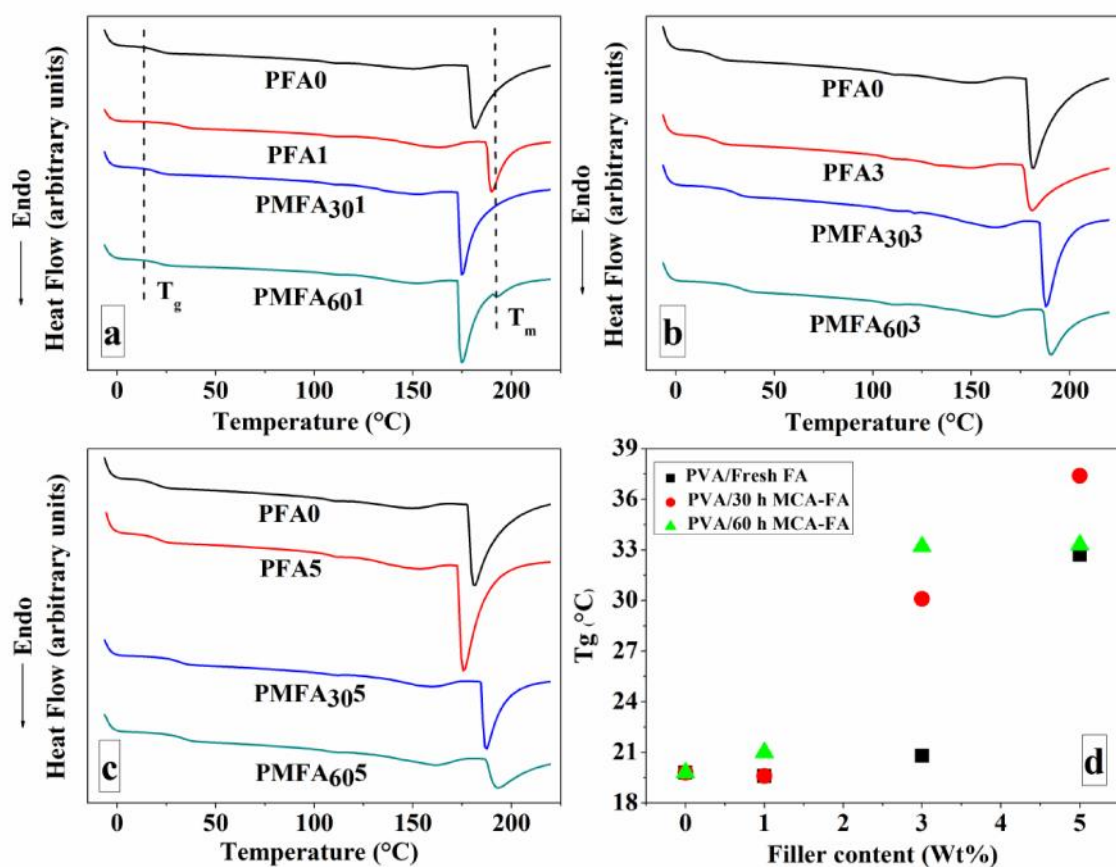
Fig. 5.9 DSC traces of neat PVA and PVA composites with (a) 1 wt%, (b) 3 wt%, (c) 5 wt% of fresh FA, 30 h and 60 h MCA-FA, and (d) T_g values of PVA composites as a function of their filler content

The incorporation of a higher amount of filler increases the T_g values of these composites (**Fig. 5.9d**). This phenomenon attributes to the reduced mobility of the polymer chains by the presence of the filler. It should be emphasized that the filler geometry could play a critical role in affecting the T_g. The polymer chains could adsorb onto or entangle with the spherical particles of fresh FA, as the diameters of the filler particles are comparable with the radii of gyration of the polymer chains. This may lead to a decreased packing density of the polymer chains. The restricted mobility originated from the denser chain packing results in higher T_g values for composites containing irregular-shaped MCA-FA particles. The MCA-FA affects the distribution of polymer chain segments, considerably higher than the typical radii of gyration of polymer chains. As a consequence, the polymer chains could wrap the MCA-FA in three dimensions, and there was no free volume and voids for the chain segments [Avella et al. 2004 and, Paul and Robeson 2008]. The maximum increase in the glass transition temperature of the PVA matrix was approximately equal to 18 °C when 5 wt% of the nanostructured FA was used as the reinforcement.

5.2 CONCLUSIONS

There is growing trend toward the development of competent composites with low environmental impact and good commercial viability. The results of this investigation indicated that the particle–particle interaction forces in MCA-FA were reduced, which played a significant role in enhancement of filler dispersion in the present composite systems. The polymer–filler interaction in these composites was thermodynamically favored as revealed by the FTIR spectroscopy. The good dispersion and distribution of the filler and the effective polymer–filler interaction helped in enhancing the mechanical properties of these composites. The nanostructured FA acted as a nucleating agent for PVA at small filler loading. The maximum increase in the T_g of the PVA matrix was about 18 °C when 5 wt% of the nanostructured FA was used as reinforcement. Overall, this study proves that mechano-chemically activated FA could be used as value-added filler for biodegradable PVA.

PART - II

CHAPTER 6

CHAPTER 6

INFLUENCE OF PLANETARY BALL MILLING PARAMETERS ON THE MECHANO-CHEMICAL ACTIVATION OF FLY ASH
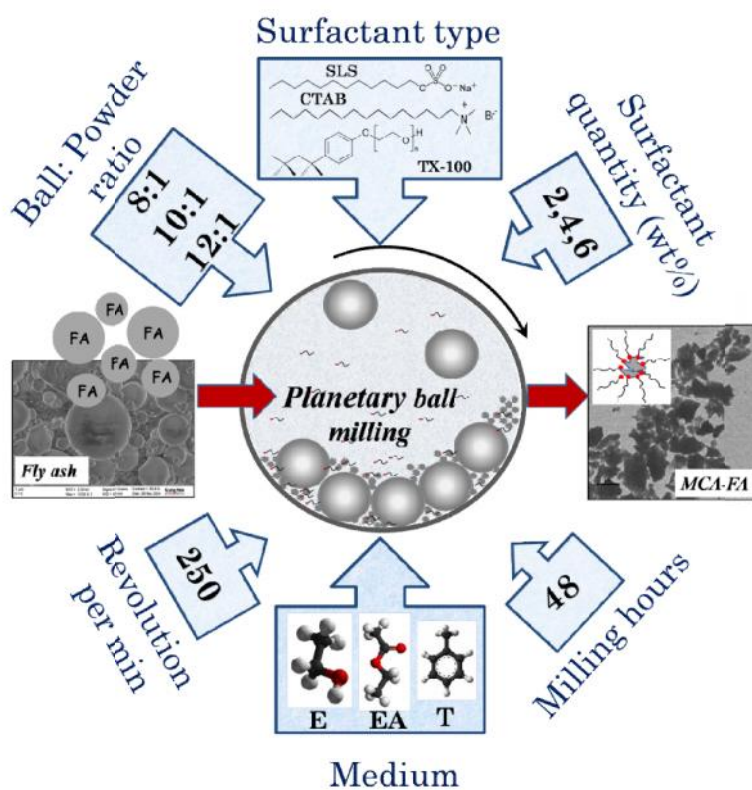
Scheme 6.1 The ball milling parameters for mechano-chemical activation of FA

This chapter illustrates the design of statistical analysis by Taguchi methodology to obtain nanostructured FA by high energy ball milling. Ball milling parameters, such as ball-to-powder weight ratio, type and quantity of surfactant and type of medium were varied as guided by Taguchi design. An orthogonal array and analysis of variance were employed to analyze the effect of milling parameters. The nanostructured FA was characterized by DLS, BET surface area analysis, XRD, XPS, FTIR spectroscopy, SEM, FESEM and TEM.

6.1 RESULTS AND DISCUSSION

6.1.1 XRF results

The detailed chemical compositions of fresh FA, sieved FA (-170#+200#) and magnetically separated FA were analyzed by XRF and are shown in **Table 6.1**. The major constituents of FA are silica, alumina and iron oxide, whereas Na_2O, K_2O, P_2O_5, CaO, MgO and TiO_2 account for minor constituents to the composition of FA. After magnetic separation, the amount of iron oxide was reduced from 4.39% to 2.75%. The remains of the iron oxide were in the combined state with other oxides, which could not be eliminated completely. The amount of the other oxides remained unaltered after magnetic separation.

Table 6.1 XRF results of fresh FA, sieved FA (-170#+200#) and magnetic separated FA

Sample	Oxide composition in percentage (%)										
	SiO_2	Al_2O_3	Fe_2O_3	CaO	K_2O	MgO	Na_2O	P_2O_5	TiO_2	W	ZrO_2
Fresh FA	62.68	27.05	3.72	2.46	1.18	0.92	0.08	0.26	1.6	0.02	0.08
Sieved FA	64.17	25.38	4.39	2.6	1.24	0.90	0.08	0.26	1.6	0.02	0.08
Magnetic separated FA	65.24	25.39	2.75	2.64	1.27	0.85	0.08	0.26	1.6	0.02	0.08

6.1.2 Experimental design

Taguchi's L_9 orthogonal array was used to achieve the control factors, which affect the output response, such as crystallite size, average particle size and specific surface area (**Table 6.2**). Each row in the table represents a trial condition with the factor levels. The columns correspond to the factors specified in this study and each column contains three levels.

Table 6.2 $L_9 (3^4)$ orthogonal array matrix and response of crystallite size, average particle size and specific surface area

Experiment number	A	B	C	D	Crystallite size (nm)			Z- avg (nm)			Specific surface area ($m^2 g^{-1}$)		
					Trial 1	Trial 2	Avg	Trial 1	Trial 2	Avg	Trial 1	Trial 2	Avg
1	1	1	1	1	13	14.4	13.7	824	726	775	6.9	7.8	7.35
2	1	2	2	2	7	7.8	7.4	454	453	454	8.18	8.8	8.49
3	1	3	3	3	12.8	14.2	13.5	573	540	557	5.95	6.79	6.37
4	2	1	2	3	15.1	16.7	15.9	673	706	690	5.15	5.33	5.24
5	2	2	3	1	13.1	14.5	13.8	660	603	632	7.78	7.36	7.57
6	2	3	1	2	10.9	12.1	11.5	694	704	699	7.95	8.57	8.26
7	3	1	3	2	8.1	9	8.55	329	328	329	8.72	8.74	8.73
8	3	2	1	3	9.6	10.6	10.1	574	479	527	1.58	4.32	2.95
9	3	3	2	1	11.1	12.3	11.7	710	633	672	4.44	4.7	4.57

6.1.3 XRD results
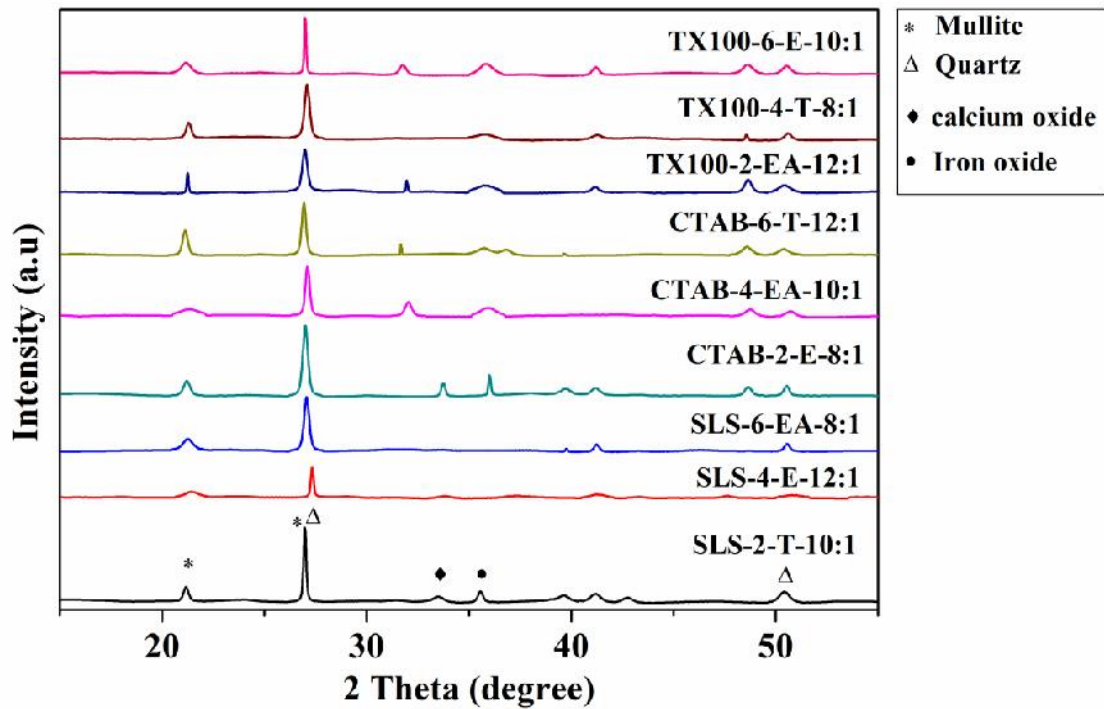
Fig. 6.1 XRD patterns of MCA-FA prepared by ball milling under different conditions designed in Table 6.2

81

The XRD patterns of the MCA-FA obtained in the 9 experiments (**Table 6.2**) are shown in **Fig. 6.1**. The analysis of XRD patterns was done using X'pert high score software, which revealed a number of crystalline peaks in the XRD curves, such as that of quartz (SiO_2), mullite ($3Al_2O_3.2SiO_2$), CaO and Fe_2O_3. In all the curves, an amorphous hump was observed in the 2 range of 14°-35°, which is due to the presence of glassy materials [Paul et al. 2007]. The average crystallite sizes of the quartz phase present in the MCA-FA were determined from the full width at half maximum (FWHM) of the XRD peaks, using Scherrer's formula given in **equation 2.3 chapter 2**.

6.1.4 FTIR spectroscopy

The interaction between the different surfactants and FA particles was examined by FTIR spectroscopy. **Fig. 6.2a, b** and **c** shows the interaction of the surfactants SLS, CTAB and TX-100 with MCA-FA. The stretching vibration bands of fresh FA were observed at 1092, 797 and 465 cm^{-1} (**Fig. 6.2a, b** and **c**). The strong broad band at 1092 cm^{-1} can be related to Si-O-Si asymmetric stretching vibration, while the 797 cm^{-1} band can be related to Si-O-Si symmetric stretching vibration [Smith 1998] as well as AlO_4 vibrations of FA. The Si-O-Si bending is observed at 465 cm^{-1}.

The vibrational spectra of the pure SLS and 2, 4 and 6 wt% of SLS on MCA-FA are shown in **Fig. 6.2a**. The FTIR spectrum of SLS shows the O-H stretching band at 3475 cm^{-1}. The 2920 and 2855 cm^{-1} bands correspond to C-H stretching. The major sulfate asymmetric and symmetric characteristic stretching vibration bands are observed at 1220 and 1080, 1140-900 cm^{-1}, respectively [Nath et al. 2010].
The peak intensity at 1092 and 797 cm^{-1} increases as the wt% of the surfactant increases, this implies the merging of sulfate bands from surfactant and silicon stretching bands of FA. The spectrum of MCA-FA treated by 6 wt% of SLS shows the presence of C-H stretching bands at 2920 and 2855 cm^{-1}, this attributes to the interaction of surfactant SLS with FA.

Fig. 6.2b shows the spectra of the pure CTAB and 2, 4 and 6 wt% of CTAB on MCA-FA; the C-H stretching is observed at 2920 and 2855 cm^{-1}. The 1480 cm^{-1} corresponds to methylene scissoring vibration. There was no major change of interactions

observed on MCA-FA, only at 6 wt% of CTAB the C-H stretching bands have interacted with MCA-FA.
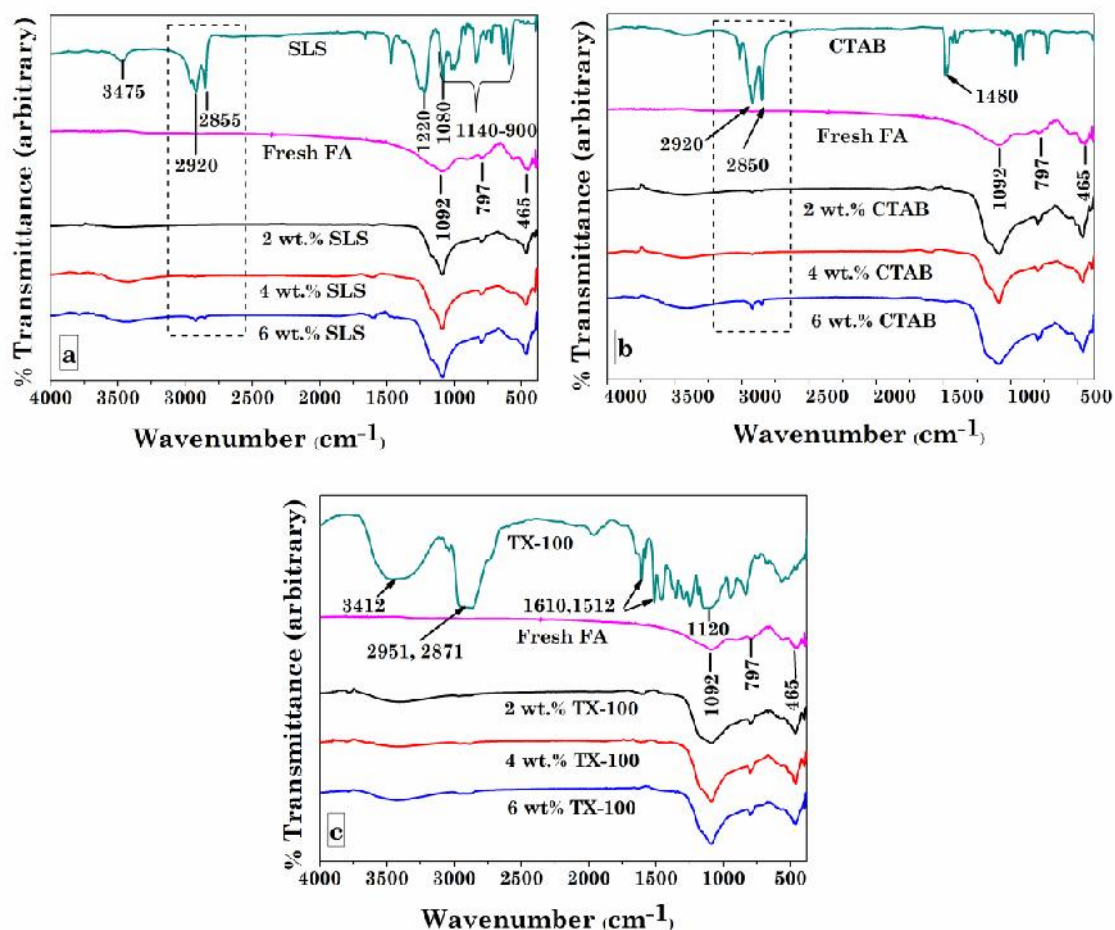
Fig. 6.2 FTIR spectra of (a) SLS, (b) CTAB and (c) TX-100

The spectrum of TX-100 surfactant (**Fig. 6.2c**) shows the O-H stretching band at 3365 cm^{-1}. The bands at 2951 and 2871 cm^{-1} correspond to asymmetric CH_2 stretch and symmetric CH_2 stretch, respectively. The symmetric stretching bands of benzenoid group vibrations are observed at 1610 cm^{-1} and 1512 cm^{-1} [Viana et al. 2012]. The absorption band near 1120 cm^{-1} is related to the stretching vibrations of the ether C-O groups of the surfactant. The peak broadens at 1092 cm^{-1} for MCA-FA as the concentration of surfactant increases. This attributes to the interaction of ether C-O groups of TX-100 and Si-O-Si stretching of FA. The peak at 3365 cm^{-1}, which is insignificant in the fresh FA,

has become conspicuous in case of MCA-FA; this is because of the interaction of the O-H stretching band of TX-100 with that of MCA-FA.

6.1.5 Design with Taguchi technique

The experimental design proposed by Taguchi was constructed using the software MINITAB-16 (Pennsylvania, USA) in the form of an orthogonal array (OA). An orthogonal array is abbreviated as L_N, where L refers to the number of levels and N indicates the number of trials that needs to be performed for a given design. In this study, the L_9 (3^4) Taguchi method indicates that 9 experiments are to be carried out for four factors at three levels. For the same factors and levels 81 experiments need to be performed by the full factorial method. By applying this orthogonal array (L_9), one can organize the factors and levels in combination with test pairs. This allows the collection of data to determine the product quality with the minimum number of experiments [Beygi et al. 2012]. The results of the Taguchi experiments were analyzed in a standard series of phases. **Table 6.2** shows the L_9 orthogonal array and the response values of crystallite size, average particle size and specific surface area of the two trials of the experiment conducted. The responses were evaluated individually.

The main effect plots are the mean values of each level, which were evaluated and the influences of the factors were determined in qualitative terms as shown in **Fig. 6.3**(**a-c**). **Fig. 6.3a, b** and **c** shows the level average response (main effect) plots of crystallite size, average particle size and specific surface area of the L_9 orthogonal array with two trials of the experiment conducted. The main effect of crystallite size (**Fig. 6.3a**), with A3B2C2D2 was found to be the best combination of the factors and their levels. By these plots, one can figure out the relative consequence of each effect, because, a particular factor for which the line is near horizontal, it has no significant effects on the response; however, if the line has the highest inclination, it will have the most significant effect. These results confirm that the factors A, B and D are strong and more significant than C. The main effect of lower average particle size and higher specific surface area (**Fig. 6.3b** and **c**), with A3B2C3D2 and A1B1C3D2 was found to be the best combination of the factors and their levels, respectively.

84

For the factor A, the best level was surfactant TX-100 for the reduced crystallite size and average particle size, where as surfactant SLS resulted in the higher specific surface area as shown in **Fig. 6.3a, b** and **c**, respectively. Surfactants basically stabilize the particle suspension and prevent agglomeration of small particles. The structures of the three types of surfactants used in the present study are shown in **Scheme 6.1**.

The mechanism of any interaction involving surfactant molecules at a surface is affected by either hydrophilic or hydrophobic adsorption. Anionic surfactant (SLS) molecules interact through their polar heads by the Coulomb electrostatic and Van der Waals forces and the nonpolar tails of the surfactant orient themselves away from the FA surface. A similar trend is observed for cationic and non-ionic surfactants having cationic and non-ionic functional groups, respectively, at their heads. The structure of the MCA-FA can hence look like an inverse micelle in which the polar heads which surround the FA particle form the inner core and the non-polar tails form the outer layer. As the type of functional groups of the surfactants determines the extent of interactions, TX-100 surfactant has a hydrophilic polyethylene oxide chain (on average it has 9.5 ethylene oxide units) and that of CTAB and SDS consists of an alkyl chain. Alternatively, the OH at the end of TX-100 has bonding tendencies toward the hydrophilic FA surface [Ghorabi et al. 2012]. Thus among the three surfactants used, TX-100 with the long chain of ethylene group forms a stronger interaction with the surface of the FA particles resulting in the lowest crystallite size and average particle size. Each type of surfactant has a critical micelle concentration (CMC), at which the solid–liquid interface becomes saturated and above the CMC; the molecules start to form aggregates or micelles. The larger the micelle size, the stronger will be the steric repulsive forces introduced by them. It is expected that the surfactant SLS with a higher critical micelle concentration (8.2 mM) in comparison with TX-100 (0.24 mM) and CTAB (1 mM) would result in a higher specific surface area. Also, the large agglomerates of MCA-FA would be more effectively deagglomerated [Hennart et al. 2012].

For factor B, 4 wt% of surfactant resulted in a lower crystallite size and average particle size, whereas 2 wt% resulted in a higher specific surface area (**Fig. 6.3a, b** and

c). The observed effect is most likely due to the stabilization of particle suspension, which prevents particle agglomeration. Some researchers [Paria and Khilar 2004] reported that adsorption of the surfactant can be divided into three different regimes; there is a linear increase in adsorption with time, a transition regime where the rate of adsorption levels off, and a plateau regime. Initially at 2 wt% of surfactant, monomer diffusion may occur at the surface of MCA-FA, later at 4 wt% of surfactant, which is considered to be the optimum concentration level for non-agglomeration and at a higher concentration (6 wt%) micellar diffusion results in saturation level.

During the milling process of FA, the viscosity and surface tension of the medium also play an important role in obtaining a finer particle size [Sakthivel et al. 2008]. For factor C, ethyl acetate was considered to be the best dispersing agent for a lower average particle size and a higher specific surface area (**Fig. 6.3b** and **c**); and ethanol for reduced crystallite size (**Fig. 2a**). If the viscosity of the suspension inside the mill becomes very high, then part of the grinding media adheres to the inner wall of the mill resulting in fewer ball-to-ball collisions.

Ethyl acetate having a lower viscosity (0.42 cP) compared with that of ethanol (1.2 cP) and toluene (0.59 cP) lowers the slurry viscosity, thereby facilitating more free flowing suspension and ball-to-ball collision. Therefore, the lower viscosity of the slurry may help to reduce the average particle size and thereby increase the specific surface area. Eventually the grinding rate decreases with the increase in surface tension of the medium. Ethanol has the minimum surface tension (22.39 mN m^{-1}) in comparison with both ethyl acetate (23.75 mN m^{-1}) and toluene (28.52 mN m^{-1}). Hence, ethanol may be adsorbed on the surface of MCA-FA and its micro-cracks, reducing the hardness of MCA-FA owing to its low surface tension, resulting in reduced crystallite size [Werth et al. 2003].
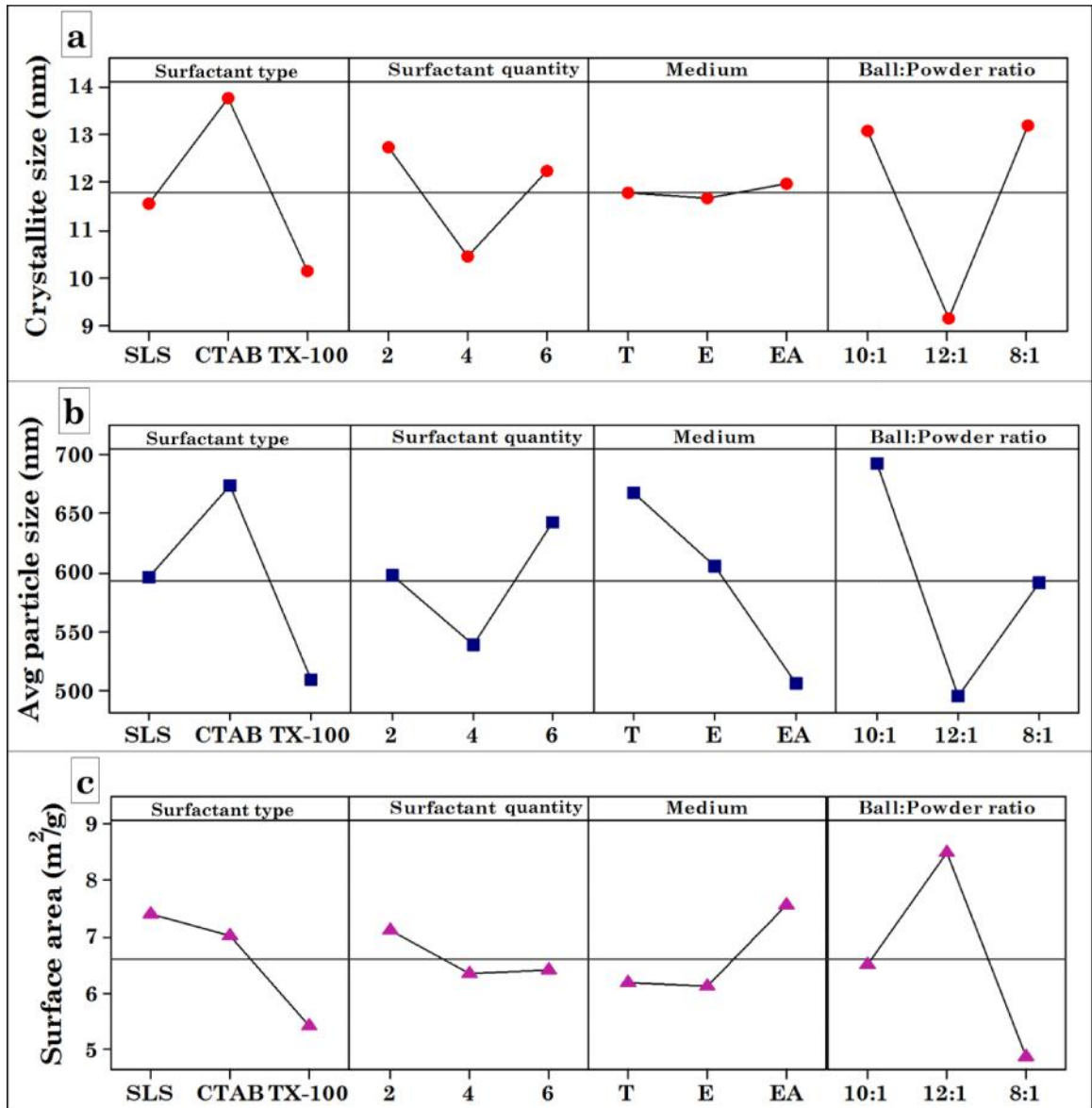
Fig. 6.3 Main effect plot for means of MCA-FA (a) crystallite size, (b) average particle size and (c) specific surface area

Table 6.3 Response table for means of crystallite size, average particle size and specific surface area

Levels	Surfactant type	Surfactant quantity	Medium	B:P ratio
Response - Means				
(a) Crystallite size (nm)				
1	11.533	12.717	11.767	13.067
2	13.733	10.433	11.667	9.15
3	10.117	12.233	11.95	13.167
Delta	3.617	2.283	0.283	4.017
Rank	2	3	4	1
(b) Average particle size (nm)				
1	595.3	598	667	693
2	673.7	537.7	605.3	494
3	509.3	642.7	506	591.3
Delta	164.3	105	161	199
Rank	2	4	3	1
(c) Specific surface area (m² g⁻¹)				
1	7.403	7.107	6.187	6.497
2	7.023	6.337	6.100	8.493
3	5.417	6.400	7.557	4.853
Delta	1.987	0.770	1.457	3.640
Rank	2	4	3	1

For factor D the best level was 12:1 for reduced crystallite size, reduced average particle size and an increased specific surface area (**Fig. 6.3a-c**). This is the only factor, which has a common level among all the characteristics of MCA-FA. The weight of balls to powder ratio (BPR) is an important variable in the milling process. At a high BPR, because of an increase in the weight proportion of the balls, the number of collisions per unit time increases and consequently more energy is transferred to the powder particles

and size reduction takes place faster [Zhang et al. 2008 and Chen et al. 2007]. But, even if the BPR exceeds the optimum value there will be excess of wear and tear between the balls, and balls and inner wall of the vial. Whereas, at lower BPR, impact energy and shear energy are not sufficient to fracture the powder particles.

The average values of means of different factors at various levels are given in the response table (**Table 6.3**). It demonstrates the average of the selected mean for each level of the factors. According to range analysis from main plot of means, the effects of each parameter can be ranked based on delta statistics as follows: factor A, factor B, factor C and factor D (**Table 6.3**). It was observed that the factors; ball-to-powder ratio and surfactant type rank 1st and 2nd, respectively, emerging as the most significant factors for all the response. A high ball-to-powder ratio provides a higher grinding energy during the rotational movement of the mill, which basically accumulates high residual stress and strain on the FA particles [Hewitt and Kibble 2009]. The surfactant forms a protective layer on the MCA-FA preventing the smaller particles from agglomeration. The factors, medium and surfactant quantity rank 3rd and 4th for response values of average particle size and specific surface area. The medium not only helps to suspend the FA particles, but, also acts as a cooling agent by absorbing the heat generated during rotation of the planetary ball mill. For the crystallite size, the 3rd and 4th ranks are surfactant quantity and medium. The amount of surfactant adsorption and the formation of micelle are basically determined by the surfactant quantity.

6.1.6 Analysis of variance (ANOVA)

The results of the Taguchi experiments were analyzed in a standard series of phases. First, the main effects were evaluated and the influences of the individual factors were determined in qualitative terms. In the second phase, the analysis of variance (ANOVA) was performed on the experimental data to identify the relative influence of the factors in discrete terms. The analysis of ANOVA was analyzed by software "WinRobust".

The ANOVA results of crystallite size, average particle size and specific surface area are shown in **Table 6.4**. According to the ANOVA, the largest contribution was by the factor D (BPR) for all the response at a 99% confidence. The contribution for factor

D (BPR) for specific surface area, crystallite size and average particle size was 56.61, 48.26 and 35.20%, respectively. The milling process involves compression, shear (attrition), impact (stroke) and impact (collision) forces acting between two grinding media beads or between grinding media beads and the inner wall of the vial. This attributes to the repeated welding, fracturing and rewelding of powder particles during mechano-chemical activation [Ali and Liwa 2013]. The % contribution by other factors: A (surfactant type), C (medium) and B (surfactant quantity) for specific surface area was 17.86, 10.1 and 1.56. Similarly for average particle size, factors A (surfactant type) and C (medium) showed equal percentage of contribution. The surfactant increases the crack propagation and medium stabilizes the particle suspension, which prevents aggregation of small particles. The factor C (medium) has zero % contribution on crystallite size, which attributes that crystallites are the sub-units of an individual particle and the medium does not influence directly the crystallite size. These results are complementary to the ranks of the response-means table (**Table 6.3**) discussed in **Section 6.1.5**.

Fig. 6.4a and **c** shows the SEM and FESEM micrographs of fresh FA. The fresh FA particles consist of solid spheres, hollow spheres (cenospheres), and irregularly shaped particles of unburnt carbon with a wide range of size distribution (**Fig. 6.4a**). The combustion temperature and cooling rate of the furnace determine the morphology of the FA particles. Smaller FA particles are adhering to the surface of large FA spheres as shown in the FESEM micrograph (**Fig. 6.4c**), which is due to the inter-particle fusion during rapid cooling. **Fig. 6.4b** and **d** shows the SEM and FESEM micrographs of the MCA-FA obtained by the factors and levels at A3B2C3D2. The rigorous impact and shear forces acting on the FA particles during mechano-chemical activation results in fractured FA particles of irregular shape and rough surface texture. **Fig. 6.4(e–f)** shows the TEM images of MCA-FA particles obtained by the factors and levels at A3B2C3D2 at different magnifications. Both these images complement the SEM and FESEM results of MCA-FA (**Fig. 6.4b** and **d**). The Image-J tool [Friel 2000] was used for the measurement of particle size distribution from these FESEM images of MCA-FA particles (**Fig. 6.4g**). Diameter of an individual particle was an average of 5

measurements taken along the particle axis. A normal distribution curve was fitted as a Gaussian function for the statistical histogram of the particle sizes in the nanometer range. The sizes of the majority of particles lie in the range of 320-380 nm, which is in line with the DLS results.
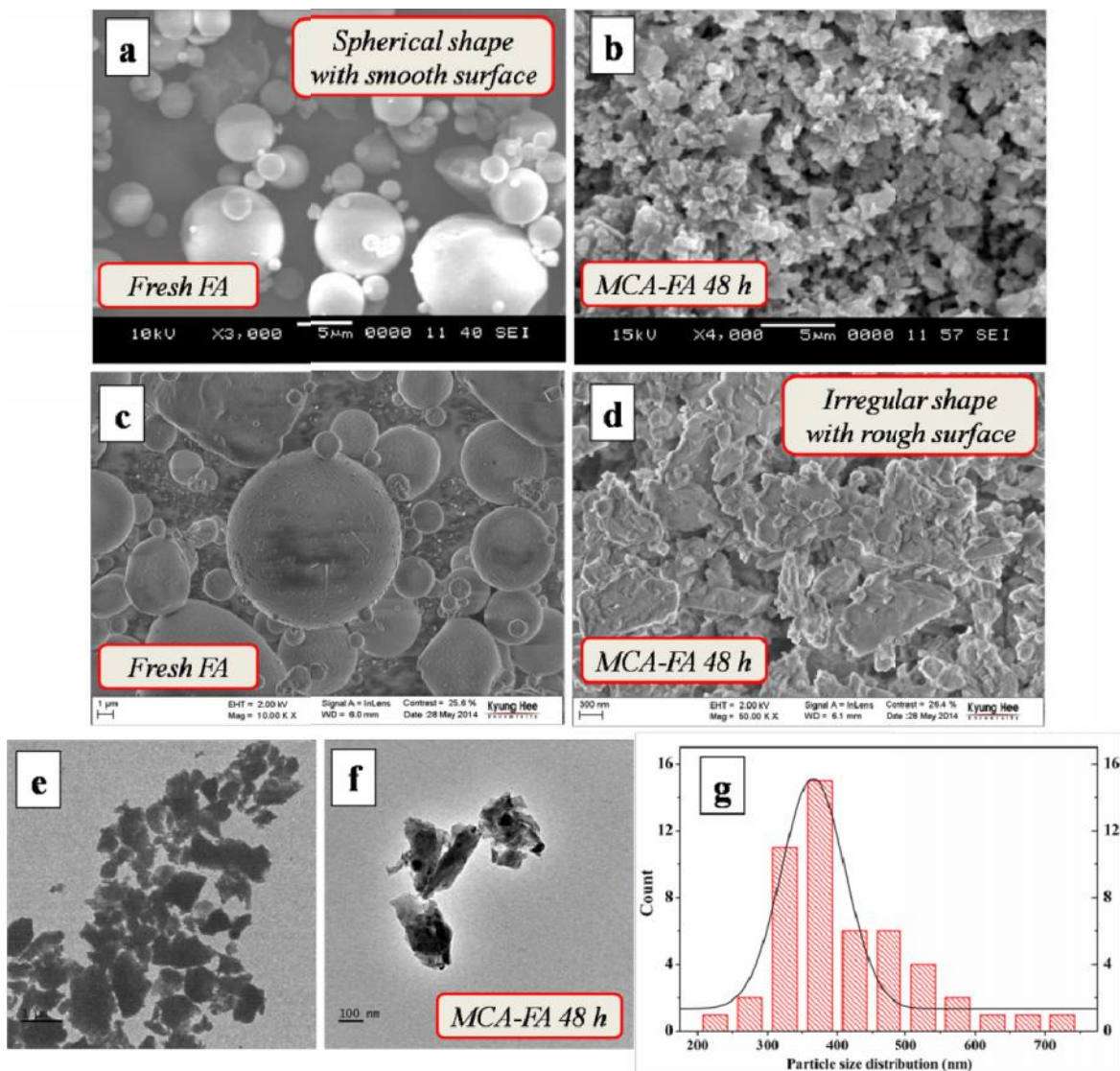
Fig. 6.4 SEM images of (a) fresh FA and (b) MCA-FA; FESEM images of (c) fresh FA and (d) MCA-FA; TEM images of MCA-FA (e and f) and (g) particle size distribution of MCA-FA

Table 6.4 Analysis of variance (ANOVA) of crystallite size, average particle size and specific surface area

Factors	Sum of square (SS)	Degree of freedom (DOF)	Mean square (MS)	Test F	F	P (%)
(a) Crystallite size						
B:P ratio	62.97	2	31.48	41.2	8.022**	48.26
Surfactant type	39.85	2	19.93	26.0	8.022**	30.10
Surfactant quantity	17.37	2	8.69	11.4	8.022**	12.44
Medium	0.25	2	0.12	0.157	-	0
Error	6.88	9	0.76			9.2
Total	127.32	17				100.00
(b) Average particle size						
B:P ratio	118824	2	59412	35.5	8.022**	35.20
Surfactant type	81241	2	40620.5	24.3	8.022**	23.74
Medium	79478	2	39739	23.8	8.022**	23.21
Surfactant quantity	33430	2	16715	10	8.022**	9.2
Error	15046.50	9	1671.83			8.7
Total	328019.5	17				100.00
(c) Specific surface area						
B:P ratio	39.87	2	19.95	35.6	8.022**	56.61
Surfactant type	13.35	2	6.67	11.9	8.022**	17.86
Medium	8.01	2	4.01	7.2	5.714*	10.1
Surfactant quantity	2.19	2	1.10	1.96	1.93$^{\#}$	1.56
Error	5.03	9	0.56			13.90
Total	68.45	17				100.00

** 99 % confidence; * 97.5 % confidence; # 80 % confidence

6.2 INTERPARTICLE INTERACTIONS AND LACUNARITY OF MECHANO-CHEMICALLY ACTIVATED FLY ASH
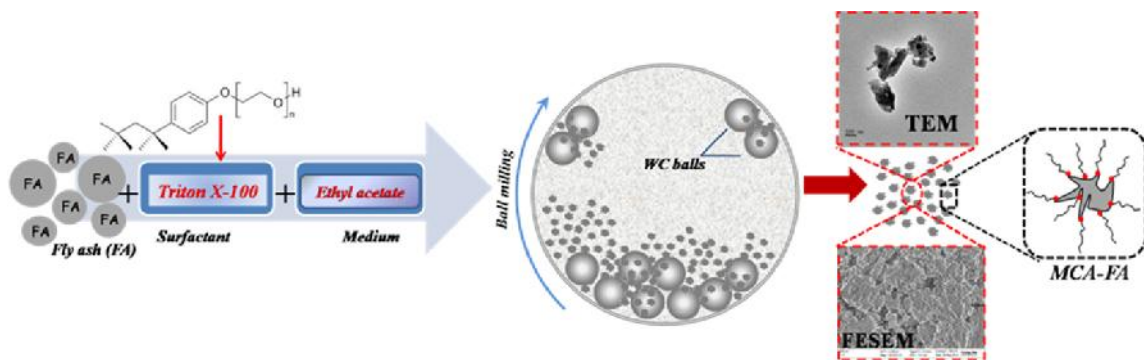
Scheme 6.2 The best combination of the factors and level for mechano-chemical activation of FA

This section discusses the detailed characterization of the MCA-FA, as one of the best combination of the factors and level of Taguchi design that resulted in lower crystallite size and average particle size and higher specific surface area, respectively. The decrease in crystallite size of MCA-FA was confirmed from a reduction in peak intensity by x-ray diffraction studies. x-ray photoelectron spectroscopic characterization illustrated that peak area of major elements (O, Si and Al) increased after milling. Morphological and FTIR studies revealed that the smooth and inert surface of the fresh FA was converted to a rough and more reactive one after mechano-chemical activation. The surface modification of FA with the surfactant was determined by dynamic contact angle measurements. Also, a fractal approach was used to characterize the lacunarity of the agglomerates in the MCA-FA.

6.2.1 Effect of mechano-chemical activation

6.2.1.1 XRD results

Dispersion and aggregation are regarded to be the two main processes taking place during grinding of solids [Fadda et al. 2009]. It has been proposed that at the first stage of grinding, dispersion is expected to be dominant, indicating a decrease in the crystallite size of the raw material. In order to study the crystallinity of the fresh FA and MCA-FA,

their XRD patterns were analyzed using X'pert High Score software. MCA-FA exhibited a number of crystalline peaks in the diffractogram even after 48 h of milling (**Fig. 6.5**); however, their intensities were diminished compared with that of fresh FA.
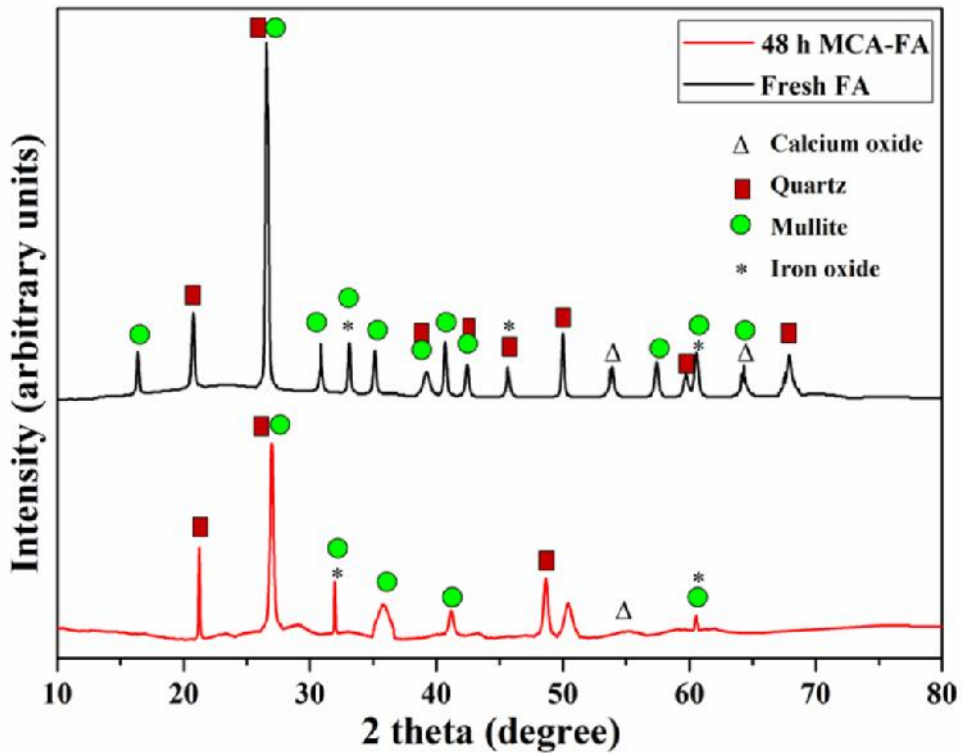
Fig. 6.5 XRD patterns of fresh FA and 48 h MCA-FA

The average crystallite sizes of the quartz phase present in the fresh FA and MCA-FA were determined using Scherrer's formula given **chapter 2 equation no. 2.3**. During high-energy milling, high stresses exerted on FA by the milling medium damage the crystalline structure causing the fragmentation of crystallites and the formation of amorphous segments as observed from the changes in the diffraction peaks at 2 values in the range of 14° to 35° (**Fig. 6.5**). It can be clearly observed that the peak intensities of quartz phase are reduced considerably and the peaks broaden after 48 h of milling. The crystallite size of the quartz phase present in fresh FA was 28 nm, which was reduced to 7.7 nm after 48 h of milling. The broadening of the peak is due to the existence of residual stress in MCA-FA, which results in lattice distortions of quartz crystallites. It can

be concluded that the crystalline structure exhibited a lower degree of crystallinity after 48 h of milling with the amorphous phase in the background.

6.2.1.2 Particle size analysis

The reaggregation of particles is a major concern with the ball milling process, which significantly increases the particle size of MCA-FA. The effects of mechano-chemical activation on the particle size of fresh FA samples are depicted in **Fig. 6.6**, representing the variation in particle diameter with respect to intensity distribution. D_{10}, D_{50} and D_{90}, which represent the average particle sizes (by volume and by number) below which 10%, 50% and 90% of their population lies, respectively, were obtained from the distribution curve.
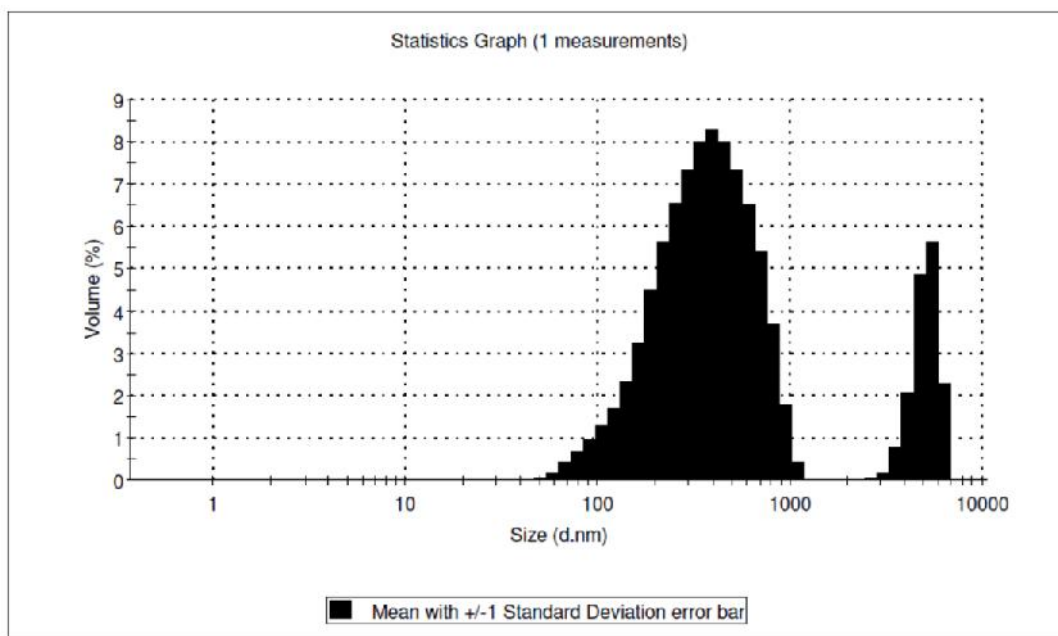
Fig. 6.6 Particle size distributions of MCA-FA

Mechano-chemical activation for 48 h caused the reduction in particle size of sieved FA (D_{50}) from 79.4 µm to 329 nm. The particle sizes at D_{10}, D_{50} and D_{90} of fresh FA and MCA-FA were obtained from DLS results and are shown in **Table 6.5**. The reduction in particle size is due to the proper milling conditions in the presence of ethyl acetate and the surfactant. Wet grinding is advantageous as it provides higher energy

efficiency, lower magnitude of excess enthalpy and the elimination of dust formation. Vigorous milling for 48 h leads to tremendous stress energy being imparted on the FA particles, resulting in massive strain in the particles. These results provide evidence supporting that more plastic deformation and disordering of the FA particles occur under intensive grinding resulting in nanoscale dimensions [Yan et al. 2010].

Table 6.5 DLS results showing particle sizes of fresh FA, sieved FA and MCA-FA

Samples	D_{10}	D_{50}	D_{90}
Fresh FA	23.2 μm	36.5 μm	58.4 μm
Sieved FA (-170# +200#)	43.2 μm	79.4 μm	99.9 μm
MCA-FA for 48 h	220 nm	329 nm	955 nm

6.2.2 Interaction between MCA-FA and surfactant

6.2.2.1 Specific surface area

Mechano-chemical activation of FA is represented schematically in **Scheme 6.1** along with the structure of surfactant used in this study. The high-energy milling process was carried out in the presence of the non-ionic surfactant to stabilize the particle suspension and prevent the aggregation of small particles, which resulted in a specific surface area value of 8.73 m^2 g^{-1} for MCA-FA. The two plausible reasons of dispersion and aggregation of the solid particles during grinding are as follows: dispersion is dominant as the collision frequency increases between particles and grinding media. Second, the increased collision probability of particles would induce cold welding to occur at the particle contacts during the milling operation. The driving forces for agglomeration are Brownian motion and fluid motion. Agglomerates are formed when particles overcome the interparticle energy barrier as the total surface area decreases [Ding et al. 2009 and Sakthivel et al. 2008].

6.2.2.2 FTIR spectroscopy

The FTIR spectra of the surfactant, fresh FA and MCA-FA are shown in **Fig. 6.7**. The spectrum of the surfactant shows O-H stretching band at 3412 cm^{-1}. The bands at 2951

and 2871 cm^{-1} correspond to asymmetric CH_2 stretch and symmetric CH_2 stretch, respectively. The symmetric stretching bands of benzenoid group vibrations are observed at 1610 cm^{-1} and 1512 cm^{-1} [Ghorabi et al. 2012]. The absorption band near 1120 cm^{-1} is related to the stretching vibrations of the ether C-O groups of the surfactant.
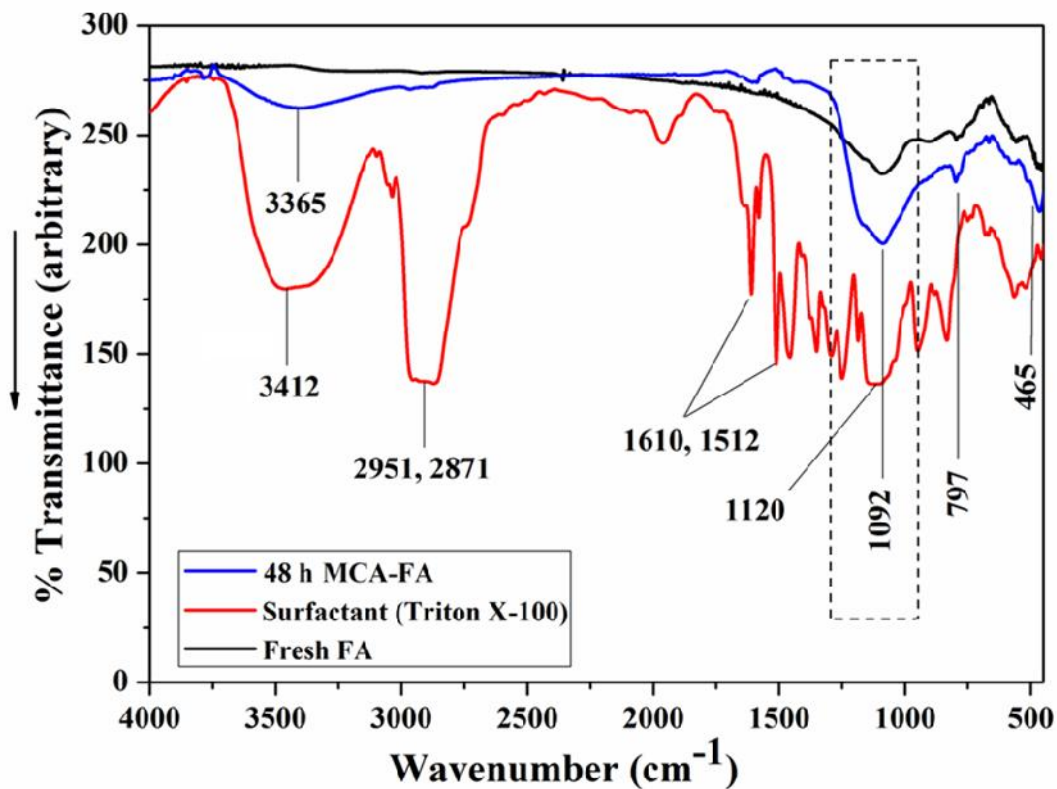
Fig. 6.7 FTIR spectra of TX-100, fresh FA and MCA-FA

FTIR spectrum of fresh FA shows characteristic stretching vibration bands at 1092, 797 and 465 cm^{-1}. The strong broad band at 1092 cm^{-1} can be related to Si-O-Si asymmetric stretching vibration, while the 797 cm^{-1} band can be related to Si-O-Si symmetric stretching vibration [Paul et al. 2007] as well as AlO_4 vibrations. The Si-O-Si bending is observed at 465 cm^{-1}. The peak at 1092 cm^{-1} has broadened and its intensity has increased for 48 h MCA-FA as compared to fresh FA, which is due to the interaction of ether C-O groups of the surfactant and Si-O-Si stretching of FA. The surfactant, TX-100, consisting of an alkyl substituted aromatic ring and a long polyether chain having an -OH terminal group, seems to form a stronger interaction with the surface of MCA-FA

through the -OH groups. The peak at 3365 cm^{-1}, which is insignificant in the fresh FA, becomes conspicuous in cases of MCA-FA; this is because of the interaction of the O-H stretching band of TX-100 with that of MCA-FA.

6.2.2.3 Contact angle measurements

The merit of using mechano-chemical activation for improving bulk and surface reactivity of metal and ceramic powders has been well accepted [Kumar and Kumar 2011]. It offers the possibility to alter the reactivity of solids through physicochemical changes in bulk and surface without altering the overall chemistry of the material. The surfactant molecules form protective layers on the surfaces of FA particles during the ball milling process, in such a way that the polar heads of the surfactant molecules orient towards the surfaces of FA particles and the non-polar tails orient themselves away from the FA surface. The structure of the MCA-FA particle can hence look like an inverse micelle in which the FA particle surrounded by the polar heads form the core and the non-polar tails form the outer shell as shown in the proposed model (**Scheme 6.1**).
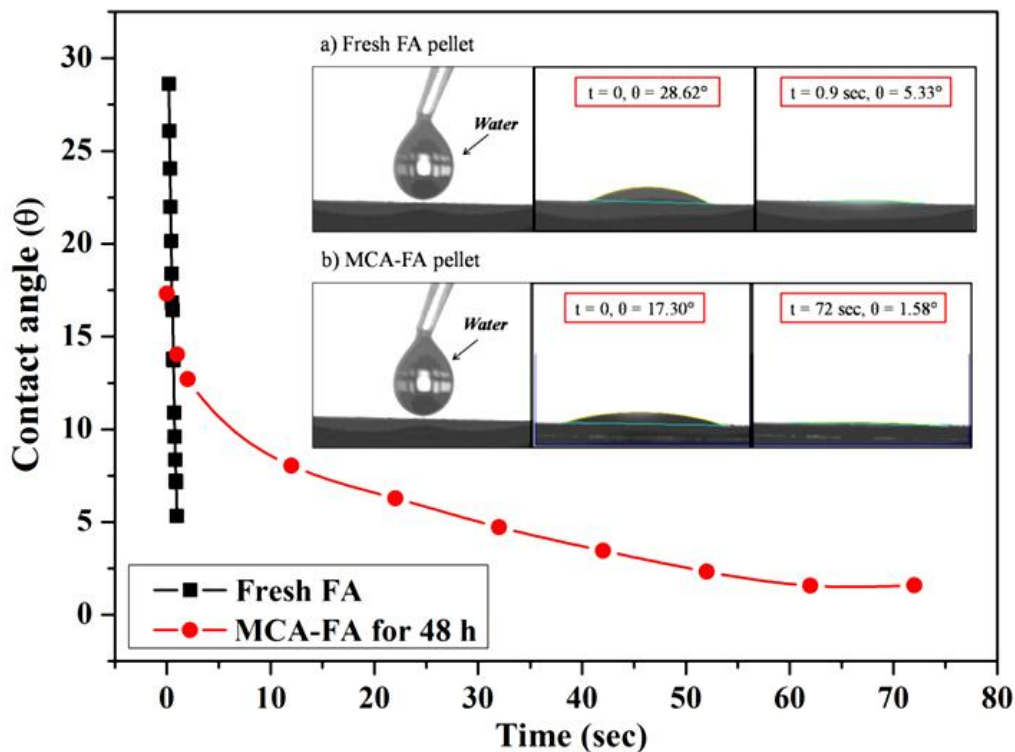
Fig. 6.8 Static contact angle measurements on fresh FA and MCA-FA pellets with water

From **Fig. 6.8**, it can be observed that fresh FA pellet is easily wetable by water. The wetability of MCA-FA by water is somewhat less considering the three processes that occur during adsorption of non-ionic surfactant: monomer diffusion, micellar diffusion and micellar dissociation [Paria and Khilar 2004]. The initial increase in adsorption for pre-micellar solution is linear with time. The critical micelle concentration (CMC) of TX-100 at 25 °C is 0.2 mM. At this CMC, the interface in MCA-FA becomes saturated, which forms micelles. These micelles introduce steric repulsive forces and disentangle agglomerates of MCA-FA. As the concentration of the surfactant increases above the CMC, the amount of water adsorbed on the surface of MCA-FA pellet approaches the plateau value; the adsorption rate begins to decrease and finally becomes zero, as shown in **Fig. 6.8a and b**.

6.2.2.4 XPS results
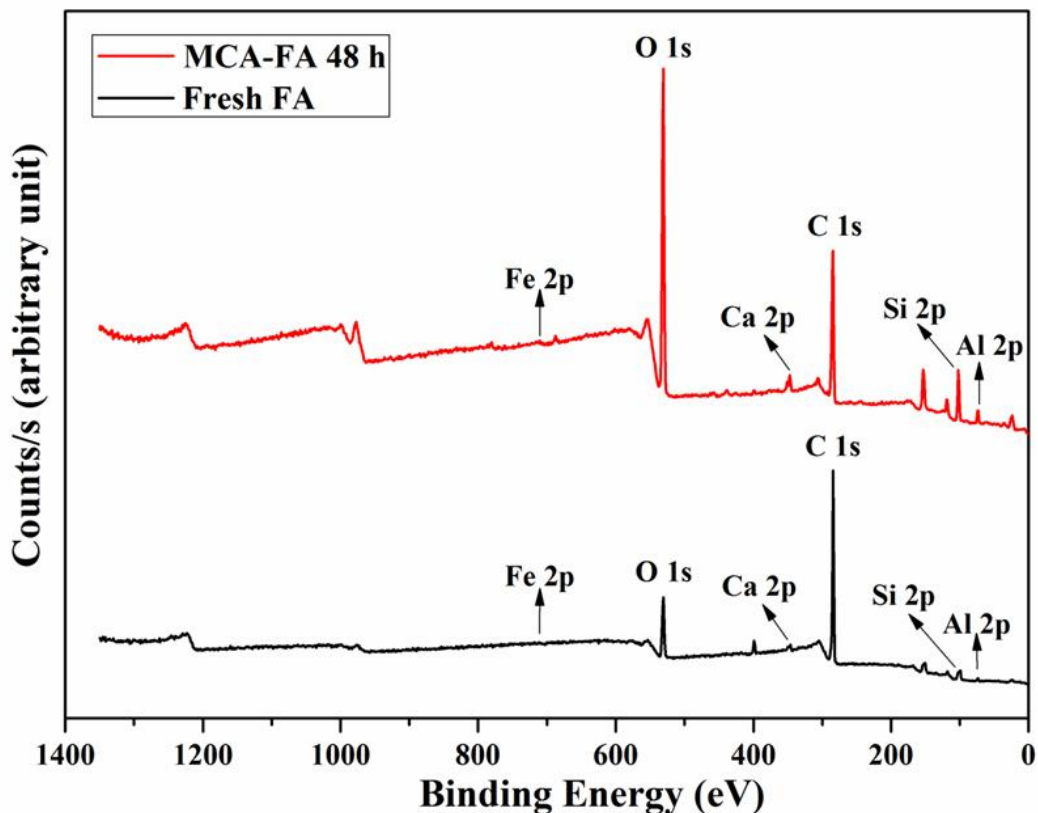
Fig. 6.9 Wide scan XPS spectra of fresh FA and MCA-FA

XPS analysis was carried out to further understand the changes in the chemical states of several typical elements of the FA particles before and after mechano-chemical activation. The wide scan XPS spectra of fresh FA and MCA-FA are shown in **Fig. 6.9**. From these spectra, one can see that the primary components of the near-surface region are oxygen, carbon, silicon, iron, calcium and aluminum. Other elements, such as sodium and potassium, are not significantly observed because of their weak binding energy signals. The chemical speciation of the elements was obtained from the high-resolution spectra of the core levels of C 1s, O 1s, Si 2p and Al 2p. Each measured XPS spectrum was fitted using Gaussian cross-product function after subtracting the background by an inelastic Shirley method. Upon deconvolution, the binding energy of each peak varied in the range of ±0.5 eV to obtain the optimum curve resolution.

Quantitative analysis (in atomic percentage, at.%) by XPS was used to determine the relative concentrations of the constituents of the fresh FA and MCA-FA samples. This was done by measuring the area under the peak using **equation** (**6.1**) [Shanmugharaj et al. 2002]:

$$C_j = \frac{A_i S_i}{\sum_j^m A_j S_j} \tag{6.1}$$

where A_i is the area under the peak of element "i", S_i is the sensitivity factor of element "i", m is the number of elements in the sample and i and j represent the elements. The atomic percentages of C, O, Si and Al are given in **Table 6.6**.

Deconvoluted peak assignments with corresponding theoretical binding energy and bond type for high-resolution XPS scan and their at.% are reported in **Table 6.6**. **Figs. 6.10**(**a-d**) and **6.11** (**a–d**) shows the assignment of deconvoluted high-resolution XPS peaks of C, O, Si and Al in fresh FA and MCA-FA, respectively. The carbon peak binding energies are located around 284.5 eV, as shown in **Fig. 6.10a**. Deconvolution of the carbon peak reveals the presence of C=O groups (287.5 eV), C-O groups (284.8 eV), C-C groups (284 eV), Fe_3C groups (283 eV) and Ca_2C (282.5 eV) in fresh FA (**Fig. 6.10a**) [Yao et al. 2013 and Xu et al. 2013]. There was a decrease in the peak intensity

and at.% of carbon-containing groups from 75.58% to 38.16% for MCA-FA (**Figs. 6.10a**, **6.11a** and **Table 6.6**). This attributes to the pre-treatment of FA, which was washed with distilled water to remove the carbon that creamed up on the surface. However, the presence of carbon was still due to the addition of surfactant during milling process. The Fe_3C group was not observed in MCA-FA, which confirms the efficient magnetic separation of iron oxide.

Table 6.6 XPS results

Elements	Type of photoelectron	Binding energy (eV)		ASF	Atomic %	
		Fresh FA	MCA-FA		Fresh FA	MCA-FA
C	1s	284.5	284.5	0.25	75.58	38.16
O	1s	531.01	531.27	0.66	13.36	41.53
Si	2p	99.31	101.91	0.27	7.7	13.74
Al	2p	73.63	73.55	0.185	2.89	6.54

Oxygen (O 1s) peaks of fresh FA and MCA-FA are shown in **Figs. 6.10b** and **6.11b**, and the peak positions are shown in **Table 6.6**. Upon deconvolution, the peak maxima occur at around 531.01 eV and 531.27 eV for fresh FA and MCA-FA, respectively [Zhang et al. 2014 and Oliveira et al. 2014]. The presence of more -OH groups leads to higher peak intensity and at.% of oxygen for MCA-FA, which attributes to its high surface reactivity.

Figs. 6.10c and **6.11c** are the deconvoluted high-resolution XPS peaks of silicon, corresponding to four types of oxidation states of Si, i.e., Si^0, Si^{2+} (SiO), Si^{3+} (Si_2O_3) and Si^{4+} (SiO_2) [Ghita et al. 2011]. There is an increase in at.% of silicon from 7.7 to 13.74 for MCA-FA. In case of MCA-FA, the Si peak at 101.9 eV corresponds to either Si-OH or Si-O-Si bonds. Also, a similar observation was made for Al, as the content of aluminol (Al-OH) at 73.5 eV and the (Al-O) bond is quite low in Al atoms of MCA-FA (**Figs. 6.10d** and **6.11d**) [Mollah et al. 1994].
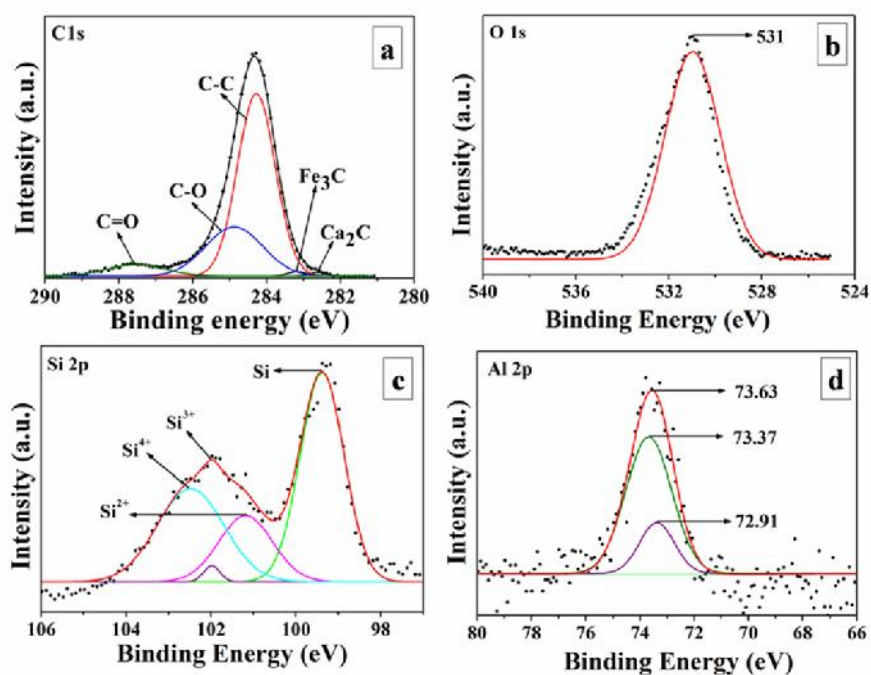
Fig. 6.10 Deconvoluted high resolution spectra of the core levels for fresh FA (a) C 1s (b) O 2s (c) Si 2p (d) Al 2p
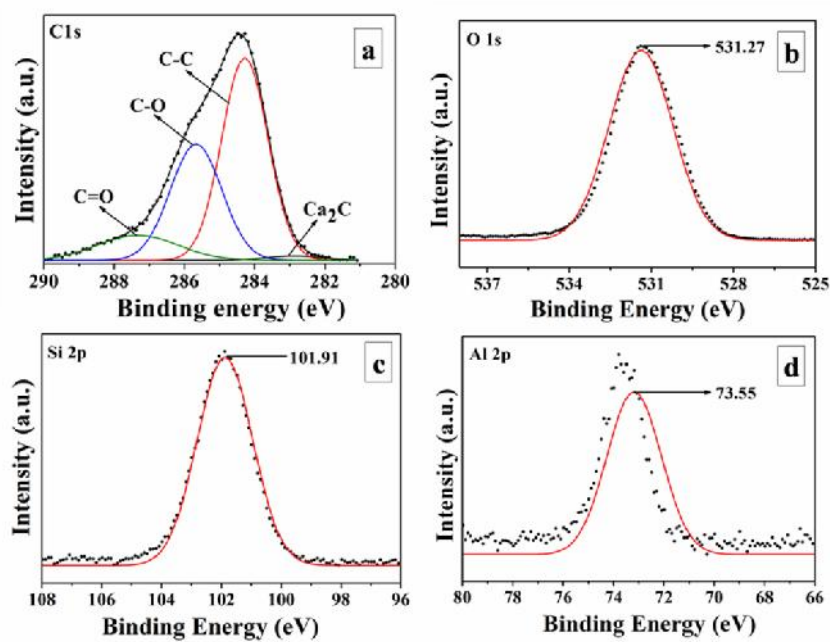
Fig. 6.11 Deconvoluted high-resolution spectra of the core levels for MCA-FA (a) C 1s (b) O 2s (c) Si 2p (d) Al 2p

102

6.2.3 Fractal dimensions of MCA-FA by image analysis of electron micrographs

As broadly reported in the literature, a ball mill is a complex system with many parameters that influence the process of grinding. In general, milling speed is chosen to achieve a steady state between the fracturing and cold welding mechanisms. Very low rotational speeds lead to increased periods of milling, thereby inducing a large inhomogeneity in the powder due to inadequate kinetic energy input and insufficient localized heat input [Chen et al. 2007]. Conversely, very high speeds can lead to excessive heating of the vessel, high wear of the balls causing increased contamination, and lower powder yields. The milling was carried out for 48 h at 250 rpm as per the optimum rotational speed of the mill, which was determined using **equation 2.1 chapter 2**.

The spherical particles of fresh FA with smooth glassy surfaces are shown in **Fig. 6.12a**. During high-energy ball milling process, the minimal particle size reachable is often limited by a process of agglomeration or compaction of product particles. The agglomerates of MCA-FA are composed of contacting primary particles (**Fig. 6.12b**). The primary particles are disposed in the agglomerate as irregular clusters, with different sizes, compactness and apparent densities as shown in **Fig. 6.12d**. Since agglomerates are considered as fractal-like structures, it is acceptable to quantify their irregularities with the fractal dimension (**D_f; Fig. 6.12c**) as originally proposed by Mandelbrot [Mandelbrot 1982 and Martínde et al. 2014]. The number of primary particles in the agglomerate (n) can be theoretically estimated from the fractal geometry given in **equation 6.2**.

$$n \approx \left(\frac{R_a}{a} \right)^{D_f}$$

(6.2)

Where R_a is the radius of the agglomerate, a the radius of the particle and D_f is the fractal dimension. This study focused on the agglomerates of nanoparticles having a fractal structure with a fractal dimension D_f close to 2.5, in agreement with the diffusion-limited agglomeration (DLA) model. However, in certain processes, such as agglomeration due to dipole-dipole interaction in the presence of externally applied magnetic or electric

fields, the agglomerates can adopt anisotropic shapes with a fractal dimension differing from the DLA value.
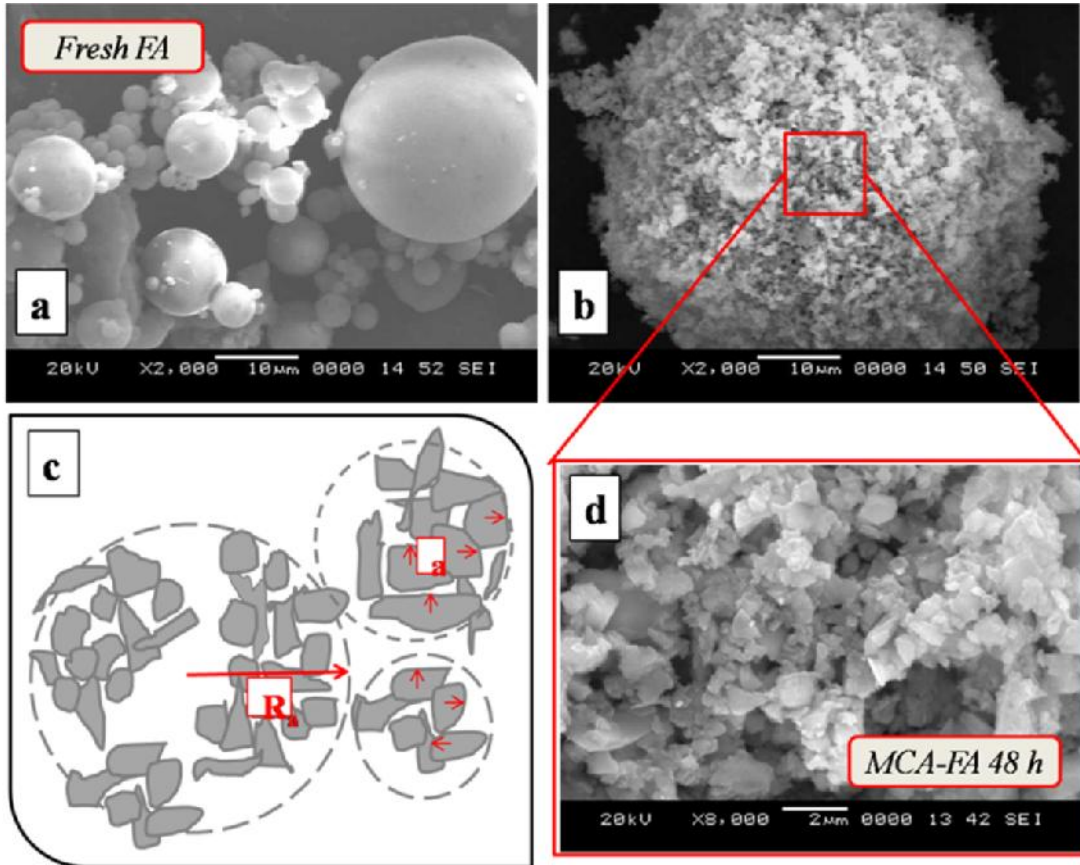
Fig. 6.12 Scanning electron micrographs of (a) fresh FA, (b) particle agglomerate of MCA-FA, (c) diffusion-limited particle-cluster agglomerate ($D_f = 2.5$), and (d) MCA-FA at 8000×

The $D_f = 2.5$ in the diffusion-limited particle–cluster agglomerate [Lapuerta et al. 2006], when the values of $a = 1$ μm to 0.1 μm and $R_a = 25$ μm were inserted in **equation 6.2**. An estimate of 3000 to more than 10, 00,000 primary particles in the cluster assembly has been made, even though the mechanical energy involved in the ball milling process is apparently critical to the breakage of large-sized FA agglomerates. Again, the milled fine agglomerates with a reduced cluster size are suspected to reagglomerate favorably during the multiple collisions of particles in the milling process [Stellacci et al. 2009]. This, in turn, prohibits a continual decrease in the mean agglomerate size as the

milling time is extended. However, mechano-chemical activation has greatly enhanced the reactivity of the solid particles as proven by the XPS results, resulting in the lacunarity of MCA-FA. In the case of nanostructured agglomerates, the structure of the particles has a direct impact on handling the final product with desired properties. Hence, this study provides an insight into the morphological changes of FA upon high-energy ball milling.

6.3 CONCLUSIONS

Using the Taguchi method, the influence of individual factors of the planetary ball milling process on the mechano-chemical activation of FA was evaluated. The results suggest that A3B2C2D2, A3B2C3D2 and A1B1C3D2 were the best possible factors and levels for lower crystallite size and average particle size and higher specific surface area, respectively. The factors such as ball-to-powder weight ratio and surfactant type rank 1st and 2nd, respectively, emerging as the most significant factors for all the response. According to the ANOVA results the two major contributing factors were ball-to-powder weight ratio and surfactant type at 99% confidence.

The MCA-FA developed in this study has shown a major improvement in properties, whereas the agglomeration of the nanoparticles was of a major concern. The high-energy ball milling-aided mechano-chemical activation of FA resulted in an average particle size of 329 nm and specific surface area of 8.73 m^2 g^{-1}. The crystallinity and crystallite size of FA decreased after the high-energy milling. The surface modification of MCA-FA by the physisorbed non-ionic surfactant was confirmed by FTIR spectroscopy, XPS and contact angle measurements. The surfactant layer formed on the MCA-FA surfaces aided in preventing the reagglomeration of its particles. Image analysis confirms the lacunarity of the MCA-FA particles, which is due to the increased reactivity of MCA-FA. XRD results reveal a reduction in crystallinity of FA upon high-energy ball milling, which might aid in improved compatibility of MCA-FA with polymer matrices. The nanostructured FA obtained by this method has a wide application potential in polymer industries as reinforcement in composites.

CHAPTER 7

CHAPTER 7

BIODEGRADABLE CHITOSAN COMPOSITES REINFORCED WITH NANOSTRUCTURED FLY ASH

This chapter outlines the preparation and characterization of chitosan (CS) composites reinforced with fresh FA and MCA-FA. The fractography of the composites was used evaluate the texture and morphology. It revealed that fresh FA with smooth surface and spherical in shape resulted in debonding and void formation in the composites. The irregular and rough surface of MCA-FA showed better distribution at lower filler loading. The key parameters for enhancement of the mechanical properties and compatibility between MCA-FA and matrix were interfacial adhesion, polymer-filler interlocking and the morphology of filler. There was a marginal change in thermal properties of CS composite with fresh FA and MCA-FA.

7.1 RESULTS AND DISCUSSION

7.1.1 Characterization of CS/fresh FA and CS/MCA-FA composites

7.1.1.1 Film solubility and swelling behavior

The film solubility and swelling behavior of CS/fresh FA and CS/MCA-FA are calculated using the **equation no. 2.7** and **2.8**, given in **chapter 2**, respectively. The results of it are shown in **Fig. 7.1**. Film solubility increases for CS/fresh FA composites with increase in filler content, this attributes to the presence of voids in the composites due to debonding between filler and matrix. These voids make an easy path way for the water to enter through the micro-cracks of the composite. The CS/MCA-FA has lower film solubility in comparison with CS/fresh FA composites. This justifies a more rigid network formed between polymer chains of the CS matrix and MCA-FA. This reduces the flexibility and number of hydrophilic groups of CS/MCA-FA composites, which is

unfavorable for the film solubility. There was no major change observed in the swelling behavior of CS/fresh FA and CS/MCA-FA composites. This is due to the cross-linking of composites with GA and physical entanglement of the CS chains with filler resulting in a lower swelling rate [Casariego et al. 2009].
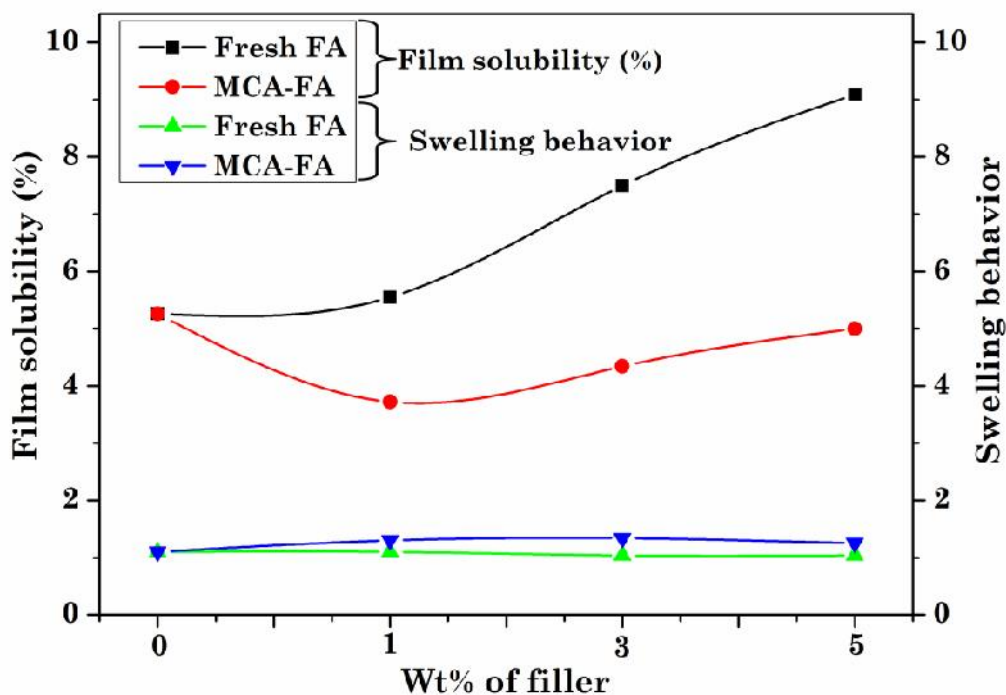
Fig. 7.1 Film solubility and swelling behavior of CS composites with 1, 3 and 5 wt% of filler content

7.1.1.2 FTIR spectroscopy

Fig. 7.2a and **b** shows the comparative study of neat CS along with the composites containing 1, 3 and 5 wt% of fresh FA and MCA-FA, respectively. CS being a hydrophilic biopolymer has three kinds of functional groups such as amino, primary hydroxyl and secondary hydroxyl groups in a glucosamine unit. For neat CS (**Fig. 7.2a** and **b**), the characteristic bands are assigned to O-H stretching and amine N-H at 3350 cm^{-1}. The low intensity peak at 2900 cm^{-1} accord with methylene (-CH$_2$) stretching. The 1650 cm^{-1} was assigned to C=O stretching of amide I and 1570 cm^{-1} was due to amine NH$_2$ bend [Yamaguchi et al. 2001]. Saccharide structure at 1150 and 890 cm^{-1} was

observed by bridge O-stretch and pyranoid ring stretch, respectively. The sharp peaks at 1060 and 1020 cm^{-1} were of C-OH stretching [Ge and Wang 2014].
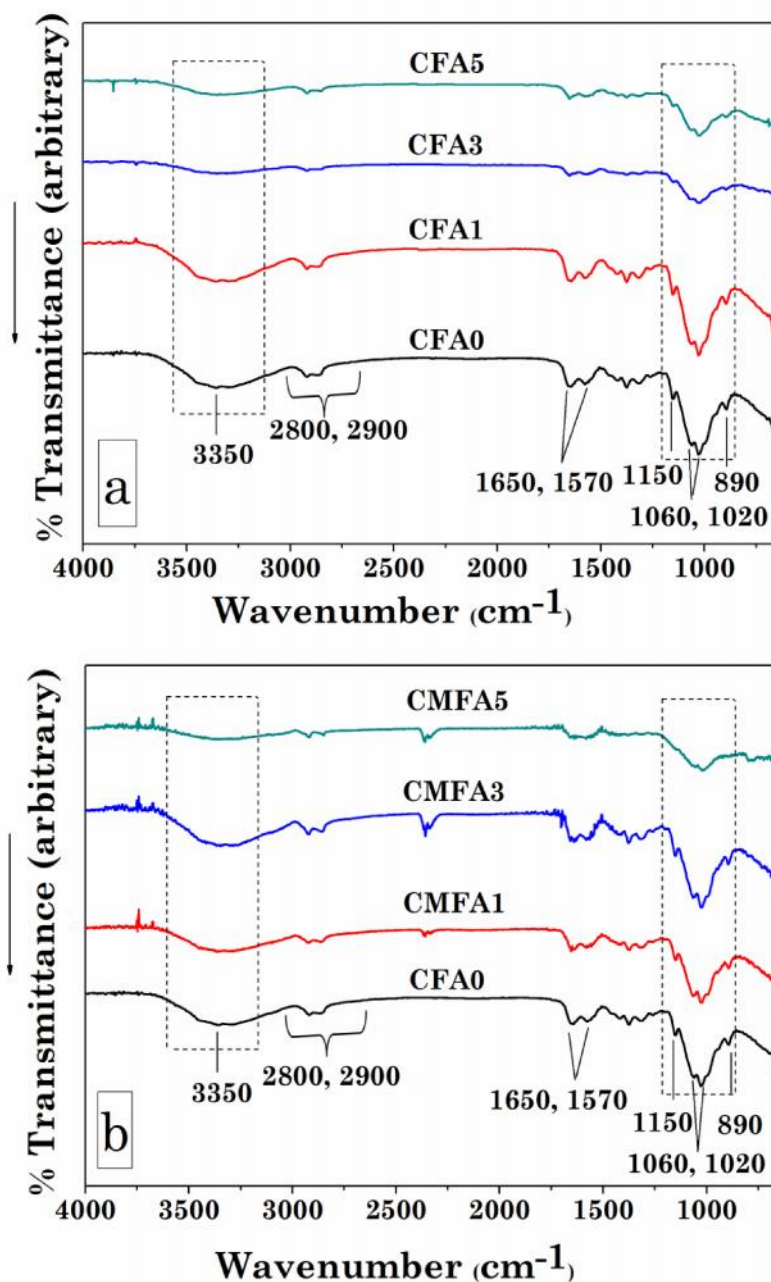
Fig. 7.2 FTIR spectra of neat CS and CS composites with 1, 3 and 5 wt% of (a) fresh FA and (b) MCA-FA

Crosslinking of CS with glutaraldehyde imparts a higher internal network with the CS backbone. The additional peak at 2800 cm^{-1} corresponds to C-H stretching vibrations related to aldehydes of gultaraldehyde. The C=N bond of Schiff base of gultaraldehyde was overlapped with the C=O stretching of amide I at 1650 cm^{-1}.

The IR spectra of CS/fresh FA composites (**Fig. 7.2a**), exhibit a decrease in the intensity of the peak around 3350 cm^{-1} as the fresh FA content was increased. This may be attributed to a decrease in the concentration of free hydroxyl (-OH) and secondary amine (-NH) groups of CS on interaction with fresh FA. But more probable that fresh FA particle may interact among themselves through hydrogen bonding.

The incorporation of nano size MCA-FA has shown noticeable interaction with hydroxyl (-OH) and secondary amine (-NH) groups of CS (**Fig. 7.2b**). This may be due to the hydrophilic surfactant (TX-100) wrapped on the MCA-FA and the long polyethylene oxide chain anchored to CS matrix. Broadening of peaks was observed at 1060 and 1020 cm^{-1}, which signifies the interaction of C-OH stretching vibration with Si-O-Si stretching of MCA-FA. This in turn greatly enhanced interfacial adhesion and significantly increased the mechanical properties of the composites.

7.1.1.3 XRD results

The XRD patterns of neat CS, CS/fresh FA and CS/MCA-FA composites with the loading of 1, 3 and 5 wt% of filler are shown in **Fig. 7.3a** and **b**. The XRD pattern of CS reveals a low intensity crystalline peak at 2 value of 11.5° and a high intensity peak at 20.0° related to and crystal forms of CS. Also, predominant amorphous phase was observed due to broadening of the peaks ranging from approximately 15° to 25°.

According to literature [Ogawa et al. 1992; Costa-Júnior et al. 2009 and Ogawa et al. 2004], CS exhibits an orthorhombic unit cell of dimensions $a = 0.826$ nm, $b = 0.95$ nm and c (fiber axis) = 1.043 nm with 2-fold helical chains, which are stabilized by hydrogen bonds with the gauche-trans orientation. Hydrogen bonds are found between adjacent chains along the a-axis, which forms a parallel sheet structure to the ac-plane in absence of hydrogen bond between the sheets. CS usually exhibits a semi-crystalline structure due to free-energy balance caused by hydrogen bond formation.
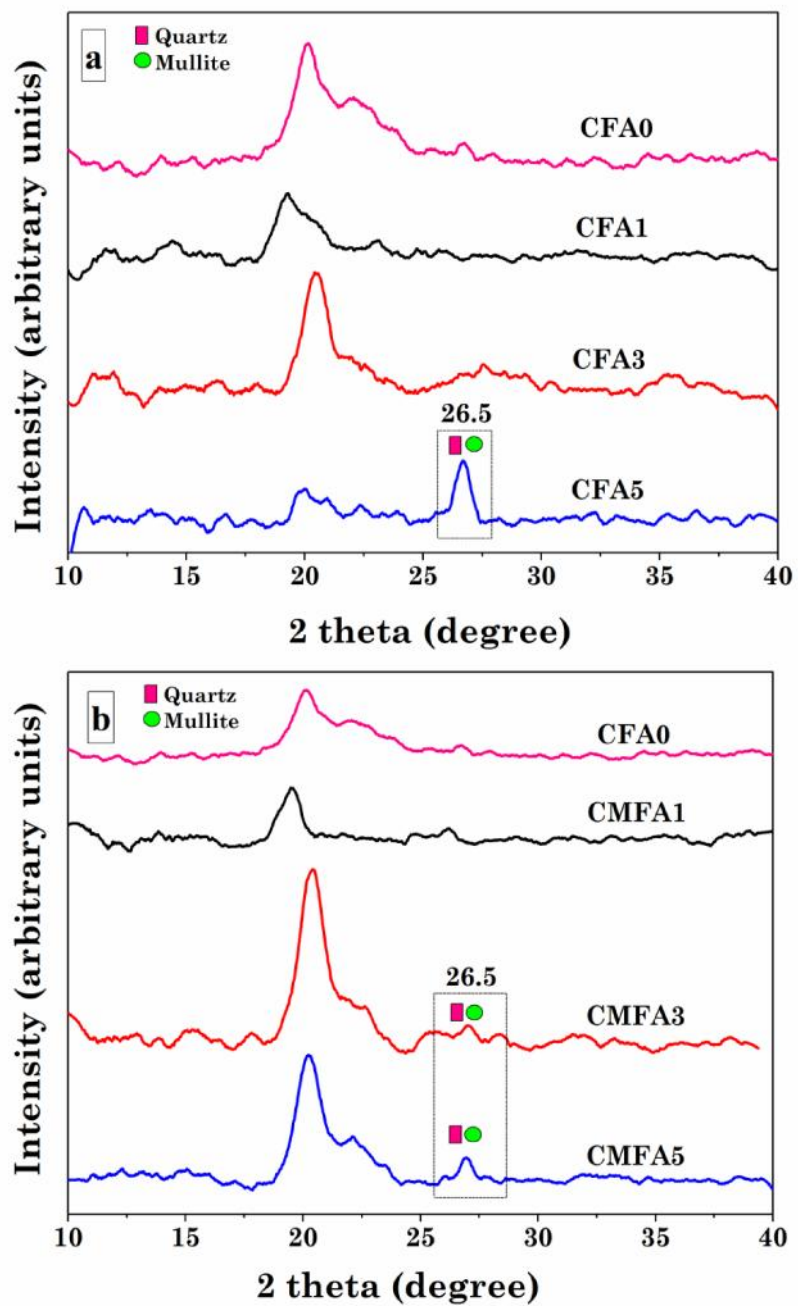
Fig. 7.3 XRD patterns of neat CS and CS composites with 1, 3 and 5 wt% of (a) fresh FA and (b) MCA-FA

The CS/fresh FA composites exhibits a prominent peak at 2 angle of 26.5° with the d-spacing of 3.4 Å at 5 wt% of filler loading (**Fig. 7.3a**), whereas it was not observed at 1 and 3 wt%. This peak corresponds to the mullite phase of FA ($3Al_2O_3.2SiO_2$) as analyzed by the X'Pert High Score Plus software (ref code: 00-002-0428). This has an orthorhombic crystal system with $a = 7.52$ Å, $b = 7.65$ Å and $c = 2.89$ Å. Similar pattern was observed for CS/MCA-FA composites at 3 and 5 wt% of filler loading (**Fig. 7.3b**), which signifies that interaction between MCA-FA and CS was possible at lower filler content. This may be due to the nano-sized particles and higher specific surface area of MCA-FA.

7.1.1.4 Mechanical properties and fractography of the CS composites

There are several parameters that affect mechanical properties of composites, such as `properties of polymer matrix, morphology and volume fraction of filler and interfacial bonding between filler and matrix.

The tensile stress-strain curves of the CS/fresh FA, CS/MCA-FA composites and their respective fractographs are shown in **Fig. 7.4(a-d)** and **Fig. 7.5(a-d)**. Mechanical properties of the CS/fresh FA and CS/MCA-FA composites tend to improve in comparison with that of neat CS. The neat CS film undergoes elastic deformation, yielding and necking without strain hardening [Justin and Chen 2014]. Like the most of the inorganic fillers, FA is hydrophilic in nature which tends to agglomerate and reduce tensile strength of the composites with increased filler loading. The incorporation fresh FA into CS matrix (**Fig. 7.4**) reduces the ductility and stiffens the composites. For CS/fresh FA composites the maximum tensile strength was observed at 1wt% of filler content, which gradually decreased at loading of 3 and 5 wt%. Crosslinking of CS with glutaraldehyde makes the film hard and brittle and the incorporation of the fresh FA at higher content has deteriorated the mechanical strength of the composites. **Fig. 7.4a** and **7.5a** reveals the morphology of neat CS to be rough woody texture. **Fig. 7.4b, c** and **d** show the fractographs of composites with 1, 3 and 5 wt% of fresh FA. The decrease in the tensile strength at 3 wt% filler loading attributes to dewetting, debonding and void formation (**Fig. 7.4c**) in CS/fresh FA composites. Similarly, at 5 wt% of filler content the

increased particle-particle interaction has reduced the strength of the composites (**Fig. 7.4d**).

Fig. 7.5 shows the higher tensile properties for CS/MCA-FA composites in comparison with that of CS/fresh FA composites. This attributes to the better mechanical interlocking between the filler particles and the CS, which was observed from the fractographs of the composites shown in **Fig. 7.5b, c** and **d**. The maximum tensile strength was observed at 1 wt% due to uniform distribution of filler throughout the matrix as shown in **Fig. 7.5b**. Some particle-rich clusters were observed at 3 and 5 wt% (**Fig. 7.5c** and **d**) of filler content, which in turn resulted in reduced tensile strength [Yan et al. 2006 and Kaully et al. 2008].
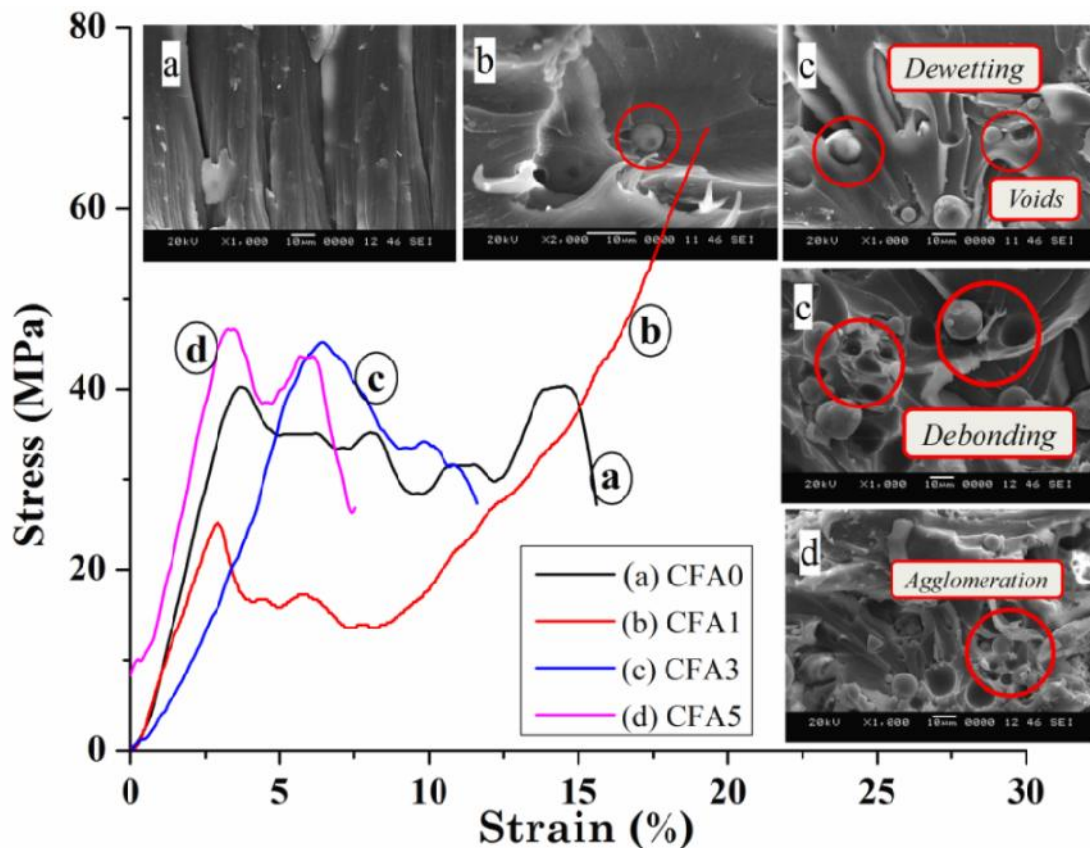
Fig. 7.4 Stress-strain graphs and fractographs of CS/fresh FA composites (a) neat chitosan (b) 1 wt% (c) 3 wt% and (d) 5 wt% of filler content

113
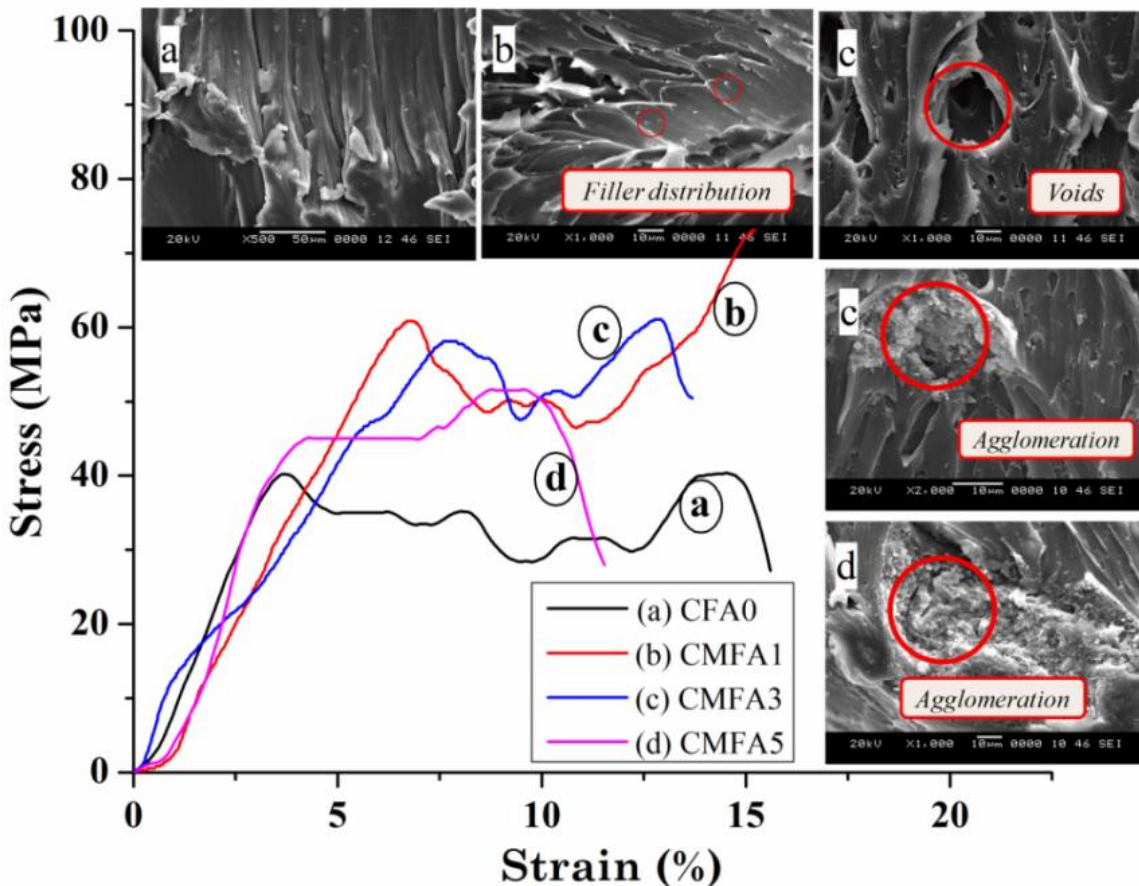
Fig. 7.5 Stress-strain graphs and fractographs of CS/MCA-FA composites (a) neat chitosan (b) 1 wt% (c) 3 wt% and (d) 5 wt% of filler content

Fig. 7.6a-b shows the bar chart of tensile strength and elongation at break of CS/fresh FA and CS/MCA-FA composites. The tensile strength of the composites of fresh FA and MCA-FA exceeds that of the neat CS film accompanied by a decrease in elongation at break (**Fig. 7.6a-b**). The maximum tensile strength was observed at 1 wt% of filler in both fresh FA and MCA-FA based composites. At higher filler content of 3 and 5 wt%, the mobility of the polymer chains is reduced between the particles causing dewetting of the fillers. This results in the formation of micro-cavities hindering the yielding of polymer matrix, which in turn increases the brittleness of the composites. Incorporation of MCA-FA showed higher tensile properties than fresh FA particles. The maximum strength was observed at 1 wt% of filler, due to stress transfer from the matrix

114

to the filler particles. The decrease in tensile strength at 3 and 5 wt% of filler is due to stress concentration caused by agglomeration of filler particles [Fu et al. 2008].
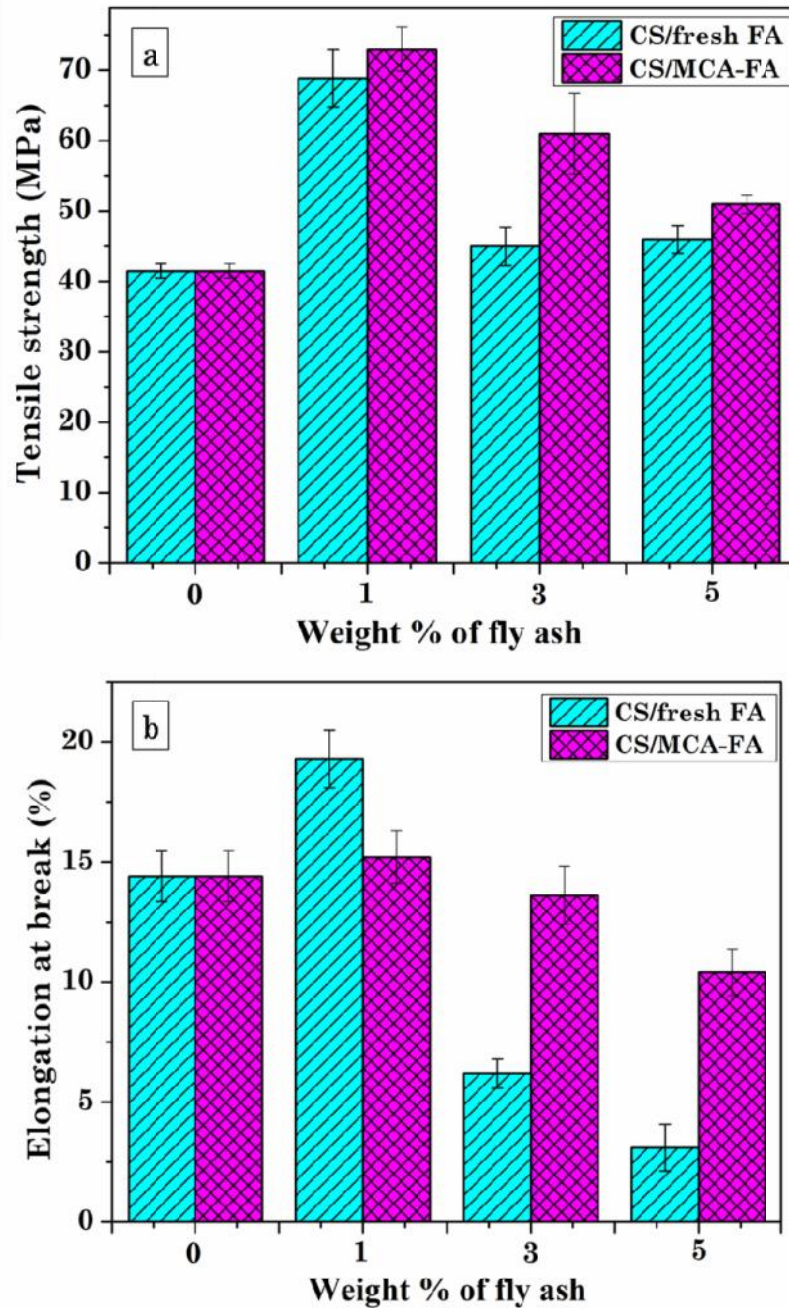
Fig. 7.6 Variations in mechanical properties of CS/fresh FA and CS/MCA-FA composites as a function of wt% of filler (a) tensile strength, (b) elongation at break

The experimental data of tensile strain variation as a function of volume fraction of filler were analyzed using Nielsen's [Nielsen 1966] model for CS/fresh FA and CS/MCA-FA composites using **equation 2.5 of chapter 2** shown in **Fig. 7.7** (**a-b**).

The theoretical values of elongation at break of the composites from **equation 2.5** were compared with the experimental ones. There was a deviation between experimental and theoretical values for the CS/fresh FA composites (**Fig. 7.7a**). The theoretical values gradually decreased with increase in filler content, whereas the experimental values for the elongation at break showed an abrupt decrease. This mismatch between theoretical and experimental data attributes to the poor mechanical properties as the rigid hollow spheres of fresh FA do not undergo elongation.

The CS/MCA-FA composites exhibits a better fit between the theoretical and experimental data presented as a function of the volume fraction of filler. The rough textured, irregularly shaped, surfactant-wrapped particles of MCA-FA have better mechanical interaction with CS (**Fig. 7.7b**). This indicates that the surfactant coated MCA-FA could effectively anchor to the CS matrix through hydrogen bonding as discussed in FTIR analysis.

To understand the mechanical results further, "interfacial interaction" between filler and the matrix was evaluated by **equation 2.6 of chapter 2** [Pukánszky et al. 1989]. **Fig. 7.7c** shows the variation of interfacial interaction parameter of the composites with volume fraction of fresh FA and MCA-FA. The interfacial adhesion was higher for MCA-FA based composites in comparison with that based on fresh FA. These results imply that the higher surface area and smaller particle size of MCA-FA provides better polymer-filler bonding. The irregular shape of MCA-FA enhances the mechanical interlocking with the matrix. This in turn can be correlated to better anchoring of MCA-FA and CS through hydrogen bonding from FTIR studies. As the MCA-FA has a surfactant coating which reduces particles clustering and provides more -OH functional sites for inter-molecular hydrogen bonding with CS matrix. At higher filler loading the particles rich clustering and agglomeration has reduced interfacial interaction [Kumar 2014]. The fresh FA particles have hydrophilic functional groups (-OH), which interact

with -NH$_2$ and -OH functional group of CS matrix through inter-molecular hydrogen bonding. But, there is a high probability that fresh FA particle might interact among themselves through hydrogen bonding, which provides less sights of interaction for the CS matrix. This might have resulted in lower interfacial interaction between fresh FA and CS polymer [Zivanovic et al. 2007].
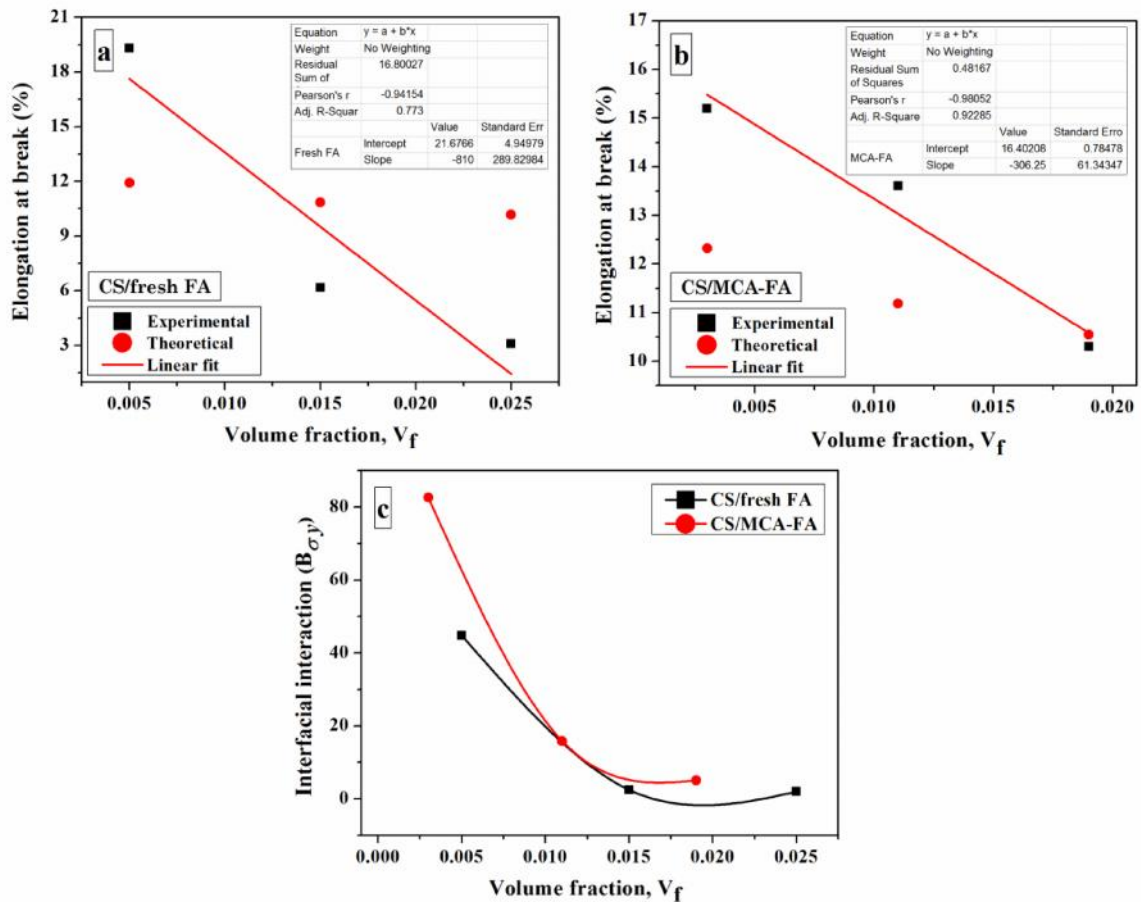
Fig. 7.7 Elongation at break versus volume fraction of filler of (a) CS/fresh FA and (b) CS/MCA-FA and (c) Interfacial interaction parameter ($B_{\dagger y}$) versus volume fraction of filler

7.1.1.5 DSC results
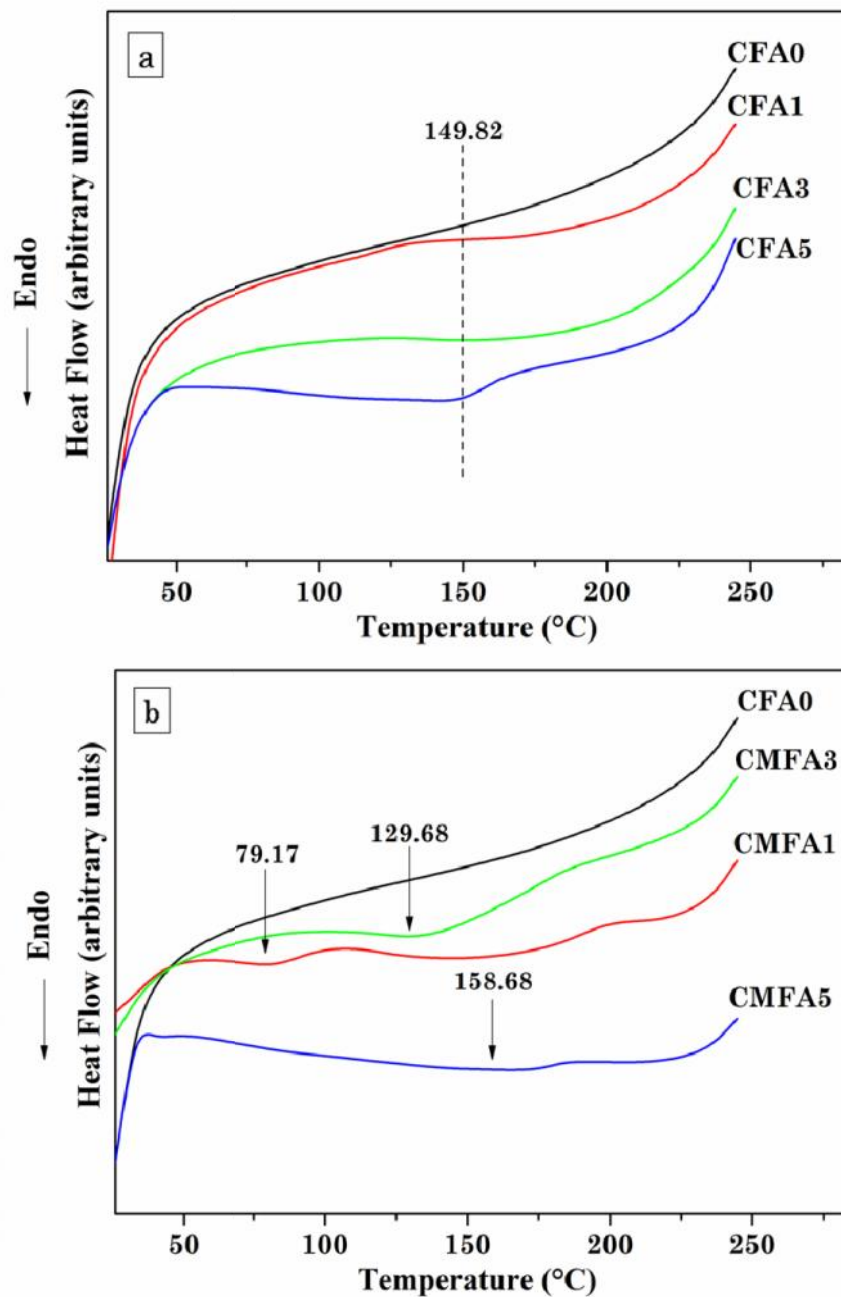
Fig. 7.8 DSC traces of neat CS and CS composites with 1, 3 and 5 wt% of (a) fresh FA and (b) MCA-FA

Fig. 7.8a-b shows the DSC traces of CS composites of fresh FA and MCA-FA. To eliminate the effect of moisture content from CS films, second heating runs were performed. Glass transition temperature (T_g) is basically used to examine the thermal behavior of the composites. The T_g of CS was difficult to measure and is still a subject of controversy. The main reasons are difficulty in sample preparation and hygroscopicity of samples. Some properties like crystallinity, molecular weight and degree of deacetylation can influence the T_g. In most of the cases the glass transition temperature increases with a decrease in the filler particle size and good polymer-filler interaction, where as if the filler size is large and its concentration increases with poor polymer-filler interaction results in decreased T_g. Many researchers have reported T_g of CS with different techniques. Syuhada et al. [Syuhada et al. 2014] observed T_g of CS at 120 °C, whereas Sakurai et al. [Sakurai et al. 2000] measured T_g of CS at 203 °C and Dong et al. [Dong et al. 2004] at 140 °C. In the present study, the DSC measurements of neat CS showed no significant evidence for occurrence of a glass transition temperature and stepwise changes in specific heat (**Fig. 7.8a and b**). This is due to the effective crosslinking of CS with glutaraldehyde, which imparts a higher internal network with the CS backbone. During crosslinking, glutaraldehyde reacts with the -NH_2 group of CS. So, the cross-linked CS film may have few -NH_2 groups available to form hydrogen bonds with H_2O molecules. This results in bonding between H_2O molecules and CS hydroxyl groups instead of amino groups. As the hydroxyl groups of CS forms stronger hydrogen bonds than with the amino groups, so it can be expected that a higher temperature would be necessary to remove such H_2O molecules [Neto et al. 2005].

CS composites with 1, 3 and 5 wt% of fresh FA, showed a small inclination of baseline around 150 °C. This attributes to the physiochemical changes influenced by addition of fresh FA, which restricts the mobility of CS chains. It could also be due to the combined effect of crystalline nature of fresh FA and CS, as evident from XRD results (**Fig. 7.8a**). **Fig. 7.8b** shows the DSC measurements of neat CS and CS composites with 1, 3 and 5 wt% of MCA-FA. The shift in the baseline peak was observed from 79 to 129 to 158 °C at 1, 3 and 5 wt% of MCA-FA, respectively. This signifies the interaction of

surfactant coated MCA-FA with CS. TX-100 surfactant provides more sites for hydrogen bonding with hydroxyl group of CS, which affects the small specific volume of rigid 2-amino-2-deoxy-d-glucopyranose chain of CS. These interactions may change with variation in the loading of MCA-FA.

7.1.1.6 TGA results
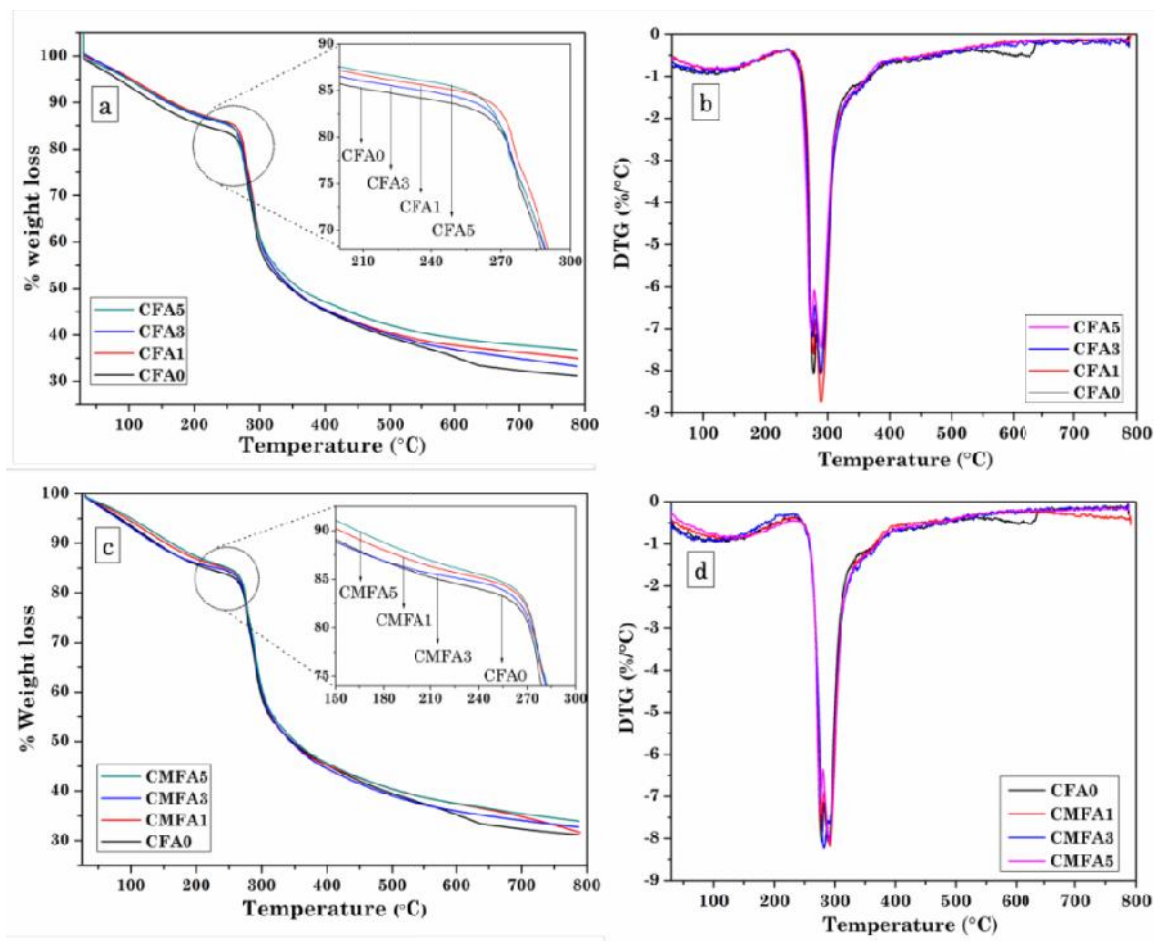
Fig. 7.9 TGA and DTG plots of neat CS and CS composites with 1, 3 and 5 wt% of (a and b) fresh FA and (c and d) MCA-FA

Fig. 7.9(**a-d**) exhibits the TGA and DTG curves of neat CS and CS composites with 1, 3 and 5 wt% of fresh FA and MCA-FA. Three consecutive steps of weight loss were observed for neat CS and CS composites with fresh FA and MCA-FA. First weight loss was observed at 65 to 105 °C, which was due to moisture vaporization indicating the

hygroscopic nature of CS composites. Second weight loss was in the range of 230 to 290 ℃, which attributes to the decomposition (thermal and oxidative) of ether linkage in CS backbone and elimination of volatile products. In third stage, the weight loss was in the range of 350 to 750 ℃, which corresponds to the partial oxidation and decomposition of glucosamine residues and then charring (**Fig. 7.9a and c**) [Swain et al. 2014]. The amount of residue left at 800 °C for neat CS was 31.17%. The onset of second and third degradation temperature of neat CS and CS composites with 1, 3 and 5 wt% of fresh FA and MCA-FA are shown in **Table 7.1**. For CS/fresh FA composites, the percentage of residue was 34.19, 32.35 and 36.68 at 1, 3 and 5 wt% of filler content, respectively. The improvement in thermal properties was due to the presence of fresh FA, which is basically a ceramic and high thermal resistance. There was no uniform interval of residue (%) left, which may be due to the non-uniform distribution of filler throughout the matrix, observed and discussed previously in fractography studies. The observations made from CS/MCA-FA composites showed uniform ascending amount of residue left, which corresponds to better distribution of filler. The amounts of residue (%) left at 800 °C for CS/fresh FA and CS/MCA-FA are given in **Table 7.1**.

Table 7.1 TGA results

Designation	Onset of second degradation step (°C)	Onset of third degradation step (°C)	Residue (wt%)
CFA0	268.58	309.15	31.17
CFA1	266.39	318.95	34.19
CFA3	265.12	317.03	32.35
CFA5	263.97	310.69	36.68
CMFA1	268.42	313.07	31.61
CMFA3	265.89	318.19	32.69
CMFA5	268.97	316.26	34.04

In the case of DTG curves (**Fig. 7.9b and d**) of CS/fresh FA and CS/MCA-FA, three major peaks were displayed prominently, indicating the step wise thermal degradation of CS composites. The three peaks at 105, 277-290 and 360 °C indicate the release of water molecules, due to scission of ether linkage in the CS backbone and pyrolysis of polysaccharides. This was consistent with the TGA results. According to most of the research work [Nieto et al. 1991], pyrolysis of polysaccharides starts by a random split of the glycosidic bonds, which results in formation of acetic and butyric acids after complete decomposition of CS composites. These findings indicate how CS behaves in the thermal analysis upon incorporating fresh FA and MCA-FA.

7.2 CONCLUSIONS

FTIR spectroscopy and XRD analyses showed good compatibility between CS matrix and MCA-FA. The surface roughness and irregularity in shape of MCA-FA resulted in its efficient mechanical interlocking with the polymer matrix. This, in turn enhanced the mechanical properties of these composites. All the composite films exhibited a higher tensile strength and a lower percentage of elongation-at-break compared with the neat CS film. The highest tensile strength was observed for the composite film with 1 wt% of filler loading and the reduction in the tensile properties at higher filler loading was due to agglomeration of filler and polymer-filler interface debonding. The tensile strength data were analyzed using Nielsen and Pukanzsky models to understand the interface formation and polymer-filler interactions. Thermal properties showed a marginal improvement due to the incorporation of MCA-FA.

CHAPTER 8

The results of this chapter have been communicated to *Silicon*

CHAPTER 8

DUCTILITY AND FLAME RETARDANCY ENHANCEMENT OF PVC BY NANOSTRUCTURED FLY ASH
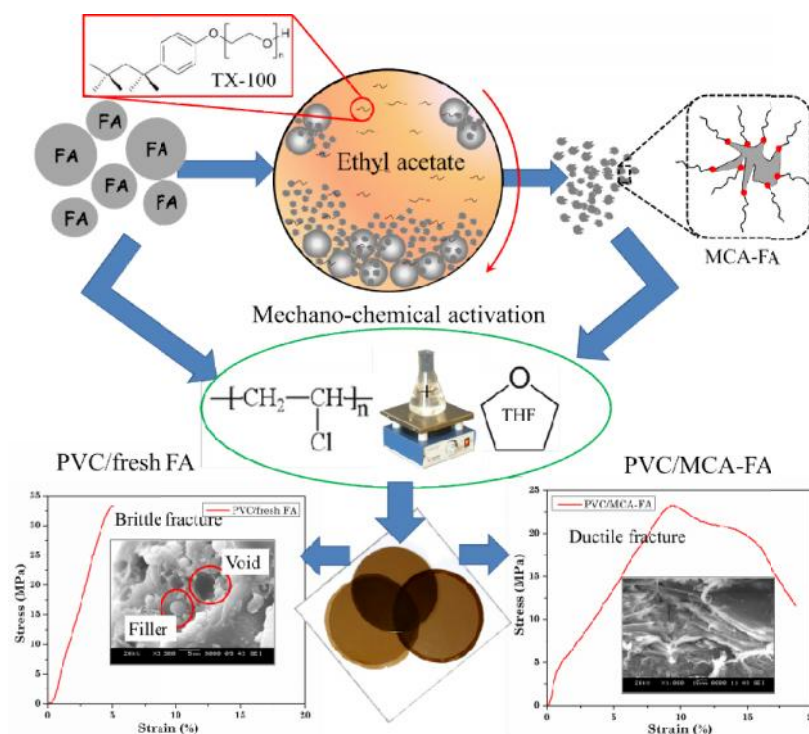
Scheme 8.1 Preparation of PVC composites with fresh FA and MCA-FA

This chapter discusses the characterization of the poly(vinyl chloride) (PVC) composites with varying amount of fresh FA and MCA-FA. FTIR spectroscopy of neat PVC and their composites with fresh FA and MCA-FA was used to study the variation in chemical functional groups. Mechanical properties of the composites revealed that incorporation of fresh FA in PVC resulted in a higher tensile strength with brittle failure. The surfactant wrapped on the MCA-FA to PVC resulted in higher elongation at break values while retaining the ductility of PVC. As fresh FA and MCA-FA contain basic oxide materials, they tend to improve the fire retardancy of PVC even at a very small filler loading determined by the flammability studies.

8.1 RESULTS AND DISCUSSION

8.1.1 Characterization of PVC/fresh FA and PVC/MCA-FA composites

8.1.1.1 FTIR spectroscopy
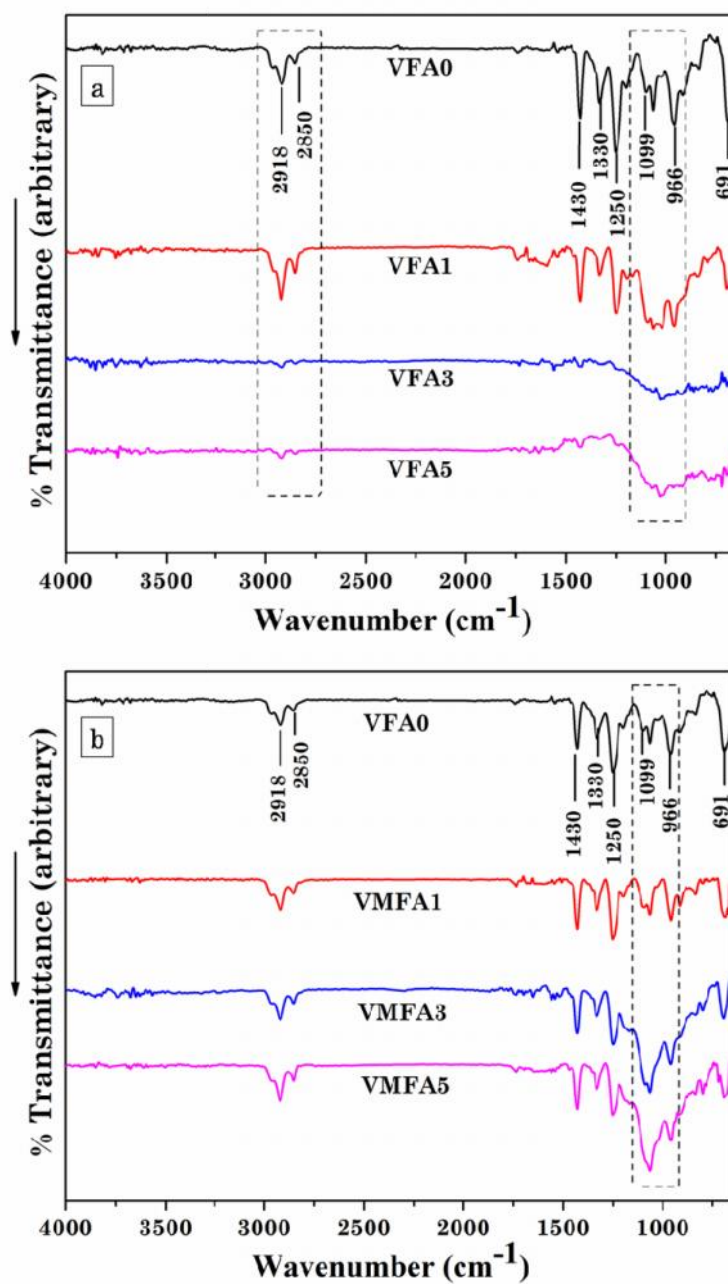
Fig. 8.1 FTIR spectra of neat PVC and PVC composites with 1, 3 and 5 wt% of (a) fresh FA and (b) MCA-FA

Fig. 8.1a and **b** shows the FTIR spectra of neat PVC and the composites with fresh FA and MCA-FA at different filler loading. The characteristic IR bands of neat PVC are broadly classified into three regions. The first region in the range of 600-700 cm^{-1} was assigned to (C-Cl) stretching. The second and third region in the range of 900-1200 cm^{-1} and 1250-2970 cm^{-1} attributed to the (C-C) stretching and numerous C-H mode, respectively. The absorption band of neat PVC at 2918 cm^{-1} and 2850 cm^{-1} are attributed to -CH asymmetric and -CH symmetric stretching. The CH$_2$ wagging, deformation and rocking were observed at 1430, 1330 and 966 cm^{-1}, respectively. The peak at 1250 cm^{-1} was due to -CH deformation from CHCl. The bands at 1099 cm^{-1} and 691 cm^{-1} correspond to C-C and C-Cl stretching, respectively [Ramesh et al. 2007 and Beltrán and Marcilla 1997].

From **Fig. 8.1a** the peak at 1099 cm^{-1} was distorted at 1 wt% of filler and the intensity of the peaks from 4000-500 cm^{-1} was diminished at 3 and 5 wt% of fresh FA. The IR spectra of the PVC/fresh FA composite with 3 and 5 wt% of filler loading resembles the spectra of fresh FA. This may be due to the excess of filler particles present in PVC composites or concentrated region of the filler in PVC matrix. In the spectra of PVC/MCA-FA composites, (**Fig. 8.1b**) the peaks at 1099 cm^{-1} of C-C stretching of PVC matrix and Si-O-Si stretching at 1092 cm^{-1} of fresh FA seems to overlap and merge resulting in higher intensity and broad peak as the filler content increases.

8.1.1.2 Mechanical properties and fractography of the PVC composites

The most important mechanical properties of particulate-polymer composites are strength and toughness, which strongly depend on surface characteristics of the filler, particle morphology and size distribution, filler-matrix interface, the filler content and the degree of filler dispersion [Fu et al. 2008].The tensile stress-strain curves and the fractographs of neat PVC, PVC/fresh FA and PVC/MCA-FA composites are shown in **Figs. 8.2** and **8.3**. The neat PVC film exhibited semi-ductile failure with low tensile strength and high elongation at break. The fracture surface of the failed specimen revealed ductile zones with peak formation and tends to have ridges and fibrous appearance (**Figs. 8.2a** and **8.3a**).
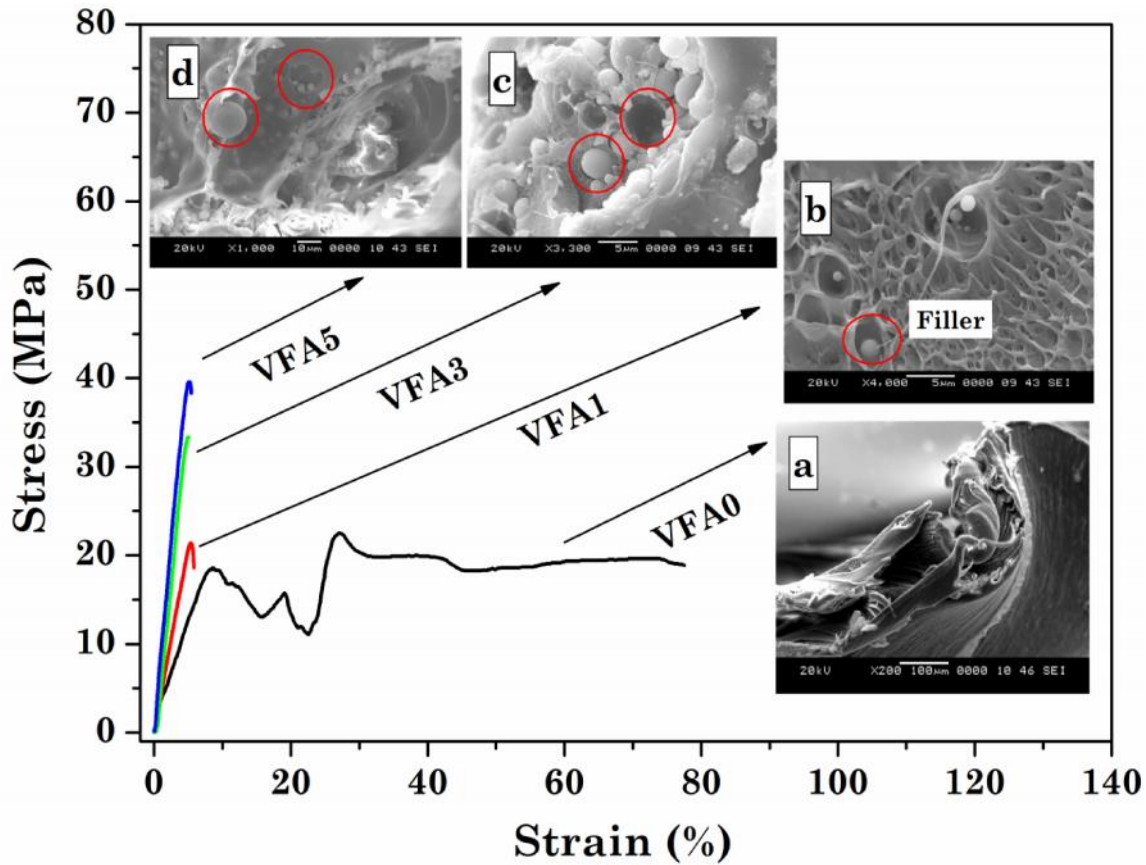
Fig. 8.2 Stress-strain graphs and fractographs of PVC/fresh FA composites (a) neat chitosan (b) 1 wt% (c) 3 wt% and (d) 5 wt% of filler content

For PVC/fresh FA composites the tensile strength increased linearly with 1, 3 and 5 wt% of filler loading (**Fig. 8.2**). This is attributed to the reinforcing effect of the rigid inorganic filler, fresh FA [Xie et al. 2004]. In **Fig. 8.2b**, the fractographs shows reduced number of fibrils and uniform distribution of filler at 1 wt% loading of fresh FA. At higher filler loading of 3 and 5 wt% of fresh FA, the interaction between the filler particles increases that affects the integrity of the PVC matrix due to which it undergoes a rapid failure. The fractographs of the samples with higher filler loading reveal the fracture surface to be rough with a few elliptical voids around FA particles due to interface debonding (**Fig. 8.2c-d**). The agglomeration, formation of voids and vacancy at pullout of the filler particles have resulted in transformation of PVC composites from semi-ductile to brittle fracture [Ghorbel et al. 2014] as shown in **Scheme 8.1**. This trend

is presumably the consequence of high stiffness of the fresh FA as filler, which alters the ductility of PVC matrix.
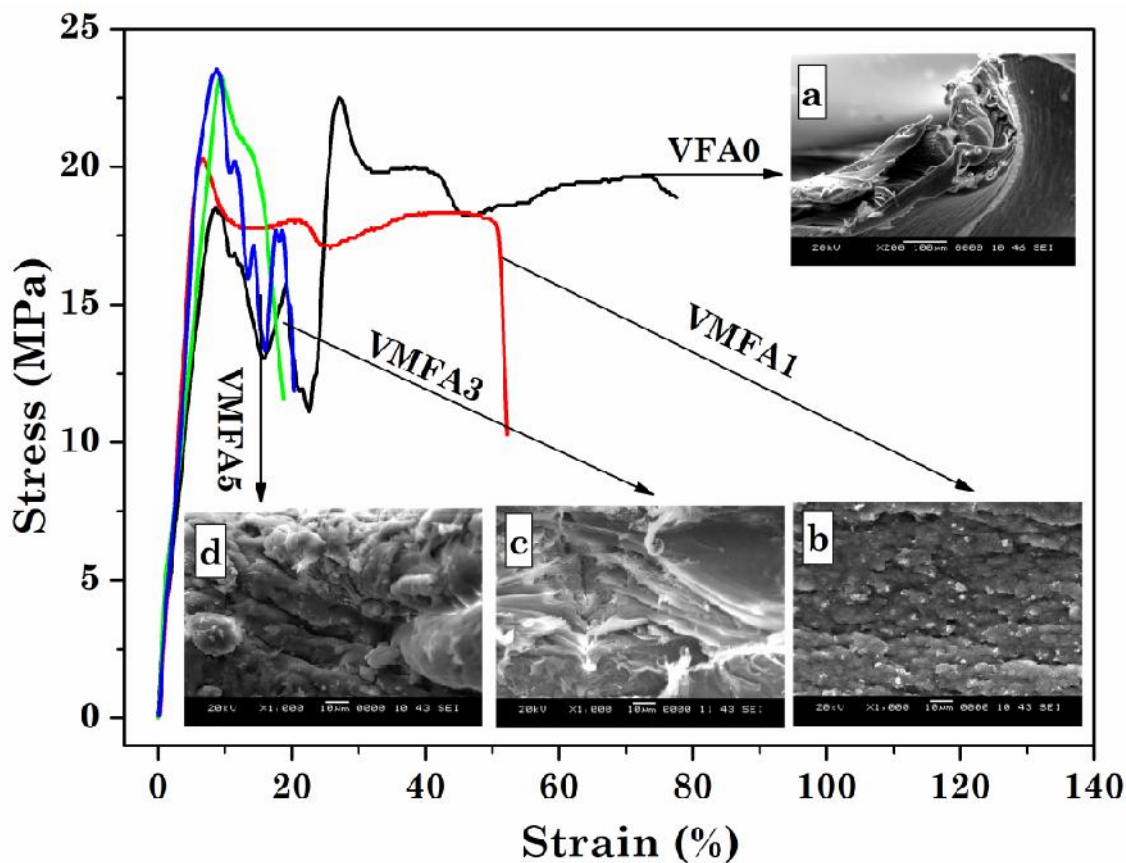
Fig. 8.3 Stress-strain graphs and fractographs of PVC/MCA-FA composites (a) neat chitosan (b) 1 wt% (c) 3 wt% and (d) 5 wt% of filler content

In contrast, it was found that the PVC/MCA-FA composites possessed lower tensile strength but their ductility was retained as that of neat PVC as shown in **Fig. 8.3**. It may be due to the decreased intermolecular forces by the interaction of the surfactant with the PVC chains, which increases the polymer chain mobility and thereby reduces the rigidity of the matrix. The fractographs of PVC/MCA-FA composites reveal uniform distribution at 1, 3 and 5 wt% of filler content and formation of fibrils and squamous structures at fracture surfaces (**Figs. 8.3b, c** and **d**). This is due to the lower particle size and higher surface area of MCA-FA, the presence of the surfactant coating on filler

particles, and also because of more number of particles encapsulated within a specified volume, as the specimen exhibits a rough fracture surface.

The variation in tensile strength and elongation at break of PVC composites with 1, 3, and 5 wt% of fresh FA and MCA-FA are represented by the bar charts in **Fig. 8.4a-b**. The tensile strength values of the PVC/fresh FA composites increased proportionately with the filler content and values of the elongation at break were reduced as the rigid FA spheres do not undergo elongation, resulting in a brittle fracture [Sombatsompop et al. 2003].

This attributes to the possible strain-induced alignment of the filler particle in the polymer matrix and strong interfacial interaction, is discussed later. The incorporation of MCA-FA has not shown any appreciable major improvement in tensile properties, but, there was an increase in the elongation at break in comparison with PVC/fresh FA composites indicating their toughening effect for PVC. This signifies that as the particle size decreases the probability of flaws existing within this volume also increases; if large flaws exist within an area of stress concentration, the tensile strength decreases [Chen et al. 2004]. This implies that ductility of the PVC/MCA-FA was retained in spite of the reduction in tensile strength as shown in **Scheme 8.1**.

A theoretical model proposed by Nielsen [Nielsen 1966] was used to analyze the relationship between the experimental values of tensile strain and the volume fraction of filler for PVC/fresh FA and PVC/MCA-FA composites from **equation 2.5 of chapter 2** shown in **Fig. 8.5(a-b)**.

Pukanszky et al. proposed an equation (**equation 2.6 of chapter 2**) for calculating the 'interfacial interaction' between filler and matrix of a composite [Pukánszky et al. 1989]. It is well known that the interfacial adhesion between filler and PVC matrix is strongly related to the tensile strength of a composite as shown in **Fig. 8.5c.**

In case of PVC/fresh FA composites (**Fig. 8.5a**), the theoretical values of $_c$ are higher than the experimental ones. In these composites the surfactant molecules are absent, and there exists hydrogen bonding between the filler and PVC matrix. This resulted in a higher interfacial interaction of spherical shaped filler particles and PVC

shown in **Fig. 8.5c**. As a result, the tensile strength of the composites improved. The fresh FA particles are micro-sized with smooth surface and therefore they can be easily dislodged from the surface [Zhu et al. 2008]. The particle dislodging was evident in the SEM micrographs of the fractured surfaces. The inherent brittle nature of fresh FA and its strong interaction with PVC has ultimately resulted in the reduction of the percentage elongation of the PVC/fresh FA composites.
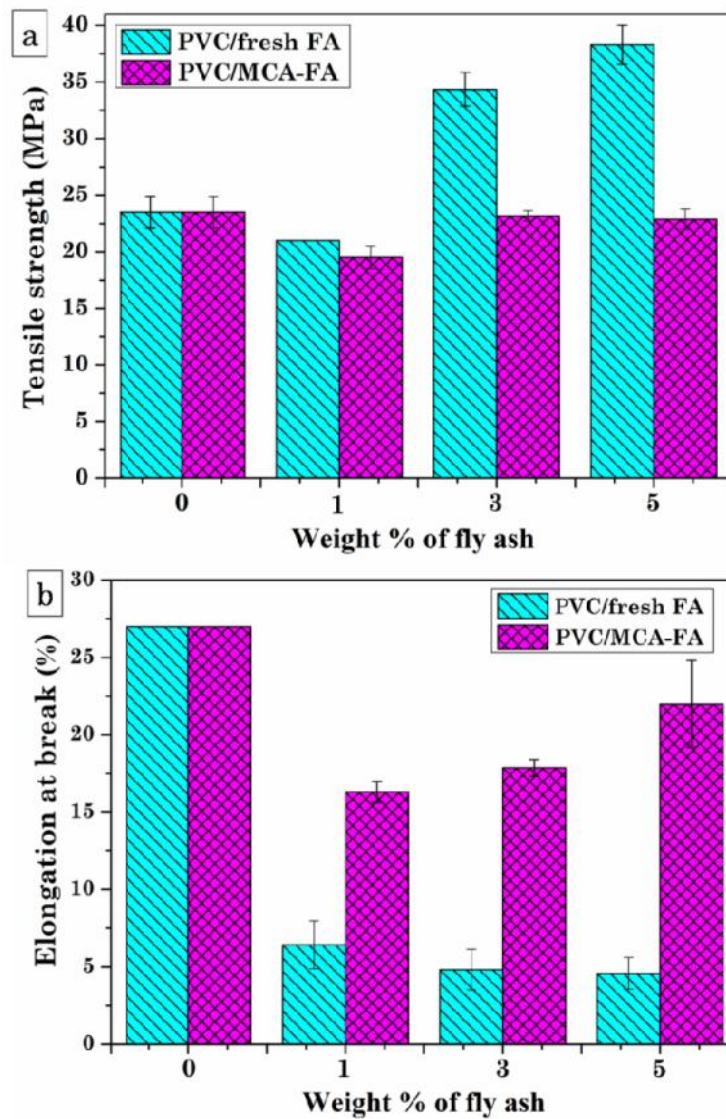
Fig. 8.4 Variations in mechanical properties of PVC/fresh FA and PVC/MCA-FA composites as a function of wt% of filler (a) tensile strength, (b) elongation at break
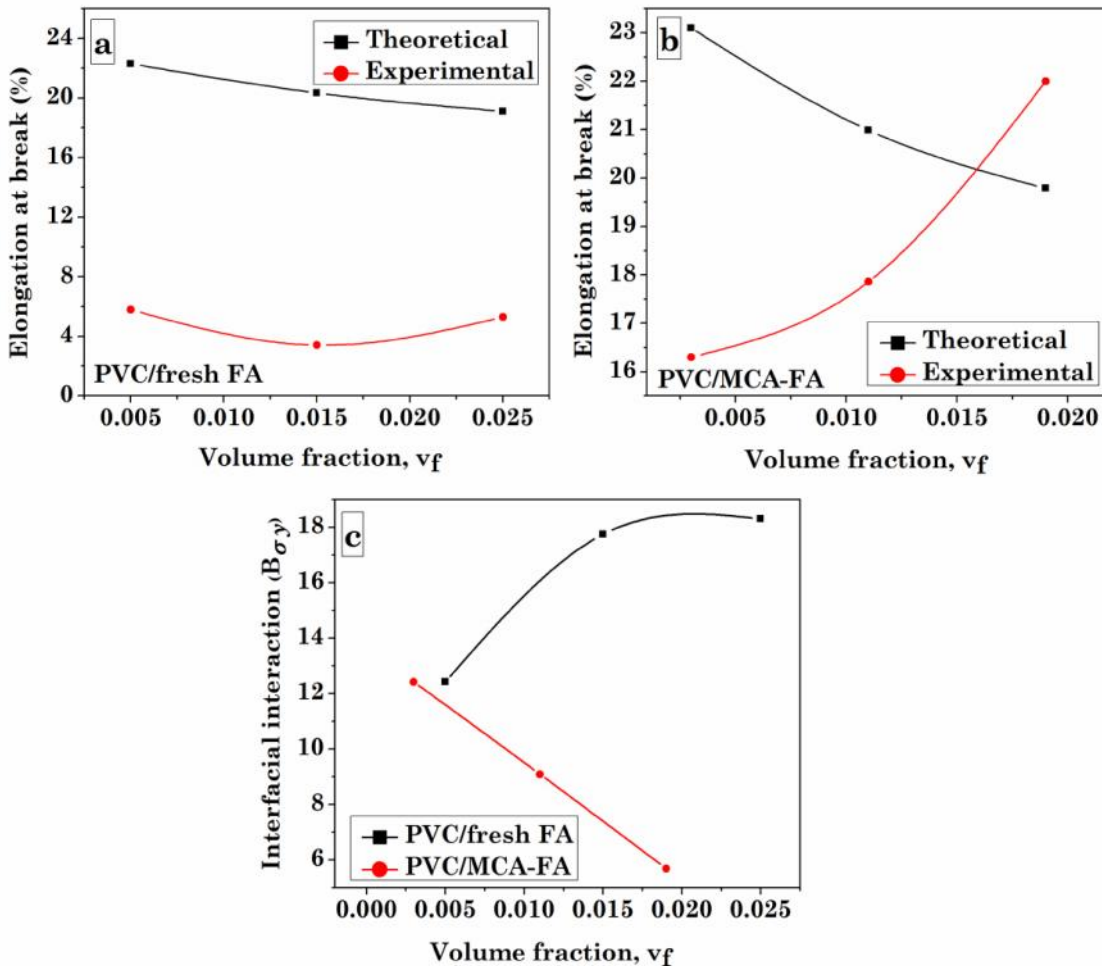
Fig. 8.5 Elongation at break versus volume fraction of filler of (a) PVC/fresh FA and (b) PVC/MCA-FA and (c) Interfacial interaction parameter ($B_{\dagger y}$) versus volume fraction of filler

Usually, in composites, the presence of the surfactant in a polymer medium can reduce the surface tension of polymer. Therefore it can increase the polymer chain mobility and improve its adhesion behavior [Funke and Starke 1992]. In the case of PVC/MCA-FA composites (**Fig. 8.5b**), the surfactants are attached only to the surface of MCA-FA particles that leads to a localized reduction in the surface tension in the premises of the particles, which can lead to a better adhesion. But the inert nature of the

130

surfactant used here could not allow any sort of interaction between the matrix and filler other than mechanical bonding (**Fig. 8.5c**). In general, any surfactant could lead to the slippage of the polymer chain as it can reduce the polymer-polymer chain interactions through hydrogen bonding. As the MCA-FA loading increases, the numbers of these surfactant molecules increases, ultimately leading to more slippage between the polymer chains thus, reducing the tensile strength in PVC/MCA-FA composites as compared with PVC/fresh FA composites.

8.1.1.3 DSC results

The influence of fresh FA and MCA-FA on the mobility of the PVC chains was investigated using DSC by measuring the glass transition temperature (T_g). The DSC curves of neat PVC, PVC/fresh FA and PVC/MCA-FA composites are shown in **Fig. 8.6a-b** and the corresponding T_g values are listed in **Table 8.1.** The T_g of PVC/fresh FA and PVC/MCA-FA composites shifted towards higher temperature in comparison with neat PVC, which is due to the interaction between the filler particles and the PVC matrix.

In PVC/fresh FA composites the glass transition temperatures is affected by the presence of fresh FA. These filler particles restrain the thermal motion of PVC molecular chains, by preventing the segmental movements of the polymer chains [Chipara et al. 2012]. The values of T_g increased persistently and lead to the enhancement of thermal stability of the PVC/FA composites. Literature studies show that the glass transition temperatures of amorphous polymers tend to increase with good filler-polymer interaction and smaller particle size of filler. For a poor interfacial interaction, there is an overall decrease in the glass transition temperature [Gacitua et al. 2005].

In case of PVC/MCA-FA composites, the filler distribution was uniform throughout the PVC matrix as observed from the fractographs, in spite of the poor polymer-filler interaction. This good dispersion is due to the poor interaction (non-agglomeration) among the particles, as each particle is wrapped with non-ionic surfactant molecules, which in turn is leading to reduced adhesion between filler and the matrix. But, the PVC chain movements are easily affected by presence of any filler or modifier, because of their completely amorphous nature [Gacitua et al. 2005]. The glass transition

temperatures of amorphous polymers are very sensitive to filler loading than the semi-crystalline ones.
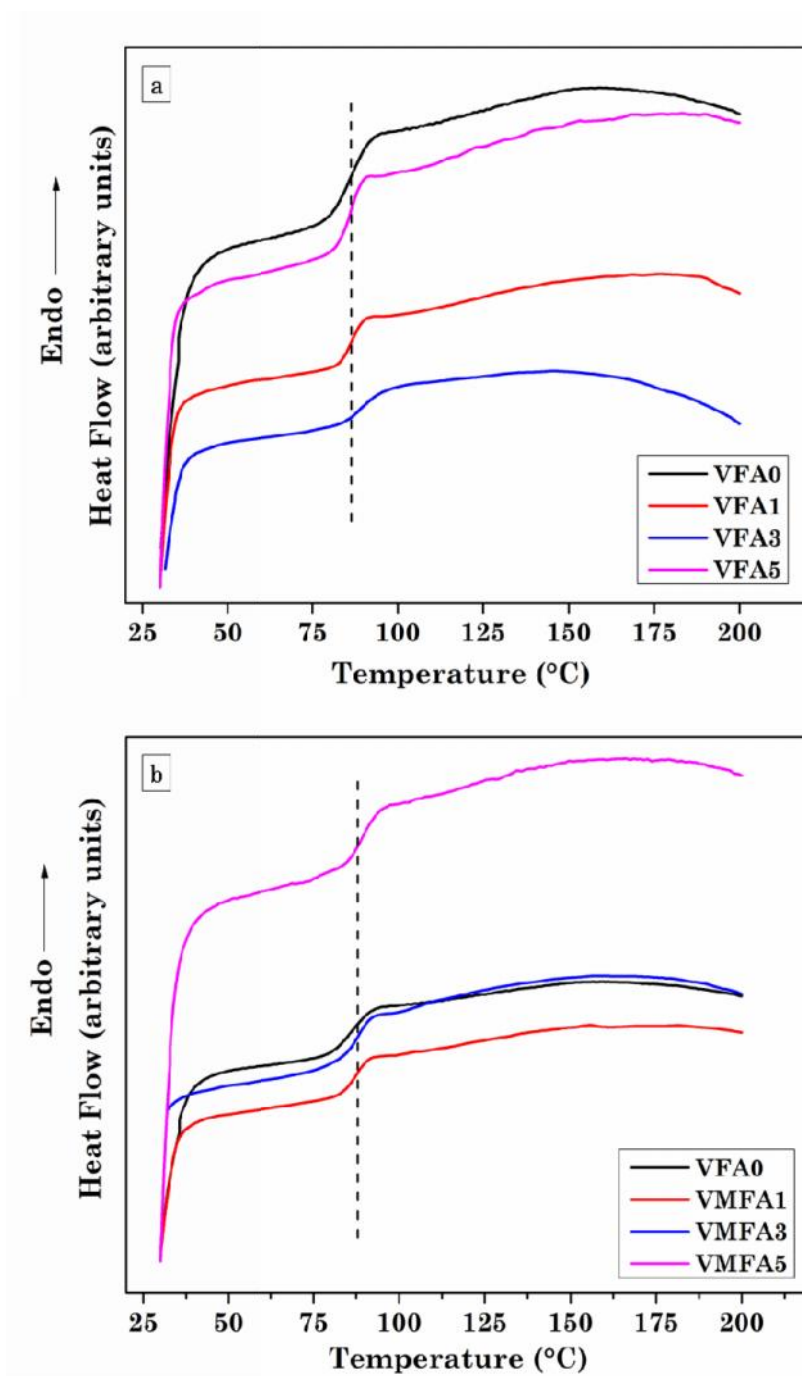
Fig. 8.6 DSC traces of neat PVC and PVC composites with 1, 3 and 5 wt% of (a) fresh FA and (b) MCA-FA

Table 8.1 LOI and T_g values of the composites

Designation	LOI (%)	T_g (°C)
VFA0	24	85.44
VFA1	24	86.41
VFA3	25	88.84
VFA5	27	86.45
VMFA1	26	87.67
VMFA3	28	88.73
VMFA5	29	89.72

8.1.1.4 Flammability study

Table 8.1 shows the LOI results of neat PVC, PVC/fresh FA and PVC/MCA-FA composites. The PVC/fresh FA composites with 3 and 5 wt% of filler loading are more fire retardant as the LOI values of these composites are superior to that of neat PVC and PVC with 1 wt% of filler loading. It is reported in literature that materials with LOI values greater than 28 are generally self-extinguishing. If a polymeric material satisfies the criterion of 28.00<LOI<100, then it is termed a 'self-extinguishing' one [Nelson 2001 and; Búcsi and Rychlý 1992]. The incorporation of 1, 3 and 5 wt% of MCA-FA in PVC matrix results in LOI of 26, 28 and 29, respectively. This study signifies that the flammable PVC could be turned into a 'self-extinguishing' material by adding just 3 wt% of MCA-FA. When compared with fresh FA, the MCA-FA enhances the fire retardancy of PVC at a much lower loading, signifying the role of its higher surface area in controlling the fire retardancy of PVC. In literature [Levchik and Weil 2005], some minerals such as alumina trihydrate, magnesium hydroxide and antimony trioxide have been reported as flame retardant additives in PVC. These mineral additives play a dual role of flame retardant and reinforcement in PVC matrix. The FA consisting of oxides such as SiO_2 and Al_2O_3 forms a sol on the burning polymeric surface which acts as smoke-suppressant, fire-retardant and thermal stabilizer. The mechanism of the control of the burning characteristics of PVC by FA will be discussed in section 8.1.1.5.

8.1.1.5 TGA results
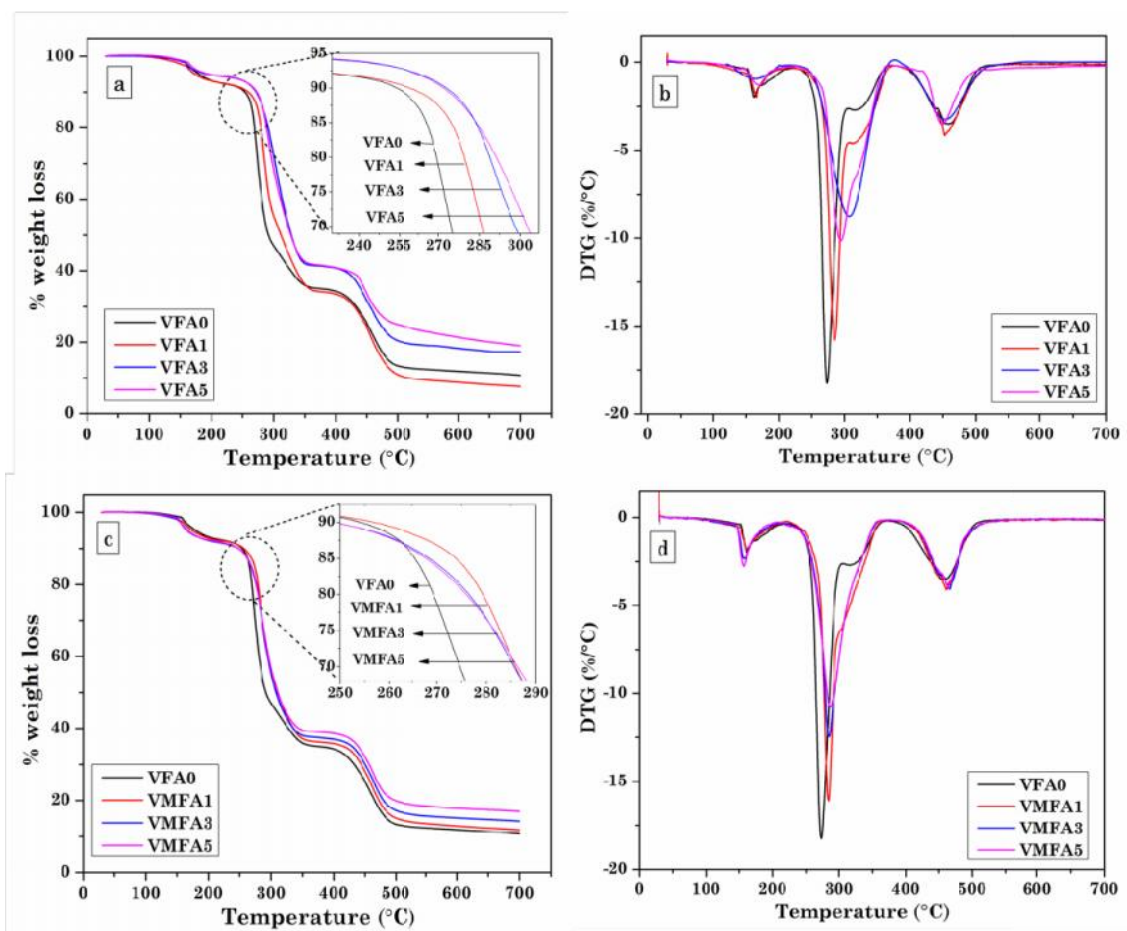
Fig. 8.7 TGA and DTG plots of neat PVC and PVC composites with 1, 3 and 5 wt% of (a-b) fresh FA and (c-d) MCA-FA

The TGA and DTG curves of neat PVC and the composites with 1, 3 and 5wt% of fresh FA and MCA-FA are presented in **Fig. 8.7**(**a-d**). In general, the thermal degradation of PVC is a two step process, but in the present study three degradation steps are observed as shown in **Fig. 8.7**. The first step in TGA curves in the neat PVC, PVC/fresh FA and PVC/MCA-FA composites may be due to the evaporation of adsorbed water molecules, which is normally adsorbed on the surface of the PVC films. The second step can be considered as actual starting of PVC degradation, which in turn is due to the dehydrochlorination of the polymer. A rapid weight loss was observed at ~250 °C in all

the samples. The catalytic influence of HCl on dehydrochlorination can accelerate the further dehydrochlorination [Hjertberg and Sörvik 1984] as shown in **Fig. 8.8a**. Dehydrochlorination is followed by several simultaneous polyene rearrangement reactions leading to conjugated double bonds and aromatic compounds [Pielichowski et al. 1998]. The amount of residue (wt%) and temperatures corresponding to onset of second and third step of degradation for all the samples are presented in **Table 8.2**. However, a number of structural defects and isomeric forms result during the main chain formation of PVC in the radical polymerization of vinyl chloride. Thermal degradation usually begins with defects in tertiary chloride structural and internal allylic chloride [Gong et al. 2004].The third degradation step, within the interval 400-550 °C, is due to the pyrolysis of the conjugated polyene structure which is formed due to dehydrochlorination reaction in the previous step. The final step observed after 580 °C is due to some structural changes such as crosslinking, crystallization, aromatization and isomerisation [Wan et al. 2004].

Table 8.2 TGA results

Designation	Onset of second degradation step (°C)	Onset of third degradation step (°C)	Residue (wt%)
VFA0	273	457	10.7
VFA1	284	452	7.7
VFA3	307	455	17.3
VFA5	294	449	19.1
VMFA1	283	461	11.8
VMFA3	284	466	14.1
VMFA5	286	464	16.9

In the case of PVC/fresh FA composites, the degradation commences at an elevated temperature than the neat PVC (**Fig. 8.7a-b**). The first step of degradation of PVC composites at 1, 3 and 5 wt% of filler loading occurs at 284, 307 and 294 °C as the HCl emissions are shifted towards a higher temperature. This is due to the HCl uptake

ability and the barrier properties of several oxides, SiO_2, Al_2O_3 Fe_2O_3 and CaO etc. composing fresh FA [Ari and Aydin 2011] as shown in **Fig. 8.8b**. Thus, HCl released at initial degradation temperature is efficiently absorbed and neutralized by fresh FA preventing the catalyzed degradation of PVC chains thereafter, despite the fact that a faster degradation is possible due to more heat transfer through the amorphous PVC chains.
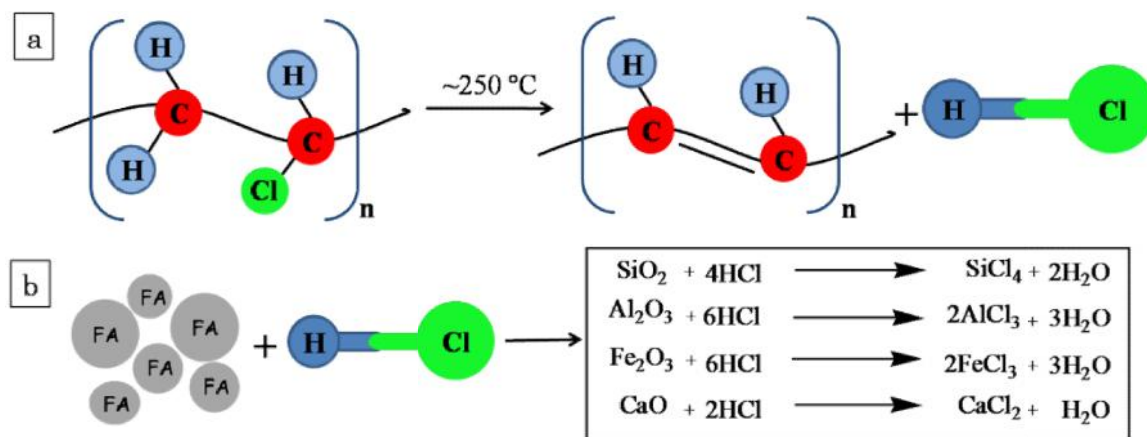
Fig. 8.8 (a) Mechanism of dehydrochlorination during thermal degradation of PVC and (b) Adsorption of HCl by various oxides present in FA

The filler and matrix interaction in the PVC/MCA-FA composites was hindered by the presence of the surfactant as observed from the FTIR results. From literature, [Liu et al. 2006 and Chen et al. 2006] it was found that the presence of $CaCO_3$ suppressed the liberation of HCl gas during combustion of PVC and the ability of adsorption of HCl gas was improved by lower particle size of $CaCO_3$. In spite of the lower particle size and higher specific surface area of MCA-FA, there was no major change in the thermal degradation temperature (**Fig. 8.7c-d**). This attributes to the modification of the filler surface by the non-ionic surfactant, which is efficient in the modification of FA but not helpful in establishing an interaction with the PVC matrix. Owing to this reason, the surfactant molecules on the surface of FA can wrap the MCA-FA particles completely, thus reducing the adsorption of HCl molecules, which are liberated at the initial stages of

136

the PVC degradation. Therefore, the degradation of PVC/MCA-FA happens at a faster rate than that of PVC/fresh FA loaded composites.

The 3rd steps of degradation of the PVC/MCA-FA composites occur at lower temperatures than that of the PVC/fresh FA composites. This may be ascribed to the surfactant covering present on the surface of MCA-FA that might have degraded along with the PVC at the 2nd step. This would have exposed the surface of the MCA-FA particles, which could protect the PVC chains until the 3rd step occurred.

8.2 CONCLUSIONS

The nanostructured MCA-FA exhibited a better dispersion and distribution throughout the PVC matrix compared with fresh FA. The surfactant wrapping on the MCA-FA surface helps PVC retain its ductility. Tensile strength of PVC/fresh FA composites increased as a function of filler loading at the cost of the ultimate elongation and ductility. The PVC/MCA-FA composites with 5 wt% filler loading retain the tensile strength with improved ductility than their fresh FA based counterparts. 5 wt% MCA-FA loading also turned the composites into 'self-extinguishing' ones. Overall, MCA-FA has shown potential as value-added multifunctional nanofiller in PVC matrix composites.

CHAPTER 9

CHAPTER 9

CONCLUSIONS

●━━━━━━━━━━━━━━━━━━━━━━━━━━━━━●

Part-I

From the results and discussions in the chapters 3, 4 and 5 the following conclusions were draw:

<u>Chapter 3</u>: EDS analysis revealed that the FA used for this study belongs to class F. Mechano-chemical activation of FA resulted in reduction of the crystallite size of the quartz phase present in fresh FA, while the relative lattice strain on it increased during milling. The average particle size decreased which led to increased specific surface area. The spherical shape with smooth surface texture of the fresh FA was converted to irregular shape and rough surface of the MCA-FA. The presence of surfactant during mechano-chemical activation of FA converted the hydrophilic surface of fresh FA to partially hydrophobic of the MCA-FA. Surface of the MCA-FA has become more active, which was evident from FTIR analysis.

<u>Chapter 4</u>: Ethylene-octene random copolymer (EOC) composites were prepared with varying amount of fresh FA and MCA-FA as filler by solution casting. The MCA-FA particles showed good interfacial interaction with the polymer matrix due its uniform distribution and dispersion in the composite, which was observed by the morphological studies from the cryo-fractured surfaces. This accounted for improved mechanical properties of the EOC/MCA-FA composites even at lower filler loading in comparison to EOC/fresh FA composites. Thermal properties and flammability of these composites was encouraging by the addition of either fresh FA or MCA-FA.

<u>Chapter 5</u>: The fresh FA and MCA-FA was incorporated with varying amount into biodegradable poly(vinyl alcohol) (PVA) matrix by solution mixing and ultrasonication. FTIR spectroscopy revealed a thermodynamically favorable interaction between the MCA-FA and PVA matrix determined by the Fowkes' equation and Gibbs free energy. This explanation was supported by a plausible mechanism. The surfactant molecules present on the surface of MCA-FA reduced the

particle-particle interaction forces among them, which played a significant role in enhancement of filler dispersion in the composite. The effective polymer–filler interaction combined with good dispersion and distribution of the filler helped in enhancing the mechanical properties of these composites. The presence of MCA-FA in PVA matrix improved crystallinity and glass transition temperature of the composites.

Part-II

From the results and discussions in the chapters 6, 7 and 8, the following conclusions were draw:

<u>*Chapter 6*</u>: *The design of statistical analysis by Taguchi methodology was successfully employed to analyze the effect of milling parameters, which resulted in nanostructured FA by mechano-chemical activation. The factors such as ball-to-powder weight ratio and surfactant type were the most significant parameters, which led to lower crystallite size and average particle size and higher specific surface area, respectively. These results were complimentary to the ANOVA analysis, which revealed ball-to-powder weight ratio and surfactant type as the major contributing factors. A fractal approach was used to determine the lacunarity of the agglomerates in the MCA-FA, which were the cluster of nanostructured FA.*

<u>*Chapter 7*</u>: *Fresh FA and MCA-FA obtained from Taguchi methodology was incorporated in varying amount in chitosan (CS) matrix by solution casting. The surface roughness and irregularity in shape of MCA-FA resulted in its efficient mechanical interlocking with the polymer matrix as it was evident from the Nielsen and Pukanzsky models. This, in turn enhanced the mechanical properties, which exhibited a higher tensile strength and a lower percentage of elongation-at-break compared with the neat CS film. Fresh FA with smooth surface and spherical in shape resulted in dewetting, debonding and void formation in the composites, which showed reduction in the tensile properties. Thermal properties showed a marginal improvement due to the incorporation of MCA-FA.*

<u>*Chapter 8*</u>: *The solution casting method was used to prepare poly(vinyl chloride) (PVC) matrix composites with varying amount of fresh FA and MCA-FA obtained*

from Taguchi methodology. Mechanical properties of the composites revealed that incorporation of fresh FA in PVC resulted in a higher tensile strength with brittle failure; addition of MCA-FA to PVC resulted in higher elongation at break values while retaining the ductility of PVC. The key parameter for enhancement of the mechanical properties and compatibility between MCA-FA and matrix was interfacial adhesion, polymer-filler interlocking and the morphology of filler, as it was evident from the Nielsen and Pukanzsky models. The basic oxide materials present in fresh FA and MCA-FA improved the thermal properties and fire retardancy of PVC composites.

Overall, this study proves that mechano-chemical activation of FA by planetary ball milling could be an efficient method to produce nanostructured FA. The design of statistical analysis by Taguchi methodology helped to reduce the number of experiments by orthogonal array. The analysis by main effect plot for means of MCA-FA and ANOVA determined the effect of milling parameters. The factors such as ball-to-powder weight ratio and surfactant type contributed majorly, which resulted in a smaller crystallite size and average particle size and higher specific surface area. The surfactant wrapped on the surface of MCA-FA particles led to their uniform distribution and dispersion in the all polymer matrices, which was confirmed from fractography studies. This enhanced the mechanical strength of all the composites. Thermal properties showed an improvement by the presence of the MCA-FA in all the polymer matrices. The MCA-FA produced by this method has shown potential as value-added multifunctional nanofiller in polymer matrix composites.

SCOPE FOR FURTHER WORK

- ❖ Preparation of the nanostructured FA by others techniques.

- ❖ The design of statistical methodology such as multiple quality criteria optimization techniques to find the optimal parameter condition of the ball milling process.

- ❖ Applications of mechano-chemically activated fly ash as filler can be explored in,

  - o Thermoset polymer matrix

  - o Ceramics matrix

  - o Metals matrix

REFERENCES

Agrawal, S.L. and Awadhia, A. (2004). "DSC and conductivity studies on PVA based proton conducting gel electrolytes." *Bull. Mater. Sci.*, *27* (6), 523–527.

Ahmaruzzaman, M. (2010). "A review on the utilization of fly ash." *Prog. Energy Combust. Sci.*, *36* (3), 327–363.

Akcay, K., Sirkecio lu, A., Tatlıer, M., Sava cı, Ö.T. and Erdem- enatalar, A. (2004). "Wet ball milling of zeolite HY." *Powder Technol.*, *142* (2-3), 121–128.

Ali, M. and Liwa, M. (2013). "Modification of parameters in mechanochemical synthesis to obtain <alpha>- and <beta>-molybdenum disilicide." *Adv. Powder Technol.*, *24* (1), 183–189.

Amin, K.A.M. and Panhuis, M. in het (2012). "Reinforced Materials Based on Chitosan, TiO_2 and Ag Composites." *Polymers*, *4* (1), 590–599.

Anandhan, S., Patil, H.G. and Babu, R.R. (2011). "Characterization of poly(ethylene-co-vinyl acetate-co-carbon monoxide)/layered silicate clay hybrids obtained by melt mixing." *J. Mater. Sci.*, *46* (23), 7423–7430.

Anandhan, S., Sundar, S.M., Senthil, T., Mahendran, A.R. and Shibulal, G.S. (2012). "Extruded poly(ethylene-co-octene)/fly ash composites – value added products from an environmental pollutant." *J. Polym. Res.*, *19* (3), 1–11.

Arbain, R., Othman, M. and Palaniandy, S. (2011). "Preparation of iron oxide nanoparticles by mechanical milling." *Miner. Eng.*, *24* (1), 1–9.

Ari, G.A. and Aydin, I. (2011). "Size-Dependent HCl Generation of PVC/SiO_2 Micro- and Nanocomposites." *J. Macromol. Sci. Part B*, *50* (5), 922–930.

Ashby, M.F., Ferreira, P.J. and Schodek, D.L. (2009). Chapter 10 - Nanomaterial Product Forms and Functions. In Nanomaterials, Nanotechnologies and Design, M.F. Ashby, P.J. Ferreira, and D.L. Schodek, eds. (Boston: Butterworth-Heinemann), pp 403–465.

ASTM C 618 − 12a. Standard specification for coal fly ash and raw or calcined natural pozzolan for use in concrete, ASTM International, 2012.

ASTM D 2863. Standard test method for measuring the minimum oxygen concentration to support candle-like combustion of plastics (oxygen index). ASTM International, May 2012.

ASTM D 412-06a. Standard test methods for vulcanized rubber and thermoplastic elastomers-tension. ASTM International, April 2013.

ASTM D 638-10. Standard test method for tensile properties of plastics. ASTM International, June 2010.

ASTM D 3037-93. Standard test methods for carbon black—surface area by nitrogen adsorption, ASTM International, 1999.

ASTM D 854-10. Standard test methods for specific gravity of soil solids by water pycnometer. ASTM International, 2010.

ASTM D 1238. Standard test methods for melt flow rates of thermoplastics by extrusion plastometer. ASTM International, 2013.

ASTM D 792. Standard test methods for density and specific gravity (relative density) of plastics by displacement. ASTM International, 2013.

ASTM D 1646. Standard test methods for rubber-viscosity, stress relaxation and pre-vulcanization characteristics (Mooney viscometer). ASTM International, 2004.

ASTM D 2240. Standard test methods for rubber property-durometer hardness. ASTM International, 2010.

Avella, M., Errico, M.E. and Rimedio, R. (2004). "PVA/PTFE nanocomposites: Thermal, mechanical, and barrier properties." *J. Mater. Sci.*, *39* (19), 6133–6136.

Baláž, P. (2008). High-Energy Milling. In Mechanochemistry in Nanoscience and Minerals Engineering, (Springer Berlin Heidelberg), pp 103–132.

Baláz, P., Nguyen, A.V., Fabián, M., Cholujová, D., Pastorek, M., Sedlák, J. and Buj áková, Z. (2011). "Properties of arsenic sulphide As4S4 nanoparticles prepared by high-energy milling." *Powder Technol.*, *211* (2-3), 232–236.

Bandyopadhyay, S., Zaeni, A., Nath, D., Yu, A., Zeng, Q., Blackburn, D. and White, C. (2010). "Advanced utilization of as received and near whitened fly ash in polypropylene polymer to improve mechanical, notched impact and whiteness colour properties." *Int. J. Plast. Technol.*, *14* (1), 51–56.

Beltrán, M. and Marcilla, A. (1997). "Fourier transform infrared spectroscopy applied to the study of PVC decomposition." *Eur. Polym. J.*, *33* (7), 1135–1142.

Beygi, H., Zare, M. and Sajjadi, S.A. (2012). "Fabrication of FeNi–Al$_2$O$_3$ nanocomposites and optimization of mechanical properties using Taguchi method." *Powder Technol.*, *232*, 49–57.

Bhadra, J. and Sarkar, D. (2011). "Size variation of polyaniline nanoparticles dispersed in polyvinyl alcohol matrix." *Bull. Mater. Sci.*, *33* (5), 519–523.

Blissett, R.S. and Rowson, N.A. (2012). "A review of the multi-component utilisation of coal fly ash." *Fuel*, *97* 1–23.

Búcsi, A. and Rychlý, J. (1992). "A theoretical approach to understanding the connection between ignitability and flammability parameters of organic polymers." *Polym. Degrad. Stab.*, *38* (1), 33–40.

Canakci, A., Erdemir, F., Varol, T. and Patir, A. (2013). "Determining the effect of process parameters on particle size in mechanical milling using the Taguchi method: Measurement and analysis." *Meas.*, *46* (9), 3532–3540.

Carraher, C.E, Jr (2003). "Seymour/Carraher's Polymer Chemistry": Sixth Edition (Boca Raton: CRC Press).

Casariego, A., Souza, B.W.S., Cerqueira, M.A., Teixeira, J.A., Cruz, L., Díaz, R. and Vicente, A.A. (2009). "Chitosan/clay films' properties as affected by biopolymer and clay micro/nanoparticles' concentrations." *Food Hydrocoll.*, *23* (7), 1895–1902.

Chaowasakoo, T. and Sombatsompop, N. (2007). "Mechanical and morphological properties of fly ash/epoxy composites using conventional thermal and microwave curing methods." *Compos. Sci. Technol.*, *67* (11–12), 2282–2291.

Chawla, K.K. (2012). "Composite Materials: Science and Engineering" (Springer Science & Business Media).

Chen, C.H., Teng, C.C., Su, S.F., Wu, W.C. and Yang, C.H. (2006). "Effects of microscale calcium carbonate and nanoscale calcium carbonate on the fusion, thermal, and mechanical characterizations of rigid poly(vinyl chloride)/calcium carbonate composites." *J. Polym. Sci., Part B: Polym. Phys.*, *44* (2), 451–460.

Chen, C.N., Chen, Y.L. and Tseng, W.J. (2007). "Surfactant-assisted de-agglomeration of graphite nanoparticles by wet ball mixing." *J. Mater. Process. Technol.*, *190* (1-3), 61–64.

Chen, N., Wan, C., Zhang, Y. and Zhang, Y. (2004). "Effect of nano-$CaCO_3$ on mechanical properties of PVC and PVC/Blendex blend." *Polym. Test.*, *23* (2), 169–174.

Chipara, M., Cruz, J., Vega, E.R., Alarcon, J., Mion, T., Chipara, D.M., Ibrahim, E., Tidrow, S.C. and Hui, D. (2012). "Polyvinylchloride-Single-Walled Carbon Nanotube Composites: Thermal and Spectroscopic Properties." *J. Nanomater.*, *2012*.

Chou, C.S., Yang, R.-Y., Chen, J.H. and Chou, S.W. (2010). "The optimum conditions for preparing the lead-free piezoelectric ceramic of $Bi_{0.5}Na_{0.5}TiO_3$ using the Taguchi method." *Powder Technol.*, *199* (3), 264–271.

Costa-Júnior, E.S., Barbosa-Stancioli, E.F., Mansur, A.A.P., Vasconcelos, W.L. and Mansur, H.S. (2009). "Preparation and characterization of chitosan/poly(vinyl alcohol) chemically crosslinked blends for biomedical applications." *Carbohydr. Polym.*, *76* (3), 472–481.

Cullity, B.D. (2001). "Elements of X-Ray Diffraction (Upper Saddle River, NJ: Prentice Hall).

D'Amore, A., Kenny, J.M. and Nicolais, L. (1988). "Viscoelastic Characterization of Reinforced Polyester Foams." *J. Cell. Plast.*, *24* (5), 473–485.

Deepthi, M.V., Sharma, M., Sailaja, R.R.N., Anantha, P., Sampathkumaran, P. and Seetharamu, S. (2010). "Mechanical and thermal characteristics of high density polyethylene–fly ash Cenospheres composites." *Mater. Des.*, *31* (4), 2051–2060.

Devi, M.S., Murugesan, V., Rengaraj, K. and Anand, P. (1998). "Utilization of flyash as filler for unsaturated polyester resin." *J. Appl. Polym. Sci.*, *69* (7), 1385–1391.

146

Dhadse, S., Kumari, P. and Bhagia, L.J. (2008). "Fly ash characterization, utilization and Government initiatives in India Œ A review." *J. Sci. Ind. Res.*, *67* (01), 11–18.

Ding, P., Orwa, M.G. and Pacek, A. W. (2009). "De-agglomeration of hydrophobic and hydrophilic silica nano-powders in a high shear mixer." *Powder Technol.*, *195* (3), 221–226.

Dong, Y., Ruan, Y., Wang, H., Zhao, Y. and Bi, D. (2004). "Studies on glass transition temperature of chitosan with four techniques." *J. Appl. Polym. Sci.*, *93* (4), 1553–1558.

Eisermann, C., Mallembakam, M.R., Damm, C., Peukert, W., Breitung-Faes, S. and Kwade, a. (2012). "Polymeric stabilization of fused corundum during nanogrinding in stirred media mills." *Powder Technol.*, *217* 315–324.

Enayati, M.H., Aryanpour, G.R. and Ebnonnasir, a. (2009). "Production of nanostructured WC–Co powder by ball milling." *Int. J. Refract. Met. Hard Mater*, *27* (1), 159–163.

Fadda, S., Cincotti, A., Concas, A., Pisu, M. and Cao, G. (2009). "Modelling breakage and reagglomeration during fine dry grinding in ball milling devices." *Powder Technol.*, *194* (3), 207–216.

Friel, J.J. (2000). "Practical Guide to Image Analysis (ASM International).

Fruhstorfer, J., Schafföner, S. and Aneziris, C.G. (2014). "Dry ball mixing and deagglomeration of alumina and zirconia composite fine powders using a bimodal ball size distribution." *Ceram. Int.*, *40* (9, Part B), 15293–15302.

Fu, S.Y., Feng, X.Q., Lauke, B. and Mai, Y.W. (2008). "Effects of particle size, particle/matrix interface adhesion and particle loading on mechanical properties of particulate–polymer composites." *Compos. Part B Eng.*, *39* (6), 933–961.

Funke, Z. and Starke, L. (1992). "The effects of surfactants on the miscibility of polymers." *Acta Polym.*, *43* (1), 21–26.

Gacitua E, W., Ballerini A, A. and Zhang, J. (2005). "Polymer nanocomposites: synthetic and natural fillers a review." *Maderas Cienc. Tecnol.*, *7* (3), 159–178.

Ge, H. and Wang, S. (2014). "Thermal preparation of chitosan–acrylic acid superabsorbent: Optimization, characteristic and water absorbency." *Carbohydr. Polym.*, *113* 296–303.

George, J.J. and Bhowmick, A.K. (2007). "Ethylene vinyl acetate/expanded graphite nanocomposites by solution intercalation: preparation, characterization and properties." *J. Mater. Sci.*, *43* (2), 702–708.

Ghani, J., Choudhury, I. and Hassan, H. (2004). "Application of Taguchi method in the optimization of end milling parameters." *J. Mater. Process. Technol.*, *145* (1), 84–92.

Ghasdi, M. and Alamdari, H. (2010). "CO sensitive nanocrystalline $LaCoO_3$ perovskite sensor prepared by high energy ball milling." *Sens. Actuators, B*, *148* (2), 478–485.

Ghita, R., Logofatu, C., Negrila, C.C., Ungureanu, F., Cotirlan, C., Manea, A.S., Lazarescu, M.F. and Ghic, C. (2011). Study of SiO2/Si Interface by Surface Techniques. In Crystalline Silicon - Properties and Uses, S. Basu, ed. (InTech),.

Ghorabi, S., Rajabi, L., Madaeni, S.S., Zinadini, S. and Derakhshan, A.A. (2012). "Effects of three surfactant types of anionic, cationic and non-ionic on tensile properties and fracture surface morphology of epoxy/MWCNT nanocomposites." *Iran Polym. J.*, *21* (2), 121–130.

Ghorbel, E., Hadriche, I., Casalino, G. and Masmoudi, N. (2014). "Characterization of Thermo-Mechanical and Fracture Behaviors of Thermoplastic Polymers." *Mater., 7* (1), 375–398.

Gong, F., Feng, M., Zhao, C., Zhang, S. and Yang, M. (2004). "Thermal properties of poly(vinyl chloride)/montmorillonite nanocomposites." *Polym. Degrad. Stab.*, *84* (2), 289–294.

Gu, J., Wu, G. and Zhang, Q. (2007). "Preparation and damping properties of fly ash filled epoxy composites." *Mater. Sci. Eng., A: A*, *452–453,* 614–618.

Guhanathan, S. and Devi, M.S. (2004). "Studies on interface in polyester/fly-ash particulate composites." *Compos. Interfaces*, *11* (1), 43–66.

Guhanathan, S., Devi, M.S. and Murugesan, V. (2001). "Effect of coupling agents on the mechanical properties of fly ash/polyester particulate composites." *Appl. Polym. Sci.*, *82* (7), 1755–1760.

Guirguis, O. W., Moselhey, M. T. H., (2011). "Thermal and structural studies of poly(vinyl alcohol) and hydroxypropyl cellulose blends." *Nat. Sci.*, *4* (1), 57–67.

Guo, Z., Zhang, D., Wei, S., Wang, Z., Karki, A.B., Li, Y., Bernazzani, P., Young, D.P., Gomes, J.A., Cocke, D.L. and Ho, T.C. (2010). "Effects of iron oxide nanoparticles on polyvinyl alcohol: interfacial layer and bulk nanocomposites thin film." *J. Nanopart. Res.*, *12* (7), 2415–2426.

Hamzaoui, R., Bouchenafa, O., Guessasma, S., Leklou, N. and Bouaziz, A. (2016). "The sequel of modified fly ashes using high energy ball milling on mechanical performance of substituted past cement." *Mater. Des.*, *90* 29–37.

He, L., Xue, R. and Song, R. (2009). "Formation of calcium carbonate films on chitosan substrates in the presence of polyacrylic acid." *J. Solid State Chem.*, *182* (5), 1082–1087.

Heng, D., Lee, S.H., Kwek, J.W., Ng, W.K., Chan, H.-K. and Tan, R.B.H. (2012). "Assessing the combinatorial influence of climate, formulation and device on powder aerosolization using the Taguchi experimental design." *Powder Technol.*, *226,* 253–260.

Hennart, S.L.A., Domingues, M.C., Wildeboer, W.J., Hee, P. van and Meesters, G.M.H. (2010). "Study of the process of stirred ball milling of poorly water soluble organic products using factorial design." *Powder Technol.*, *198* (1), 56–60.

Hennart, S.L.A., Hee, P. van, Drouet, V., Domingues, M.C., Wildeboer, W.J. and Meesters, G.M.H. (2012). "Characterization and modeling of a sub-micron milling process limited by agglomeration phenomena." *Chem. Eng. Sci.*, *71,* 484–495.

Hewitt, S. a. and Kibble, K. a. (2009). "Effects of ball milling time on the synthesis and consolidation of nanostructured WC–Co composites." *Int. J. Refract. Met. Hard Mater.*, *27* (6), 937–948.

Hjertberg, T. and Sörvik, E.M. (1984). Thermal Degradation of PVC. In Degradation and Stabilisation of PVC, E.D. Owen, ed. (Springer Netherlands), pp 21–79.

Ho, W.-H., Tsai, J.-T., Lin, B.-T. and Chou, J.-H. (2009). "Adaptive network-based fuzzy inference system for prediction of surface roughness in end milling process using hybrid Taguchi-genetic learning algorithm." *Expert Syst. Appl.*, *36* (2, Part 2), 3216–3222.

https://www.fishersci.com/shop/products/retsch-pm-100-planterary-ball-mill-grinding-jars-5/p-3039698

http://www.surface-tension.de/. Accessed 10 Aug 2013

Ikejima, T., Yoshie, N. and Inoue, Y. (1999). "Influence of tacticity and molecular weight of poly(vinyl alcohol) on crystallization and biodegradation of poly(3-hydroxybutyric acid)/poly(vinyl alcohol) blend films." *Polym. Degrad. Stab.*, *66* (2), 263–270.

Iyer, R.S. and Scott, J.A. (2001). "Power station fly ash - a review of value-added utilization outside of the construction industry." *Resour. Conserv. Recycl.*, *31* (3), 217–228.

Jamshidi, A., Nourbakhsh, A.A., Naghibi, S. and MacKenzie, K.J.D. (2014). "Application of the statistical Taguchi method to optimize X-SiAlON and mullite formation in composite powders prepared by the SRN process." *Ceram. Int.*, *40* (1, Part A), 263–271.

Jung, H.J., Sohn, Y., Sung, H.G., Hyun, H.S. and Shin, W.G. (2015). "Physicochemical properties of ball milled boron particles: Dry vs. wet ball milling process." *Powder Technol.*, *269,* 548–553.

Justin, R. and Chen, B. (2014). "Characterisation and drug release performance of biodegradable chitosan–graphene oxide nanocomposites." *Carbohydr. Polym.*, *103* 70–80.

Kader, M. a., Kim, K., Lee, Y.-S. and Nah, C. (2006). "Preparation and properties of nitrile rubber/montmorillonite nanocomposites via latex blending." *J. Mater. Sci.*, *41* (22), 7341–7352.

Kaully, T., Siegmann, A. and Shacham, D. (2008). "Mechanical behavior of highly filled natural $CaCO_3$ composites: Effect of particle size distribution and interface interactions." *Polym. Compos.*, *29* (4), 396–408.

Khan, M.J., Al-Juhani, A.A., Shawabkeh, R., Ul-Hamid, A. and Hussein, I.A. (2011). "Chemical modification of waste oil fly ash for improved mechanical and thermal properties of low density polyethylene composites." *J. Polym. Res.*, *18* (6), 2275–2284.

Kim, K.D., Choi, D.W., Choa, Y.-H. and Kim, H.T. (2008). "The effect of parameters on the formation of ZnO nanoparticles by statistical experimental design method in vibrating milling process." *J. Mater. Process. Technol.*, *202* (1–3), 569–573.

Kishore, Kulkarni, S.M., Sunil, D. and Sharathchandra, S. (2002). "Effect of surface treatment on the impact behaviour of fly-ash filled polymer composites." *Polym. Int.*, *51* (12), 1378–1384.

Kong, L.B., Ma, J., Zhu, W. and Tan, O.K. (2001). "Preparation and characterization of translucent PLZT8 / 65 / 35 ceramics from nano-sized powders produced by a high-energy ball-milling process." *Mater. Res. Bull.*, *36,* 1675–1685.

Kong, L.B., Ma, J., Zhu, W. and Tan, O.K. (2001). "Preparation of $Bi_4Ti_3O_{12}$ ceramics via a high-energy ball milling process." *Mater. Lett.*, *51,* 108–114.

Kong, L.B., Zhu, W. and Tan, O.K. (2001). "Preparation and characterization of PLZT ceramics using high-energy ball milling." *J. Alloys Compd.*, *322,* 290–297.

Kulkarni, M.B., Bambole, V.A. and Mahanwar, P.A. (2014). "Effect of particle size of fly ash cenospheres on the properties of acrylonitrile butadiene styrene-filled composites." *J. Thermoplast. Compos. Mater.*, *27* (2), 251–267.

Kulkarni, S.M. and Kishore (2002). "Effects of surface treatments and size of fly ash particles on the compressive properties of epoxy based particulate composites." *J. Mater. Sci.*, *37* (20), 4321–4326.

Kumar, S., Jaganathan, S.K., Nando, G.B. and Chattopadhyay, S.C. (2015). "Synthesis and Characterization of Novel Polycarbonate Based Polyurethane/Polymer

Wrapped Hydroxyapatite Nanocomposites: Mechanical Properties, Osteoconductivity and Biocompatibility." *J. Biomed. Nanotechnol.*, *11* (2), 291–305.

Kumar, S. and Kumar, R. (2011). "Mechanical activation of fly ash: effect on reaction, structure and properties of resulting geopolymer." *Ceram. Int.*, *37* (2), 533–541.

Kuram, E. and Ozcelik, B. (2013). "Multi-objective optimization using Taguchi based grey relational analysis for micro-milling of Al 7075 material with ball nose end mill." *Meas.*, *46* (6), 1849–1864.

Lapuerta, M., Ballesteros, R. and Martos, F.J. (2006). "A method to determine the fractal dimension of diesel soot agglomerates." *J. Colloid Interface Sci.*, *303* (1), 149–158.

Lee, J.S., Choi, M.S., Hung, N.V., Kim, Y.S., Kim, I.W., Park, E.C., Jeong, S.J. and Song, J.S. (2007). "Effects of high energy ball-milling on the sintering behavior and piezoelectric properties of PZT-based ceramics." *Ceram. Int.*, *33* (7), 1283–1286.

Levchik, S.V. and Weil, E.D. (2005). "Overview of the recent literature on flame retardancy and smoke suppression in PVC." *Polym. Adv. Technol.*, *16* (10), 707–716.

Li, Y., White, D.J. and Peyton, R. Lee (1998). "Composite material from fly ash and post-consumer PET." *Resour. Conserv. Recycl.*, *24* (2), 87–93.

Liu, M., Guo, B., Du, M. and Jia, D. (2007). "Drying induced aggregation of halloysite nanotubes in polyvinyl alcohol/halloysite nanotubes solution and its effect on properties of composite film." *Appl. Phys. A*, *88* (2), 391–395.

Liu, M., Guo, B., Du, M., Chen, F. and Jia, D. (2009). "Halloysite nanotubes as a novel -nucleating agent for isotactic polypropylene." *Polymer*, *50* (13), 3022–3030.

Liu, P., Zhao, M. and Guo, J. (2006). "Thermal Stabilities of Poly(Vinyl Chloride)/Calcium Carbonate (PVC/CaCO$_3$) Composites." *J. Macromol. Sci. Part B*, *45* (6), 1135–1140.

Lomayeva, S.F., Yelsukov, E.P., Konygin, G.N., Dorofeev, G.A., Povstugar, V.I., Mikhailova, S.S., Zagainov, A.V. and Maratkanova, A.N. (2000). "The influence of a

surfactant on the characteristics of the iron powders obtained by mechanical milling in organic media." *Colloids Surf., A*, *162* (1999), 279–284.

Mandelbrot, B.B. (1982). "The Fractal Geometry of Nature (San Francisco: W. H. Freeman and Company).

Mansur, H.S., Sadahira, C.M., Souza, A.N. and a.P. Mansur, A. (2008). "FTIR spectroscopy characterization of poly (vinyl alcohol) hydrogel with different hydrolysis degree and chemically crosslinked with glutaraldehyde." *Mater. Sci. Eng. C*, *28* (4), 539–548.

Martín, L. de, Fabre, A. and Ruud van Ommen, J. (2014). "The fractal scaling of fluidized nanoparticle agglomerates." *Chem. Eng. Sci.*, *112* 79–86.

Maweja, K., Montong, T., Moyo, L. and Phasha, M.J. (2012). "Mechanical alloying and magnetic saturation of tungsten–nickel powders." *Int. J. Refract. Met. Hard Mater.*, *31,* 247–252.

Mio, H., Kano, J., Saito, F. and Kaneko, K. (2002). "Effects of rotational direction and rotation-to-revolution speed ratio in planetary ball milling." *Mater. Sci. Eng., A*, *332,* 75–80.

Mollah, M.Y.A., Hess, T.R. and Cocke, D.L. (1994). "Surface and bulk studies of leached and unleached fly ash using XPS, SEM, EDS and FTIR techniques." *Cem. Concr. Res.*, *24* (1), 109–118.

Mustapha, M., Othman, E.A., Norsal, K., Mustapha, F., Mamat, O. and Ramesh, S. (2013). "Carbothermal nitridation process of mechanically milled silica sand using Taguchi's method." *Ceram. Int., 39* (6), 6119–6130.

Muzzy, J.D. (2000). 2.02 - Thermoplastics—Properties. In Comprehensive Composite Materials, A.K. Zweben, ed. (Oxford: Pergamon), pp 57–76.

Nath, D.C.D., Bandyopadhyay, S., Boughton, P., Yu, A., Blackburn, D. and White, C. (2010). "Chemically modified fly ash for fabricating super-strong biodegradable poly(vinyl alcohol) composite films." *J. Mater. Sci.*, *45* (10), 2625–2632.

Nath, D.C.D., Bandyopadhyay, S., Campbell, J., Yu, A., Blackburn, D. and White, C. (2010). "Surface-coated fly ash reinforced biodegradable poly(vinyl alcohol)

composite films: part 2-analysis and characterization." *Appl. Surf. Sci.*, *257* (4), 1216–1221.

Nath, D.C.D., Bandyopadhyay, S., Gupta, S., Yu, A., Blackburn, D. and White, C. (2010). "Surface-coated fly ash used as filler in biodegradable poly(vinyl alcohol) composite films: Part 1—The modification process." *Appl. Surf. Sci.*, *256* (9), 2759–2763.

Nath, D.C.D., Bandyopadhyay, S., Rider, J., Yu, A., Blackburn, D. and White, C. (2011). "Study of dynamic mechanical properties and morphological behaviours of fly ash reinforced polypropylene composites." *Macromol. Res.*, *19* (4), 338–344.

Nath, D.C.D., Bandyopadhyay, S., Yu, A., Blackburn, D. and White, C. (2010). "High strength bio-composite films of poly(vinyl alcohol) reinforced with chemically modified-fly ash." *J. Mater. Sci.*, *45* (5), 1354–1360.

Nath, D.C.D., Bandyopadhyay, S., Yu, A., Blackburn, D. and White, C. (2010). "Novel observations on kinetics of nonisothermal crystallization in fly ash filled isotactic-polypropylene composites." *J. Appl. Polym. Sci.*, *115* (3), 1510–1517.

Nath, D.C.D., Bandyopadhyay, S., Yu, A., Blackburn, D., White, C. and Varughese, S. (2010). "Isothermal crystallization kinetics of fly ash filled iso-polypropylene composite- and a new physical approach." *J. Therm. Anal. Calorim.*, *99* (2), 423–429.

Nath, D.C.D., Bandyopadhyay, S., Yu, A., Zeng, Q., Das, T., Blackburn, D. and White, C. (2009). "Structure–property interface correlation of fly ash–isotactic polypropylene composites." *J. Mater. Sci.*, *44* (22), 6078–6089.

Neam u, B.V., Chicina , I., Isnard, O., Popa, F. and Pop, V. (2011). "Influence of wet milling conditions on the structural and magnetic properties of Ni_3Fe nanocrystalline intermetallic compound." *Intermetallics*, *19* (1), 19–25.

Nelson, M.I. (2001). "A dynamical systems model of the limiting oxygen index test: II. Retardancy due to char formation and addition of inert fillers." *Combust. Theory Model.*, *5* (1), 59–83.

Neto, C.G.T., Giacometti, J.A., Job, A.E., Ferreira, F.C., Fonseca, J.L.C. and Pereira, M.R. (2005). "Thermal Analysis of Chitosan Based Networks." *Carbohydr. Polym.*, *62* (2), 97–103.

Nielsen, L.E. (1966). "Simple theory of stress-strain properties of filled polymers." *J. Appl. Polym. Sci.*, *10* (1), 97–103.

Nieto, J.M., Peniche-Covas, C. and Padro´n, G. (1991). "Characterization of chitosan by pyrolysis-mass spectrometry, thermal analysis and differential scanning calorimetry." *Thermochim. Acta*, *176* 63–68.

Ogawa, K., Yui, T. and Miya, M. (1992). "Dependence on the Preparation Procedure of the Polymorphism and Crystallinity of Chitosan Membranes." *Biosci. Biotechnol. Biochem.*, *56* (6), 858–862.

Ogawa, K., Yui, T. and Okuyama, K. (2004). "Three D structures of chitosan." *Int. J. Biol. Macromol.*, *34* (1–2), 1–8.

Oliveira, R.C., Hammer, P., Guibal, E., Taulemesse, J.M. and Garcia Jr., O. (2014). "Characterization of metal–biomass interactions in the lanthanum(III) biosorption on Sargassum sp. using SEM/EDX, FTIR, and XPS: Preliminary studies." *Chem. Eng. J.*, *239* 381–391.

Ortiz, A.L., Zamora, V. and Rodríguez-Rojas, F. (2012). "A study of the oxidation of ZrB2 powders during high-energy ball-milling in air." *Ceram. Int.*, *38* (4), 2857–2863.

Othman, M.B.H., Md Akil, H., Md Rasib, S.Z., Khan, A. and Ahmad, Z. (2015). "Thermal properties and kinetic investigation of chitosan-PMAA based dual-responsive hydrogels." *Ind. Crops Prod.*, *66* 178–187.

Pal, K., Banthia, A.K. and Majumdar, D.K. (2007). "Preparation and characterization of polyvinyl alcohol-gelatin hydrogel membranes for biomedical applications." *AAPS Pharm. Sci. Tech.*, *8* (1), 21.

Paria, S. and Khilar, K.C. (2004). "A review on experimental studies of surfactant adsorption at the hydrophilic solid-water interface." *Adv. Colloid Interface Sci.*, *110* (3), 75–95.

Parvaiz, M.R., Mohanty, S., Nayak, S.K. and Mahanwar, P.A. (2011). "Effect of surface modification of fly ash on the mechanical, thermal, electrical and morphological properties of polyetheretherketone composites." *Mater. Sci. Eng., A*, *528* (13–14), 4277–4286.

Paul, D.R. and Robeson, L.M. (2008). "Polymer nanotechnology: Nanocomposites." *Polymer*, *49* (15), 3187–3204.

Paul, K.T., Satpathy, S.K., Manna, I., Chakraborty, K.K. and Nando, G.B. (2007). "Preparation and Characterization of Nano structured Materials from Fly Ash: A Waste from Thermal Power Stations, by High Energy Ball Milling." *Nanoscale Res. Lett.*, *2* (8), 397.

Pelovski, Y., Dombalov, I. and Petkova, V. (2001). "Mechano-chemical Activation of Dolomite." *J. Therm. Anal. Calorim.*, *64* (3), 1257–1263.

Pielichowski, K., Hamerton, I., Pielichowski, J. and Stanczyk, P. (1998). "A study of the thermal properties of blends of poly(vinyl chloride) with novel epoxypropanecarbazole-based dyes by TGA/FTIR." *Eur. Polym. J.*, *34* (5-6), 653–657.

Pukánszky, B., Tüdös, F., Jan a , J. and Kola ik, J. (1989). "The possible mechanisms of polymer-filler interaction in polypropylene-$CaCO_3$ composites." *J. Mater. Sci. Lett.*, *8* (9), 1040–1042.

Qiao, J. and Wu, G. (2011). "Tensile properties of fly ash/polyurea composites." *J. Mater. Sci.*, *46* (11), 3935–3941.

Rabiezadeh, A., Hadian, A. M. and Ataie, A. (2012). "Preparation of alumina/titanium diboride nano-composite powder by milling assisted sol–gel method." *Int. J. Refract. Met. Hard Mater.*, *31,* 121–124.

Ramesh, S., Leen, K.H., Kumutha, K. and Arof, A.K. (2007). "FTIR studies of PVC/PMMA blend based polymer electrolytes." *Spectrochim. Acta. A. Mol. Biomol. Spectrosc.*, *66* (4–5), 1237–1242.

Ramos, V.D., Costa, H.M. da, Soares, V.L.P. and Nascimento, R.S.V. (2005). "Hybrid composites of epoxy resin modified with carboxyl terminated butadiene acrilonitrile copolymer and fly ash microspheres." *Polym. Test.*, *24* (2), 219–226.

Reynaud, E., Jouen, T., Gauthier, C., Vigier, G. and Varlet, J. (2001). "Nanofillers in polymeric matrix: a study on silica reinforced PA6." *Polym.*, *42* (21), 8759–8768.

Rohatgi, P.K., Matsunaga, T. and Gupta, N. (2009). "Compressive and ultrasonic properties of polyester/fly ash composites." *J. Mater. Sci.*, *44* (6), 1485–1493.

Rose, H.E. and Sullivan, R.M.E. (1953). "A Treatise on the Internal Mechanics of Ball, Tube & Rod Mills (London: Constable).

Ross, P.J. (1996). "Taguchi Techniques for Quality Engineering: Loss Function, Orthogonal Experiments, Parameter and Tolerance Design (McGraw Hill Professional).

Roy, R.K. (2001). "Design of Experiments Using The Taguchi Approach: 16 Steps to Product and Process Improvement (New York: Wiley-Interscience).

Rudin, A. and Choi, P. (2012). "The Elements of Polymer Science & Engineering" (Academic Press).

Sakthivel, S., Krishnan, V.V. and Pitchumani, B. (2008). "Influence of suspension stability on wet grinding for production of mineral nanoparticles." *Particuology*, *6* (2), 120–124.

Sakurai, K., Maegawa, T. and Takahashi, T. (2000). "Glass transition temperature of chitosan and miscibility of chitosan/poly(N-vinyl pyrrolidone) blends." *Polymer*, *41* (19), 7051–7056.

Sarbak, Z. and Kramer-Wachowiak, M. (2002). "Porous structure of waste fly ashes and their chemical modifications." *Powder Technol.*, *123* (1), 53–58.

Saroj, A.L. and Singh, R.K. (2012). "Thermal, dielectric and conductivity studies on PVA/Ionic liquid [EMIM][EtSO$_4$] based polymer electrolytes." *J. Phys. Chem. Solids*, *73* (2), 162–168.

Satapathy, B.K., Das, A. and Patnaik, A. (2011). "Ductile-to-brittle transition in cenosphere-filled polypropylene composites." *J. Mater. Sci.*, *46* (6), 1963–1974.

Satapathy, S., Nag, A. and Nando, G.B. (2012). "Effect of electron beam irradiation on the mechanical, thermal, and dynamic mechanical properties of flyash and nanostructured fly ash waste polyethylene hybrid composites." *Polym. Compos.*, *33* (1), 109–119.

Satapathy, S., Nando, G.B., Nag, A. and Raju, K.V.S.N. (2013). "HDPE-Fly Ash/Nano Fly Ash Composites." *J. Appl. Polym. Sci.*, *130* (6), 4558–4567.

Sengupta, S., Pal, K., Ray, D. and Mukhopadhyay, A. (2011). "Furfuryl palmitate coated fly ash used as filler in recycled polypropylene matrix composites." *Composites Part B*, *42* (7), 1834–1839.

Shangguan, Y., Song, Y., Peng, M., Li, B. and Zheng, Q. (2005). "Formation of - crystal from nonisothermal crystallization of compression-molded isotactic polypropylene melt." *Eur. Polym. J.*, *41* (8), 1766–1771.

Shanmugharaj, A.M., Sabharwal, S., Majali, A.B., Tikku, V.K. and Bhowmick, A.K. (2002). "Surface characterization of electron beam modified dual phase filler by ESCA, FT-IR and surface energy." *J. Mater. Sci.*, *37* (13), 2781–2793.

Sharafi, S. and Gomari, S. (2012). "Effects of milling and subsequent consolidation treatment on the microstructural properties and hardness of the nanocrystalline chromium carbide powders." *Int. J. Refract. Met. Hard Mater.*, *30* (1), 57–63.

Sharma, A.K. and Mahanwar, P.A. (2010). "Effect of particle size of fly ash on recycled poly (ethylene terephthalate) / fly ash composites." *Int. J. Plast. Technol.*, *14* (1), 53–64.

Shawabkeh, R., Khan, M.J., Al-Juhani, A.A., Al-Abdul Wahhab, H.I. and Hussein, I.A. (2011). "Enhancement of surface properties of oil fly ash by chemical treatment." *Appl. Surf. Sci.*, *258* (5), 1643–1650.

Shi, X. M., Zhang, J., Jin, J., and Chen, S. J., (2008). "Non-isothermal crystallization and melting of ethylene-vinyl acetate copolymers with different vinyl acetate contents." *eXPRESS Polym. Lett.*, *2* (9), 623–629.

Shinohara, K., Golman, B., Uchiyama, T. and Otani, M. (2000). "Fine-grinding characteristics of hard materials by attrition mill." *Powder Technol.*, *103,* 292–296.

Shrivastava, A., Sakthivel, S., Pitchumani, B. and Rathore, A. S. (2011). "A statistical approach for estimation of significant variables in wet attrition milling." *Powder Technol.*, *211* (1), 46–53.

Smith, B.C. (1998). "Infrared Spectral Interpretation: A Systematic Approach (Boca Raton: CRC Press).

Sombatsompop, N., Chaochanchaikul, K., Phromchirasuk, C. and Thongsang, S. (2003). "Effect of wood sawdust content on rheological and structural changes, and thermo-mechanical properties of PVC/sawdust composites." *Polym. Int.*, *52* (12), 1847–1855.

Stankovich, S., Dikin, D.A., Dommett, G.H.B., Kohlhaas, K.M., Zimney, E.J., Stach, E.A., Piner, R.D., Nguyen, S.T. and Ruoff, R.S. (2006). "Graphene-based composite materials." *Nature*, *442* (7100), 282–286.

Stellacci, P., Liberti, L., Notarnicola, M. and Bishop, P.L. (2009). "Valorization of coal fly ash by mechano-chemical activation Part I. Enhancing adsorption capacity." *Chem. Eng. Sci.*, *149* 11–18.

Su, L., Xing, Z., Wang, D., Xu, G., Ren, S. and Fang, G. (2013). "Mechanical Properties Research and Structural Characterization of Alkali Lignin/Poly(vinyl alcohol) Reaction Films." *Bioresour.*, *8* (3), 3532–3543.

Sudhamani, S.R., Prasad, M.S. and Udaya Sankar, K. (2003). "DSC and FTIR studies on Gellan and Polyvinyl alcohol (PVA) blend films." *Food Hydrocoll.*, *17* (3), 245–250.

Swain, S.K., Dash, S., Kisku, S.K. and Singh, R.K. (2014). "Thermal and Oxygen Barrier Properties of Chitosan Bionanocomposites by Reinforcement of Calcium Carbonate Nanopowder." *J. Mater. Sci. Technol.*, *30* (8), 791–795.

Swami, P.N., Raju, B.N., Rao, D.V. and Rao, J.B. (2009). "Synthesis and Characterization of Nano-Structured Fly Ash: A Waste from Thermal Power Plant." *Proceedings of the Institution of Mechanical Engineers, Part N: J. Nanoeng. and Nanosys.*, *223* (2), 35–44.

Syuhada, N.I., Huang, N.M., Vijay Kumar, S., Lim, H.N., Rahman, S.A., Thien, G.S., Ibrahim, N.A., Ahmad, M. and Moradihamedani, P. (2014). "Enhanced mechanical properties of chitosan/EDTA-GO nanocomposites thin films." *Sains Malaysiana*, *43* (6), 851–859.

Taguchi, G. (1986). "Introduction to Quality Engineering: Designing Quality into Products and Processes (Tokyo: Quality Resources).

Tan, O.K., Cao, W., Hu, Y. and Zhu, W. (2004). "Nanostructured oxides by high-energy ball milling technique: application as gas sensing materials." *Solid State Ionics*, *172* (1-4), 309–316.

Tanabe, T., Okitsu, N., Tachibana, A. and Yamauchi, K. (2002). "Preparation and characterization of keratin–chitosan composite film." *Biomaterials*, *23* (3), 817–825.

Tjong, S.C. (2006). "Structural and mechanical properties of polymer nanocomposites." *Mater. Sci. Eng. R Rep.*, *53* (3–4), 73–197.

Varma, I.K. and Gupta, V.B. (2000). 2.01 - Thermosetting Resin—Properties. In Comprehensive Composite Materials, A.K. Zweben, ed. (Oxford: Pergamon), pp 1–56.

Viana, R.B., Silva, A.B.F. da and Pimentel, A.S. (2012). "Infrared Spectroscopy of Anionic, Cationic, and Zwitterionic Surfactants." *Adv. Phys. Chem.*, *2012*.

Wan, C., Tian, G., Cui, N., Zhang, Y. and Zhang, Y. (2004). "Processing thermal stability and degradation kinetics of poly(vinyl chloride)/montmorillonite composites." *J. Appl. Polym. Sci.*, *92* (3), 1521–1526.

Wang, M.R., Jia, D.C., He, P.G. and Zhou, Y. (2011). "Microstructural and mechanical characterization of fly ash cenosphere/metakaolin-based geopolymeric composites." *Ceram. Int.*, *37* (5), 1661–1666.

Wang, Y., Ni, Q.Q., Zhu, Y. and Natsuki, T. (2014). "Fabrication of functionally graded nano-TiO_2-reinforced epoxy matrix composites." *Polym. Compos.*, *35* (3), 557–563.

Watanabe, H. (1999). "Critical rotation speed for ball-milling." *Powder Technol.*, *104* (1), 95–99.

Werth, J.H., Linsenbühler, M., Dammer, S.M., Farkas, Z., Hinrichsen, H., Wirth, K.E. and Wolf, D.E. (2003). "Agglomeration of charged nanopowders in suspensions." *Powder Technol.*, *133* (1-3), 106–112.

Xiao, C. and Yang, M. (2006). "Controlled preparation of physical cross-linked starch-g-PVA hydrogel." *Carbohydr. Polym.*, *64* (1), 37–40.

Xie, X.L., Liu, Q.X., Li, R.K.Y., Zhou, X.-P., Zhang, Q.X., Yu, Z.Z. and Mai, Y.W. (2004). "Rheological and mechanical properties of PVC/CaCO$_3$ nanocomposites prepared by in situ polymerization." *Polymer*, *45* (19), 6665–6673.

Xu, G., Wang, L., Liu, J. and Wu, J. (2013). "FTIR and XPS analysis of the changes in bamboo chemical structure decayed by white-rot and brown-rot fungi." *Appl. Surf. Sci.*, *280* 799–805.

Xu, M., Bahl, C.R.H., Frandsen, C. and Mørup, S. (2004). "Interparticle interactions in agglomerates of alpha-Fe$_2$O$_3$ nanoparticles: influence of grinding." *J. Colloid Interface Sci.*, *279* (1), 132–6.

Yamaguchi, I., Tokuchi, K., Fukuzaki, H., Koyama, Y., Takakuda, K., Monma, H. and Tanaka, J. (2001). "Preparation and microstructure analysis of chitosan/hydroxyapatite nanocomposites." *J. Biomed. Mater. Res.*, *55* (1), 20–27.

Yan, W., Lin, R.J.T. and Bhattacharyya, D. (2006). "Particulate reinforced rotationally moulded polyethylene composites – Mixing methods and mechanical properties." *Compos. Sci. Technol.*, *66* (13), 2080–2088.

Yan, Z.X., Deng, J. and Luo, Z.M. (2010). "A comparison study of the agglomeration mechanism of nano- and micrometer aluminum particles." *Mater. Charact.*, *61* (2), 198–205.

Yang, Q., Zhao, L., Xiao, H., and Zhao, N. (2000). "Analysis of intrinsic stress in diamond films by X-ray diffraction." International centre for diffraction data. Adv. X-Ray Anal., 43, 151-156.

Yang, Y.F., Gai, G.S., Cai, Z.F. and Chen, Q.R. (2006). "Surface modification of purified fly ash and application in polymer." *J. Hazard. Mater.*, *133* (1-3), 276–82.

Yao, N., Zhang, P., Song, L., Kang, M., Lu, Z. and Zheng, R. (2013). "Stearic acid coating on circulating fluidized bed combustion fly ashes and its effect on the mechanical performance of polymer composites." *Appl. Surf. Sci.*, *279* 109–115.

Yao, Z.T., Ji, X.S., Sarker, P.K., Tang, J.H., Ge, L.Q., Xia, M.S. and Xi, Y.Q. (2015). "A comprehensive review on the applications of coal fly ash." *Earth Sci. Rev.*, *141,* 105–121.

Yo urtcuo lu, E. and Ucurum, M. (2011). "Surface modification of calcite by wet-stirred ball milling and its properties." *Powder Technol.*, *214* (1), 47–53.

Yunsheng, Z., Wei, S. and Zongjin, L. (2006). "Impact behavior and microstructural characteristics of PVA fiber reinforced fly ash-geopolymer boards prepared by extrusion technique." *J. Mater. Sci.*, *41* (10), 2787–2794.

Zaeni, A., Bandyopadhyay, S., Yu, A., Rider, J., Sorrell, C.S., Dain, S., Blackburn, D. and White, C. (2010). "Colour control in fly ash as a combined function of particle size and chemical composition." *Fuel*, *89* (2), 399–404.

Zhang, D.L. (2004). "Processing of advanced materials using high-energy mechanical milling." *Prog. Mater. Sci.*, *49* (3-4), 537–560.

Zhang, F.L., Zhu, M. and Wang, C.Y. (2008). "Parameters optimization in the planetary ball milling of nanostructured tungsten carbide/cobalt powder." *Int. J. Refract. Met. Hard Mater.*, *26* (4), 329–333.

Zhang, J., Cui, H., Wang, B., Li, C., Zhai, J. and Li, Q. (2014). "Preparation and characterization of fly ash cenospheres supported $CuO–BiVO_4$ heterojunction composite." *Appl. Surf. Sci.*, *300* 51–57.

Zhang, L., Xu, Z., Feng, Y., Hu, Y. and Yao, X. (2008). "Synthesis, sintering and characterization of PNZST ceramics from high-energy ball milling process." *Ceram. Int.*, *34,* 709–713.

Zheng, L., Cui, B., Zhao, L., Li, W. and Hadjipanayis, G.C. (2012). "Sm_2Co_{17} nanoparticles synthesized by surfactant-assisted high energy ball milling." *J. Alloys Compd.*, *539,* 69–73.

Zhu, A., Shi, Z., Cai, A., Zhao, F. and Liao, T. (2008). "Synthesis of core–shell PMMA–SiO$_2$ nanoparticles with suspension–dispersion–polymerization in an aqueous system and its effect on mechanical properties of PVC composites." *Polym. Test.*, *27* (5), 540–547.

Zivanovic, S., Li, J., Davidson, P.M. and Kit, K. (2007). "Physical, mechanical, and antibacterial properties of chitosan/PEO blend films." *Biomacromolecules*, *8* (5), 1505–1510.

LIST OF PUBLICATIONS

IN PEER-REVIEWED JOURNALS

A. G. Patil, A. Mahendran, S. Anandhan, "Nanostructured fly ash as reinforcement in a plastomer-based composite: A new strategy in value addition to thermal power station fly ash", *Silicon,* DOI: 10.1007/s12633-014-9194-2, (2014).

A. G. Patil, M. Selvakumar, S. Anandhan**, "Characterization of composites based on biodegradable poly(vinyl alcohol) and nanostructured fly ash with an emphasis on polymer-filler interaction", *Journal of Thermoplastic Composite Materials*, DOI: 10.1177/0892705714563130.

A. G. Patil, A. M. Shanmugharaj, S. Anandhan, "Interparticle interactions and lacunarity of mechano-chemically activated fly ash", *Powder Technology*, 272, 241-249 (2015).

A. G. Patil, S. Anandhan, "Influence of planetary ball milling parameters on the mechano-chemical activation of fly ash", *Powder Technology*, 281, 151-158 (2015).

A. G. Patil, Poornachandra, Ramesh Gumageri, K. Rajkumar and S. Anandhan**, "**Biodegradable Chitosan Composites Reinforced with Nanostructured Waste Fly Ash", *Journal of material cycles and waste management* (*under review*).

A. G. Patil, A. Mahendran, M. Selvakumar and S. Anandhan**, "**Ductility and flame retardance improvement of PVC by Nanostructured fly ash", *Silicon* (*under review*).

BOOK CHAPTER

A. G. Patil, S. Bandyopadhyay and S. Anandhan, "Fly ash based polymer matrix composites", in 'Advances in Polymer Materials and Technology', S. Anandhan and S. Bandyopadhyay, Eds., CRC Press, Boca Raton, USA (*Communicated*).

IN CONFERENCE PROCEEDINGS

A. G. Patil, S. Anandhan, "Ethylene-octene copolymer/ball milled Fly Ash Composites", *Third International Conference on Natural Polymers, Bio-Polymers, Bio-Materials, their Composites, Blends, IPNs, Polyelectrolytes and Gels: Macro to Nano Scales (ICNP – 2012)*, India, October 2012 (Invited paper).

A. G. Patil, S. Anandhan, "Preparation and characterization of poly(vinyl alcohol)/mechanochemically activated fly ash composites", *International Conference on Rubber and Rubber like Materials (ICRRM–2013)*, organized by the Rubber Technology Center (IIT Kharagpur – India) India, March 2013.

A. G. Patil, S. Anandhan, "Optimization of parameters of mechano-chemical activation of fly ash by Taguchi method". *6th Bangalore Nano 2013 Poster -Walkway of Discovery* organized by the Dept. of IT, BT and ST, Govt of Karnataka; VGST and JNCASR (Bangalore- India), December 2013.

A. G. Patil, S. Anandhan**, "Interparticle interactions and lacunarity of mechano-chemically activated fly ash", *International seminar on Frontiers of Ceramic & Material Technologies for Cement Industries (CEMSEM-2014),* India, organized by Indian ceramic society, November 2014, *"Awarded as best paper presentation".*

A. G. Patil, S. Anandhan, "Preparation and characterization of nano-structured fly ash, a potential reinforcement for polymer matrices", *International Conference on Advancements in Polymeric Materials APM-2015*, CIPET-Chennai and IISc, Bangalore, India, February 2015.

A. Mahendran, **A. G. Patil**, S. Anandhan, H. Lammer, 'Nanostructured fly ash as reinforcement in a plastomer-based composite: A new Strategy to reduce greenhouse emission from thermal power station', *International Conference on Biopolymer Materials and Engineering*, Slovenj Gradec, April 2015.

BIO-DATA

Akshata G. Patil

Permanent address:

Plot No. 306-307

Godutai Nagar

Gulbarga **-** 585102

Karnataka, India

Contact Details:

Email ✉: akshatagpatil@gmail.com

Phone ☎: +91-9535821103

Academic Qualifications:

Bachelor of Engineering in Ceramic and Cement Technology (2009), Department Ceramic and Cement Technology from Poojya Doddappa Appa College of Engineering, Gulbarga, Karnataka, India.

Master of Technology in Materials Engineering (2011), Department of Metallurgical and Materials Engineering from National Institute of Technology Karnataka, Surathkal, India.

Research publications:

Articles in International Journals: 04

Articles in Conference Proceedings: 06